Title
Non-invasive Optical Measurement of arterial blood flow speed

Permalink
https://escholarship.org/uc/item/6fn6g2m4

Author
Zhang, Ce

Publication Date
2020

UNIVERSITY OF CALIFORNIA SAN DIEGO

Non-invasive Optical Measurement of arterial blood flow speed

A dissertation submitted in partial satisfaction of the
requirements for the degree
Doctor of Philosophy

in

Electrical Engineering (Electronic Circuits & System)

by

Alex Ce Zhang

Committee in charge:

Professor Yu-Hwa Lo, Chair
Professor Prabhakar R. Bandaru
Professor Stephanie Fraley
Professor Drew A. Hall
Professor Yuan Taur

2020

The dissertation of Alex Ce Zhang is approved, and it is acceptable in quality and form for publication on microfilm and electronically:

Chair

University of California San Diego

2020

DEDICATION

To my parents.

EPIGRAPH

The hard way is the only way.

TABLE OF CONTENTS

LIST OF FIGURES

ACKNOWLEDGEMENTS

First of all, I would like to dedicate my special thanks to my advisor Professor Yu-Hwa Lo for his thoughtful guidance, patience and support during my Ph.D study. Any of the work done during my Ph.D study could not have been completed without his tireless guidance and tremendous input. His dedication to student development, breadth of experience, and commitment to research is inspiring and amazing. He taught me how to make vague ideas into concrete mathematical formulation with scientific rigor in a systematic way. He is extremely intelligent and can always quickly out-think student like me by many steps which we truly find amazing and helpful. Despite overseeing so many projects, he never fail to know every details of each projects and provides insightful feedback. I would also like to give special thanks to Professor Taur for choosing me to be his teaching assistant for many quarters which means a lot to me. I would also like to thank my committee members, Professor Prabhakar R. Bandaru, Professor Stephanie Fraley and Professor Drew A. Hall for their time giving me advise on the projects which has been greatly helpful.

I also wish to thank all the Lo group members, and I could have finish the journey without their help, support, discussion. In particular,Dr. Tsung-Feng Wu, Dr. Zhe Mei, Dr. Iftikhar Ahmed Niaz, Dr. Yi Gu, Dr. Yuanyuan Han, Dr. Yuchun Zhou, Dr. Yu-Hsin Liu, Dr. David Hall, Dr. Lujiang Yan, Dr. Zihan Xu, Dr. Wei Cai, Dr. Tiantian Zhang, Dr. Ping-Wei Chen, Dr. Sung Hwan Cho, Yugang Yu, Mahammad Abu Raihan Miah,Jiayun Zhou, Rui Tang, Zunming Zhang, Chi-Yang Tseng, Edward Wang, Shih-Yun Chiu, Shaurya Ayra, Xinyu Chen, Lauren Walker, and Zhilin Guo.

Most importantly, I would like to thank my parents and friends for their support and patience throughout my Ph.D. study.

Portions of Chapter 1,2,3,9 has been submitted in Zhang, A.C., Lo, Y.H., 2020. Non-invasive optical Measurement of arterial blood flow speed. *Biomedical Optics Express (under peer review).* The dissertation author was the primary author of this material.

Portions of Chapter 6,7,8 are currently being prepared for submission for publication in Zhang, A.C., Lo,Y.H.,2020. Theoretical Analysis of non-invasive measurement of arterial blood flow speed. IEEE Journal of Selected Topics in Quantum Electronics. The dissertation author was the primary author of this material.

VITA

2012	B. S. in Microelectronics, Xidian University, Xi’an
2018	M. S. in Electrical Engineering (Electronic Circuits & System), University of California San Diego
2020	Ph. D. in Electrical Engineering (Electronic Circuits & System), University of California San Diego

PUBLICATIONS

1. **Zhang, A.C.**, Gu, Y., Han, Y., Mei, Z., Chiu, Y.J., Geng, L., Cho, S.H. and Lo, Y.H., 2016. Computational cell analysis for label-free detection of cell properties in a microfluidic laminar flow. *Analyst*, 141(13), pp.4142-4150.
2. **Zhang, A.C.**, Lo, Y.H., 2020. Non-invasive optical Measurement of arterial blood flow speed. *Biomedical Optics Express (under peer review)*
3. **Zhang, A.C.**, Lo, Y.H., 2020. Theoretical analysis of non-invasive artertial blood flow measurement(in preparation)
4. Gu, Y.,**Zhang, A.C.** , Han, Y., Li, J., Chen, C. and Lo, Y.H., 2019. Machine learning based real-time image-guided cell sorting and classification.*Cytometry Part A*, 95(5), pp.499-509.
5. Han, Y., Gu, Y., **Zhang, A.C** and Lo, Y.H., 2016. imaging technologies for flow cytometry. *Lab on a Chip*,16(24), pp.4639-4647.
6. Liu, Y.H., Yan, L., **Zhang, A.C.**, Hall, D., Niaz, I.A., Zhou, Y., Sham, L.J. and Lo, Y.H., 2015. Cycling excitation process: An ultra efficient and quiet signal amplification mechanism in semiconductor.*Applied Physics Letters*,107(5), p.053505.
7. Han, Y., Tang, R., Gu, Y., **Zhang, A.C.**, Cai, W., Castor, V., Cho, S.H., Alaynick, W. and Lo, Y.H., 2019. Cameraless high-throughput three-dimensional imaging flow cytometry. *Optica*, 6(10), pp.1297-1304.
8. Yan, L., Yu, Y., **Zhang, A.C.**, Hall, D., Niaz, I.A., Raihan Miah, M.A., Liu, Y.H. and Lo, Y.H., 2017. An amorphous silicon photodiode with 2 THz gain-bandwidth product based on cycling excitation process.*Applied Physics Letters*,111(10), p.101104.
9. Yu, Y., Xu, Z., Li, S., **Zhang, A.C.**, Yan, L., Liu, Z. and Lo, Y.H., 2019. Plasmonically Enhanced Amorphous Silicon Photodetector With Internal Gain.*IEEE Photonics Technology Letters*,31(12), pp.959-962.
10. Gu, Y., Tang, R., **Zhang, A.C.**, Han, Y. and Lo, Y.H., 2019, May. Image-guided microfluidic cell sorter with machine learning. In *CLEO: Science and Innovations* (pp. STu4H-3). Optical Society of America.

11. Han, Y., Tang, R., Gu, Y., **Zhang, A.C.**, Cai, W., Castor, V., Cho, S.H., Alaynick, W. and Lo, Y.H., 2019. Cameraless High-throughput 3D Imaging Flow Cytometry.*arXiv preprint arXiv:1902.01393.*
12. Yan, L., Yu, Y., Xu, Z., Niaz, I., Miah, M.A.R., **Zhang, A.C.**, Zhou, J. and Lo, Y., 2018, June. Low Noise, High Gain-Bandwidth Photodetectors Using Cycling Exciting Process (CEP) as Amplification Mechanism. In*2018 IEEE International Conference on Electron Devices and Solid State Circuits (EDSSC)(pp. 1-2). IEEE.*
13. Niaz, I.A., Miah, M.A.R., Yan, L., Yu, Y., He, Z.Y., Zhang, Y., **Zhang, A.C.**, Zhou, J., Zhang, Y.H. and Lo, Y.H., 2019. Modeling Gain Mechanisms in Amorphous Silicon Due to Efficient Carrier Multiplication and Trap-Induced Junction Modulation.*Journal of Lightwave Technology*,37(19), pp.5056-5066.
14. Xu, Z., Yu, Y., Niaz, I.A., Chen, Y., Arya, S., Lei, Y., Miah, M.A.R., Zhou, J., **Zhang, A.C.**, Yan, L. and Xu, S., 2019. Discovery of Ionic Impact Ionization (I3) in Perovskites Triggered by a Single Photon.*arXiv preprint arXiv:1906.02475.*
15. Yu, Y., Yan, L., **Zhang, A.**, Liu, Y.H., Hall, D., Zhou, J., Chiang, L. and Lo, Y., 2017, October. Quantum detectors using cycling excitation process in disordered medium. In*2017 IEEE Photonics Conference (IPC)(pp. 563-564). IEEE.*
16. Zhou, J., Miah, M.A.R., Yu, Y., **Zhang, A.C.**, Zeng, Z., Damle, S., Niaz, I.A., Zhang, Y. and Lo, Y.H., 2019. Room-temperature long-wave infrared ,detector with thin double layers of amorphous germanium and amorphous silicon.*Optics Express,27(25), pp.37056-37064.*
17. Liu, Y.H., **Zhang, A.**, Miah, M.A.R., Hall, D., Niaz, I.A., Yan, L., Yu, Y., Kavrik, M.S. and Lo, Y.H., 2016, September. Cycling excitation process for light detection and signal amplification in semiconductors. In*Optical Sensing, Imaging, and Photon Counting: Nanostructured Devices and Applications* 2016(Vol. 9933, p. 99330C). International Society for Optics and Photonics.
18. Liu, Y.H., Yan, L., **Zhang, A.**, Hall, D., Niaz, I.A., Kavrik, M.S. and Lo, Y.H., 2016, July. An ultra-efficient internal mechanism to amplify photoresponse for Si and compound semiconductor devices. In*2016 IEEE Photonics Society Summer Topical Meeting Series* (SUM)(pp. 17-18). IEEE.
19. Image-based cell sorting systems and methods, Y Lo, Y Han, Y Gu, **C Zhang** - US Patent App. 16/307,449, 2019
20. Chen, X., Gu, Y., Chen, J., Lee, C.H., Gagne, I., Tang, R., Waller, L., Zhang, Z., **Zhang, A.C.**, Han, Y. and Wang, W., 2020. Image-guided cell sorting using fast scanning lasers. *APL Photonics,5(4), p.040801.*
21. Tang, R., Chen, X., Zhang, Z., Waller, L., Chen, J., Gu, Y., Han, Y., Lee, C.H., Gagne, I., **Zhang, A.C** and Cho, S.H., 2020, February. 2D image-guided cell sorter and 3D imaging flow cytometer. In*High-Speed Biomedical Imaging and Spectroscopy V(Vol. 11250, p. 112500H).* International Society for Optics and Photonics.
22. Xu, Z., Yu, Y., Arya, S., Niaz, I.A., Chen, Y., Lei, Y., Miah, M.A.R., Zhou, J., **Zhang, A.C.**,

Yan, L. and Xu, S., 2020. Frequency-and Power-Dependent Photoresponse of a Perovskite Photodetector Down to the Single-Photon Level.*Nano Letters*,20(3), pp.2144-2151.

23. Xu, Z., Yu, Y., Niaz, I.A., Chen, Y., Arya, S., Lei, Y., Miah, M.A.R., Zhou, J., **Zhang, A.C.**, Yan, L. and Xu, S., 2019. Discovery of Ionic Impact Ionization (I3) in Perovskites Triggered by a Single Photon.*arXiv preprint arXiv:1906.02475*.

ABSTRACT OF THE DISSERTATION

Non-invasive Optical Measurement of arterial blood flow speed

by

Alex Ce Zhang

Doctor of Philosophy in Electrical Engineering (Electronic Circuits & System)

University of California San Diego, 2020

Professor Yu-Hwa Lo, Chair

Non-invasive measurement of the arterial blood speed gives rise to important health information such as cardio output and blood supplies to vital organs. The magnitude and change in arterial blood speed are key indicators of the health conditions and development and progression of diseases. We demonstrated a simple technique to directly measure the blood flow speed in main arteries based on the diffused light model. The concept is demonstrated with a phantom that uses intralipid hydrogel to model the biological tissue and an embedded glass tube with flowing human blood to model the blood vessel. The correlation function of the measured photocurrent was used to find the electrical field correlation function via the Siegert relation. We have shown that the characteristic decorrelation rate (i.e. the inverse of the decoherent time) is linearly proportional to

the blood speed and independent of the tube diameter. This striking property can be explained by an approximate analytic solution for the diffused light equation in the regime where the convective flow is the dominating factor for decorrelation. As a result, we have demonstrated a non-invasive method of measuring arterial blood speed without any prior knowledge or assumption about the geometric or mechanic properties of the blood vessels.

Chapter 1

Introduction

Oxygenated red blood cells in the blood flow deliver essential nutrients and oxygen to organs and limbs to maintain their homeostatic conditions and proper functions. Oximeter detects the oxygen saturation level of red blood cells by using wavelength dependent absorption for oxygenated and deoxygenated blood [Wang et al., 2018]. Such measurements can be done with wearable devices such as smart watches. On the other hand, there has been no convenient and non-invasive method to measure the amount of blood supply or blood speed in major arteries.

Reduced blood supply is usually a sign of diseases and medical conditions. Dehydration, thromboses formation, and other physiological and pathological conditions can cause short term or long term changes in the blood speed at a given location of the artery [Stewart et al., 2019]. The information helps early diagnosis and monitoring of diseases with impaired blood flow [Jayanthy et al., 2011, Poelma et al., 2012, Blumgart and Yens, 1927]. Therefore, it is desirable to directly measure the travelling velocity of red blood cells at well-defined locations such as the carotidal artery to the head, femoral artery to the lower limb, brachial artery to the upper arm, spinal arteries to the spinal cord, renal arteries to the kidneys, hepatic artery to the liver, and pulmonary artery to the lungs, etc. Since the arterial blood speed at the well-defined positions provide direct and unambiguous information about blood supply to the sites of health concerns.

Doppler frequency shift of ultrasonic waves offers a non-invasive measurement of the blood flow speed at the well-defined position. However, acoustic measurements require close physical contacts of the ultrasound transducers with the tissue to allow efficient coupling of the acoustic wave, and gel is needed to assure the quality and reliability of the contact. Furthermore, the measured signal is highly dependent on the angle between the probe and the blood flow direction. The most convenient and ergonomic direction is to have the transducer perpendicular to the blood vessel. However, this arrangement will produce no Doppler shift signal, thus making the measurement less convenient in a homecare or nursing home setting for self-administered operation[Pietrangelo et al., 2018]. In this regard, an optical method is potentially more desirable because a light wave can enter the tissue via free space coupling and once entering the tissue, as we will discuss later, it travels diffusively. In addition, the optical hardware including semiconductor light sources and detectors are more compact than acoustic transmitters and receivers.

People have used dynamic scattering of laser light by red blood cells to measure the speed for blood vessels near the tissue surface [Kashima et al., 1992, Kashima et al., 1993]. Similar to the Doppler effect of sound propagation, the frequency of the scattered light by moving particles is also shifted. Although the operation principle seems to be straightforward, the physical model of the “optical Doppler device” is based on a key assumption that the light is only scattered once by a moving object (e.g. a traveling red blood cell) and the rest of the scatterings is produced by quasi static objects such as skin and fat. This assumption may be reasonable for probing near surface tissue blood flow, but not for major arteries where around 40% of the volume of the blood vessel with a diameter of a few millimeters is occupied by traveling red blood cells. Under the approximation of single light scattering by moving particles, the detected scattered light will display a frequency shift proportional to the velocity of the particle and the amount of frequency shift can be detected using the homodyne coherent detection technique. However, the above technique cannot be applied to multiple scatterings by a large number of moving particles. In such situations, the frequency spectrum of the light wave is broadened, making the interpretation of signal difficult. Because of this limit, the current technique of optical Doppler shift has been limited to measuring the blood flow in microflow channels near the skin although the blood supply by major arteries produces more valuable information for health and disease conditions. In addition, the laser Doppler flowmetry can only measure relative speed. [Rajan et al., 2009].

To measure the blood flow speed in major arteries, we extend the technique of optical scattering method by taking into account the effect of multiple scattering by red blood cells. Instead of measuring the Doppler shift in the optical frequency, we measure the decorrelation time of the reflected light. The key results of our work are (a) we have shown experimentally and theoretically that one can measure the arterial blood flow velocity using a simple optical setup comprised of a single semiconductor laser and a single detector, both coupled to a multi-mode fiber bundle, and (b) we discovered that for main arteries where the diffused light model applies, the decorrelation time is inversely proportional to the RBC speed and we can measure its value without any prior knowledge about the anatomy and tissue mechanic properties of the artery.

Once entering the tissue, light has a very short scattering mean free path and the light becomes diffusive. Modelling of light propagation in this regime has led to the development of oximeter back in 70s [Ishimaru, 1978] and many researchers have utilized the diffused light to construct images through highly diffusive biological media, such as reconstructed breast cancer images [Wang and Wu, 2012]. The standard configuration for diffused light correlation spectroscopy includes a point source and a point detector, and the measured correlation function depends on the relative position between the source and the detector[Durduran et al., 2010, Vishwanath and Zanfardino, 2019, Zanfardino and Vishwanath, 2018]. The method of diffused light correlation spectroscopy has been used in blood perfusion measurement [Boas et al., 2016], including brain circulations [Durduran and Yodh, 2014, Torricelli et al., 2014]. The setup uses a single-mode fiber coupled detector to allow single-mode transmission of two orthogonal light polarizations [Rička, 1993]. The single spatial mode yields the best signal-to-noise ratio since it detects one speckle. However, this setup produces very low light intensity and requires a single photon detector (e.g. a single-photon avalanche detector (SPAD) or a photomultiplier tube (PMT)), making the setup quite sophisticated and subject to interference and stray light.

To make the system robust and easy to operate, in this paper we use multimode fiber and a regular photodetector to detect temporal fluctuations of the light intensity. In the following we first present our experimental setup and measurement results, and then describe the physical model to show how the measured results can be used to find the red blood cell velocity. We will show that in a simple and robust setup that is relatively insensitive to the optical alignment between the fiber bundle and the tissue, where we can reliably measure the absolute value of the traveling speed of red blood cells in a blood vessel that has a millimeter diameter embedded in a layer of tissue. The results offer a promising solution for non-invasive measurement of the blood supply into organs and limbs.

Chapter 1 is based on a reprint of Zhang, A.C., Lo, Y.H., 2020. Non-invasive optical Measurement of arterial blood flow speed. *Biomedical Optics Express (under peer review)*. The dissertation author was the primary author of this material.

Chapter 2

Experimental Setup

The experimental setup and measured results are first presented here, followed by the theoretical analysis in the later sections.

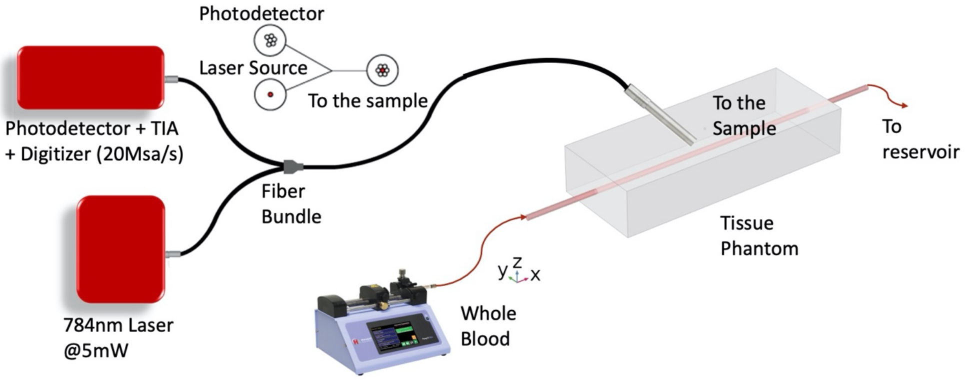

Figure 2.1: Experimental Setup. The laser light illuminates the tissue phantom surface at a 45-degree angle and the scattered diffused light is collected through the reflection probe fiber bundle which is coupled to a photoreceiver. The glass tube that emulates a blood vessel is embedded in the tissue phantom 5mm below the surface.

2.1 Tissue Phantom Fabrication

Wwe used intralipid as the scattering agent to reproduce keymimic the tissue by making its optical properties of tissue to make the scattering coefficient μ_s and anisotropy factor g similar to the the values of real tissue. Because of its similar optical properties to the bilipid membrane of cells, intralipid is commonly used to simulate tissue scattering [Lai et al., 2014, Pogue and Patterson, 2006, Flock et al., 1992]. In addition, the absorption coefficient of intralipid is low and its refractive index is close to that of soft tissue[Ding et al., 2005]. The tissue phantom is created using intralipid (Sigma-Aldrich 20%) in gelatin gel. One percent concentration of intralipid was chosen to achieve a scattering coefficient of around $10cm^{-1}$ at 784 nm. The phantom was initially prepared at $90°C$, and then poured into a mold where a glass tube was pre-inserted at a depth of 5mm from the phantom surface (measured from the center of the tube).The liquid phantom was immediately placed into a freezer at -18 $°C$ for 30 minutes for rapid solidification to prevent sedimentation of intralipid to achieve a uniform scattering property. Then the sample was placed in a refrigerator at 6 $°C$ for 30 minutes to further solidify. The subsequent experiment was usually completed within 30 minutes after the phantom fabrication to prevent evaporation induced dehydration of the phantom, which could reduce the surface height. Glass tubes of three different inner diameters were used to mimic the arteries. Tygon tubing was connected to both ends of the glass tube, with one end connected to a $10mL$ syringe mounted on a syringe pump and the other end connected to a reservoir (See figure 2.1).

2.2 Blood Preparation

12 mL of human whole blood collected on the same day of the experiment was purchased from the San Diego Blood Bank. EDTA was added to the blood sample to prevent coagulation.

2.3 Optical and electronics setup

We used an off-the-shelf multi-core reflection fiber bundle probe (Model:RP21 from Thorlabs) that consists of one center core surrounded by 6 peripheral cores to couple the input and reflected light. The center core was used to deliver the laser light to the blood vessel and the 6 peripheral cores that are merged into a single output are coupled to the photodetector (see figure 2.1). The fiber bundle was mounted about 45 degrees relative to the surface of the tissue phantom to prevent specular refection from the tissue surface. The fiber bundle was coarsely aligned to the position of the glass tube in the tissue phantom. The laser used in the experiment was an off-the-shelf fiber coupled laser diode at 785nm, biased slightly above its threshold current to produce an output of 5 mW. The output of the detection fiber was coupled to a silicon APD with an integrated transimpedance amplifier (Thorlabs APD410A) to achieve a transimpedance gain of 500 kV/A at 10MHz bandwidth. The APD multiplication gain was set to be the lowest ($M \sim 10$). The output signal from the APD photoreceiver entered a data acquisition board (Advantech PCI-E 1840) at a sampling rate of 20 Msps, yielding a Nyquist bandwidth of 10 MHz. The total data acquisition time for the measurement was 25 seconds. We treated each 5ms duration as one recording section, so 25 seconds of measurement produced 5,000 sections for analysis and noise cancellation. In all the data presented next, we used the average data over 25 seconds for the mean and over 1 second to determine the variations shown in error bars.

We tested blood flows with three tube inner diameters: 0.93mm, 1.14mm, and 1.68mm. The tube diameters were measured by a digital microscope to assure high accuracy. For each tube diameter, we flow the blood at different speeds.

2.4 Experimental Results

We have used the setup in figure 2.1 to measure the photocurrent correlation defined as $\frac{\langle i(t)i(t+\tau)\rangle}{\langle i(t)\rangle^2}$ where i(t) is the photocurrent at time “t” and $\langle\rangle$ is the ensemble average. For a 25 second measurement that can be divided into 5,000 5ms sections, the ensemble average is the average of these 5,000 sections. τ is the time delay between the instantaneous photocurrents, and is the variable for the correlation function.

One important relation is to convert the photocurrent correlation into the normalized electrical field correlation function g_1 represented by equation (2.1):

$$g_1(\tau) = \frac{\langle E(t)E^*(t+\tau)\rangle}{\langle E(t)E^*(t)\rangle} \tag{2.1}$$

Using the Siegert Relation[Cummins and Swinney, 1970], we can obtain a relation between the magnitude of $g_1(\tau)$ and the photocurrent correlation as shown in equation (2.2):

$$\frac{\langle i(t)i(t+\tau)\rangle}{\langle i(t)\rangle^2} = 1 + \frac{1}{N}|g_1(\tau)|^2 + \frac{e\delta(t)}{\langle i(t)\rangle} \tag{2.2}$$

where $i(t)$ is the measured photocurrent, N is the number of spatial modes coupled into the detection fiber bundle and collected by the detector, $\delta(t)$ is a delta function, and e is the electron charge. The last term in equation (2.2) represents the shot noise.

The magnitude of electrical field correlation g_1 under different flow speeds of blood is shown in semi-log plots in Figure 2.2 to 2.4, (a), where each figure shows measurements performed with a different tube diameter. The x-axis of each plot is the logarithmic of τ in the correlation function. From these plots we made two interesting observations: (a) At relatively low blood flow speed, the curve shows a characteristic analogous to the "Fermi-Dirac distribution function" if we treat "$\ln(\tau)$ as "energy"; (b) at high blood speed, the curve behaves like a superposition of two Fermi-Dirac distribution functions, one at lower "energy" and another at higher "energy". These characteristics become more apparent if we take the derivative of g_1 with $\ln(\tau)$, showing that the "Fermi level", $\ln(T_F)$, occurs at the inflection point where the magnitude of slope reaches the maximum.

We will discuss the physics of such characteristics in the later section. By examining the interesting features of the measured electrical field correlation g_1, we can extract the “Fermi energy, ε_F” or $\ln(T_F)$. In the low blood speed regime where the$|g_1|$ plot shows two superimposed Fermi-like functions, we chose the inflection point of the lower energy function (i.e. in the regime of smaller $\ln(\tau)$ values). We will elucidate the reasons for such a choice in the next section. Essentially each of the two superimposed Fermi-like functions represents a corresponding regime of light scattering mechanisms. Figure 2.2 to 2.4 (b) show the plot of $1/T_F$ (which is equivalent to $e^{-\varepsilon_F}$) versus the blood flow velocity with different tube diameters. Amazingly, we obtain a simple linear relation between $1/T_F$ and the blood speed. More interestingly, we have found that the $1/T_F$ versus speed curve is independent of the tube diameter. As shown in figure 2.5, the three curves of $1/T_F$versus speed measured from different tube diameters completely overlap and can be represented by one simple relation independent of the tube diameter. This result suggests that our measurement setup can potentially measure the blood speed in different artery sizes without having to know the exact dimension of the blood vessel diameter. This discovery is very important in practical applications because it shows that from the $g_1(\tau)$ curve, which can be obtained from the correlation of the photocurrent, we can obtain the speed of the blood directly for different arteries at a given position without any prior knowledge of the anatomy of the blood vessel. The discovery of this important relation requires a sound physical foundation, to rule out the possibility for being simply coincidental. The physical model and mathematical analysis will be discussed next.

Chapter 2 is based on a reprint of Zhang, A.C., Lo, Y.H., 2020. Non-invasive optical Measurement of arterial blood flow speed. *Biomedical Optics Express (under peer review)*.The dissertation author was the primary author of this material.

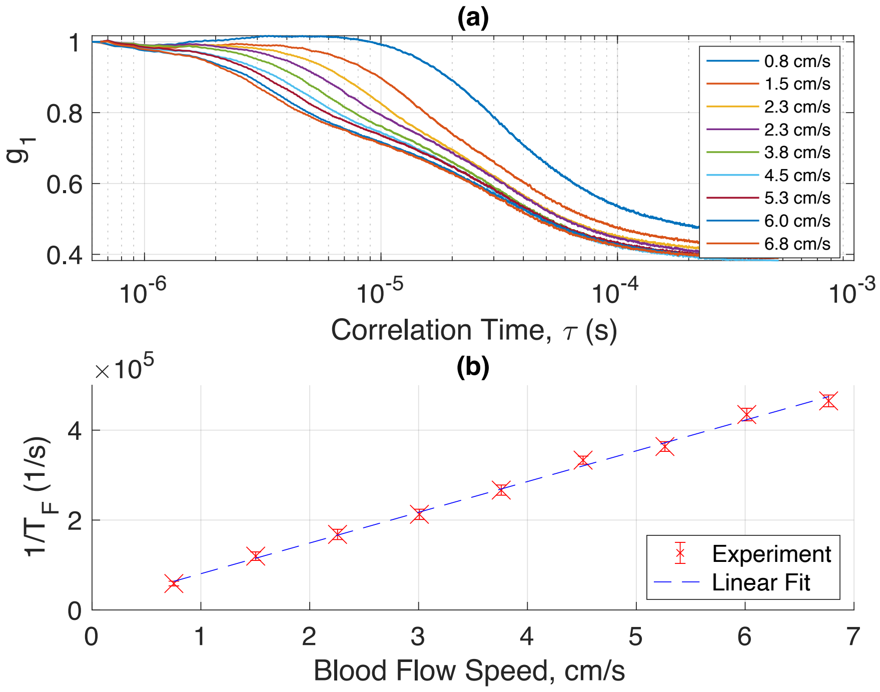

Figure 2.2: (a) Measured E-field correlation function (g_1) versus flow speed of whole blood for a tube diameter of 1.68mm. (b) By taking the inverse of the correlation time at the first inflection point in (a), the decorrelation rate ($1/T_F$) is plotted versus the flow speed. The scattered data set with error bars represents the 95% confidence interval over 25 measurements, each for a duration of 1 second. The dashed line is a linear fit of the measured data.

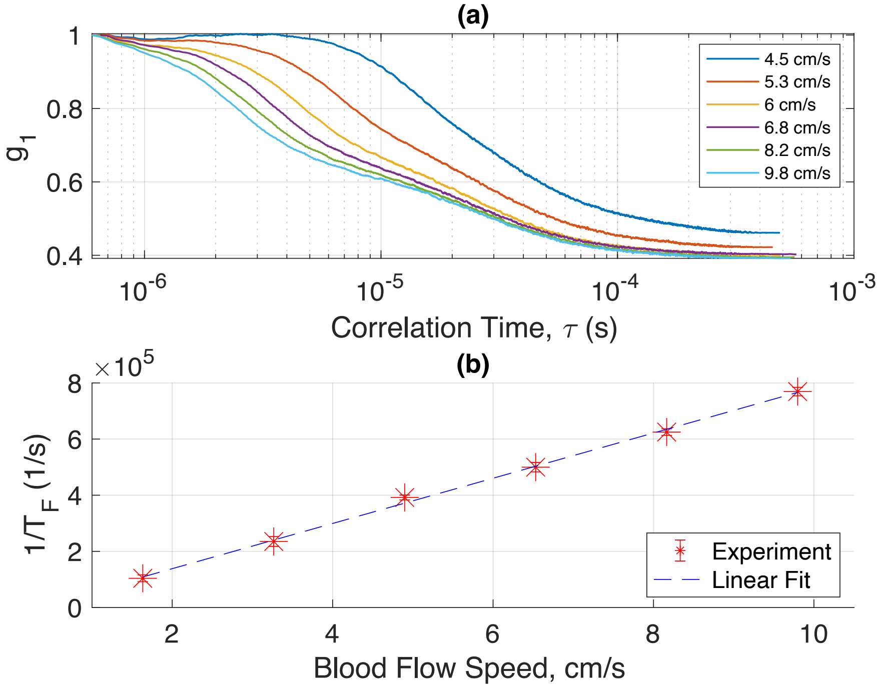

Figure 2.3: (a) Measured E-field correlation function (g_1) versus flow speed of whole blood for a tube diameter of 1.14mm. (b) By taking the inverse of the correlation time at the first inflection point in (a), the decorrelation rate ($1/T_F$) is plotted versus the flow speed. The scattered data set with error bars represents the 95% confidence interval over 25 measurements, each for a duration of 1 second. The dashed line is a linear fit of the measured data.

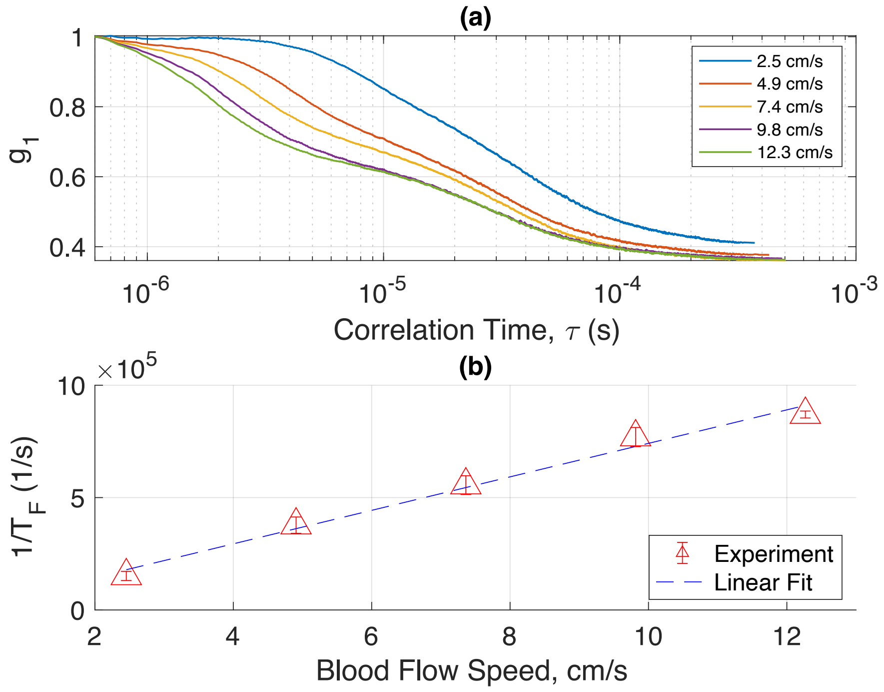

Figure 2.4: (a) Measured E-field correlation function (g_1) versus flow speed of whole blood for a tube diameter of 0.93mm. (b) By taking the inverse of the correlation time at the first inflection point in (a), the decorrelation rate ($1/T_F$) is plotted versus the flow speed. The scattered data set with error bars represents the 95% confidence interval over 25 measurements, each for a duration of 1 second. The dashed line is a linear fit of the measured data.

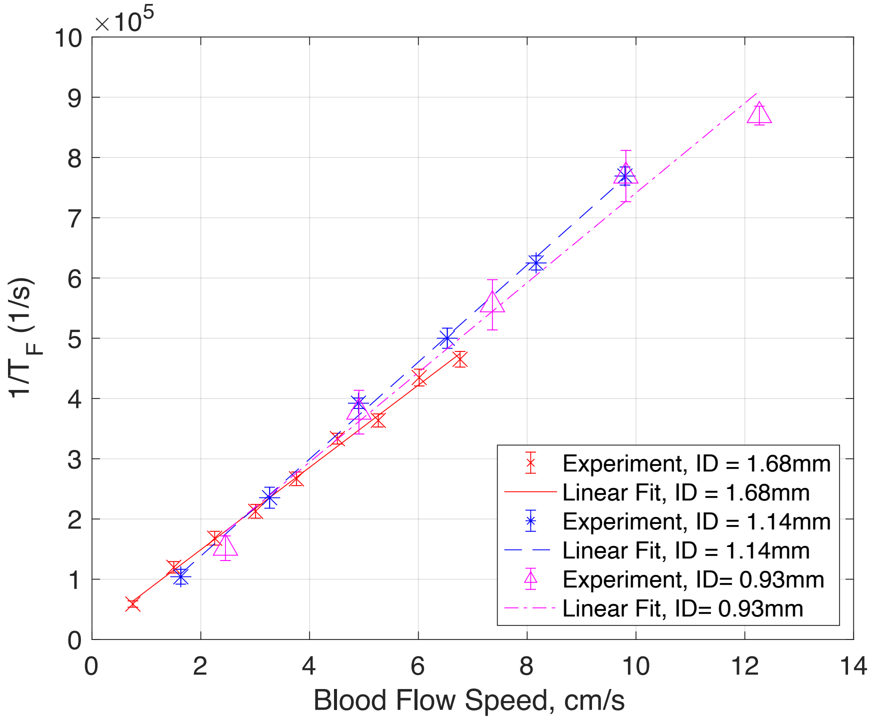

Figure 2.5: Combined decorrelation rate $(1/T_F)$ versus blood flow speed plot for different tube ID. The scattered data set with the error bar represents the 95% confidence interval over 25 measurements, each for a duration of 1 second. The line plots are linear fits of the measured data. The fact that plots for different tube ID collapse into one single line demonstrates the existence of a simple relation between the decorrelation rate and the blood speed and the relation is independent of the tube diameter.

Chapter 3

Outline of Physical Models

3.1 Diffused Light Equation for Moving Scatters:

In order to understand the underlining physics of the relation between the inverse of characteristic decorrelation time, $1/T_F$, and the flow speed of the blood, we describe the physical model and mathematical formulation for our experiment in this section. We will outline the key steps and, through approximations, produce an analytical relation between the blood speed and the decorrelation time. The detailed numerical results for more general analyses without approximations will be presented in a separate paper.

People usually take two approaches to model light propagation in a strongly scattered biological medium. In one approach, we start with the wave equation and introduce the scattering and absorption characteristics along the optical path. Despite its rigor in the mathematical formulation, to make the result useful, approximations have to be made to make the problem solvable. Twersky's theory and Dyson's equation fall into this category [Ishimaru, 1978]. In another approach, we can formulate the problem in a transport equation that deals with photon energy transport. These two methods eventually give rise to the same result. In this paper we take the second approach because of its relative simplicity.

The governing equation is a radiative transfer equation (RTE) in the following form:

$$\frac{dI(\vec{r},\hat{s})}{ds} = -\rho\ \sigma_t I(\vec{r},\hat{s}) + \rho\sigma_s \int_{4\pi} p(\hat{s},\hat{s}')I(\vec{r},\hat{s}')\ d\Omega' + S(\vec{r},\hat{s}) \tag{3.1}$$

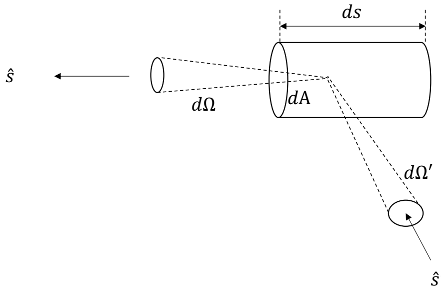

Figure 3.1: Illustration of the elementary scattering volume for equation (3.1), *ds* represents the differential length, *dA* is the differential area, $d\Omega$ is the differential solid angle.

in which I is the light specific intensity with a unit $Wm^{-2}sr^{-1}$,ρ is the particle concentration, σ_s is the scattering cross section, σ_t is the total scattering cross section which is the summation of scattering cross section and absorption cross section. $p(\hat{s},\hat{s}')$ is the normalized differential scattering cross section which is sometimes called the phase function and it's unitless, and $S(\vec{r},\hat{s})$ is the source intensity which has a unit of $Wm^{-3}sr^{-1}$. Figure 3.1 illustrates the orientations and coordinates for an infinitesimal scattering volume. Equation (3.1) contains 5 coordinates: x,y,z,θ,ϕ where x,y,z define the position vector $\vec{r}$ of the light intensity, and θ,ϕ represent the beam's propagation direction. The unit vectors $\hat{s}$' and $\hat{s}$ represent the direction of the incident light and the propagation direction after scattering.

Solving equation (3.1) would produce the full solution for the light scattering problem for any scatter concentration. However, equation (3.1) is very complicated to solve. Fortunately, in most biological samples, the scatter density is so high that photons quickly lose the memory of their path histories after multiple scatterings and it can be justified to assume the light intensity depends on its position (x,y,z) with a slight flux flow in the direction of propagation (θ,ϕ). This would lead to a simplification of the problem, and the average intensity could be described by the diffusion equation which is only dependent on the position (x,y,z). Mathematically, it means that we can expand the light intensity in spherical harmonics by keeping the zero order and first order term.

$$I(\vec{r},\hat{s}) \simeq \frac{1}{4\pi}U(\vec{r}) + \frac{3}{4\pi}\vec{F}(\vec{r})\cdot\hat{s} \tag{3.2}$$

where the first term is the average intensity and the second term is the small photon flux in the direction of propagation. Applying the diffusion approximation to the RTE, we can obtain a steady state diffusion equation (3.3) to model light propagation in a diffusive medium when the scatters are not moving. As light needs to be scattered multiple times to become diffusive, an important requirement for the diffusion approximation is that the cross section for light scattering is much stronger than the cross section for light absorption. A problem would arise when dealing with light intensity close to the boundary since the light is highly directional at the boundary, violating the diffusive condition. Different boundary conditions have been explored to resolve this problem, including adoption of an extended boundary condition which uses Taylor expansion to convert the Robin boundary condition into a Dirichlet type boundary condition to simplify the solution for equation (3.3) [Haskell et al., 1994].

$$[D\nabla^2 - \mu_a]U(\vec{r}) = -S(\vec{r}) \tag{3.3}$$

where $D = 1/3\mu_s'$ is the photon diffusivity with a unit of meter and μ_s' is the reduced scattering coefficient. μ_a is the absorption coefficient with a unit m^{-1}. $S(\vec{r})$ is the source (unit of Wm^{-3}) that depends only on the location but not on the propagation direction, different from $S(\vec{r},\hat{s})$ in equation (3.1).When the scatters exhibit motions, the scattered intensity would include time as a parameter. For statistical optics, it is natural to use field correlation function to capture this dynamic process. Here, we are still talking about the steady state response of the system so that the time dependence can be represented as a parameter in the differential equation.

We start with the case of single scattering event by a moving object. The normalized single scattering function can be written as:

$$g_1^s(\tau) = \frac{\langle E(t)E^*(t+\tau)\rangle}{\langle E(t)E^*(t)\rangle} = \exp\left(-\frac{1}{6}q^2\langle\Delta r_i^2(\tau)\rangle\right) \tag{3.4}$$

where g_1^s is the single scattering normalized correlation function, E is the scalar electrical field of light, q is the photon momentum transfer by each scattering, $\langle\Delta r_i^2(\tau)\rangle$ is the RMS displacement of the scatters in a duration of τ. The above equation describes the electrical field correlation function due to single scattering. This single scattering function can be incorporated into the radiative transfer equation, yielding the so-called correlation transfer equation which is the dynamic counter part of the static radiative transfer equation [Boas and Yodh, 1997]:

$$\frac{dG_1(\vec{r},\hat{s},\tau)}{ds} = -\rho\sigma_t G_1(\vec{r},\hat{s},\tau) \ + \ \rho\sigma_s\int_{4\pi} p(\hat{s},\hat{s}') \ \ g_1^s(\hat{s},\hat{s}',\tau)G_1(\vec{r},\hat{s},\tau)\, d\Omega' + S(\vec{r},\hat{s}) \tag{3.5}$$

Similarly, the diffusion approximation can also be applied to obtain the correlation diffusion equation which is again the counterpart of the static diffusion equation described previously. Equation (3.5) is the correlation diffusion equation. The diffusion equation can then be solved with appropriate boundary conditions to be compared with experimental results.

$$[D\nabla^2 - \mu_a - \frac{1}{3}\mu_s' k_0^2\langle\Delta r^2(\tau)\rangle]G_1(\vec{r},\tau) = -S(\vec{r}) \tag{3.6}$$

where n is the refactive index of scattering media, k_0 is the wavevector in vacuum, μ_s' is the reduced scattering coefficient which is the scattering coefficient modified due to scattering anisotropy. For isotropic scattering, the scattering coefficient would be the same reduced scattering coefficient.

3.2 Analytic Relation Between Decorrelation Time and RBC Flow Speed

We assume a plane wave illumination at the surface. Despite the simplification, the approximation can yield a satisfactory result in good agreement with the experiment. To simplify the practical application, we adopted an experimental design where a single detector covers an area defined by the numerical aperture of 6 hexagonally arranged multimode fiber surrounding the light source (see figure 2.1). Assuming the blood vessel is cylindrically symmetric, we used a 2D model as shown in figure 3.2. We can reduce equation (3.6) into the following diffusion equation,

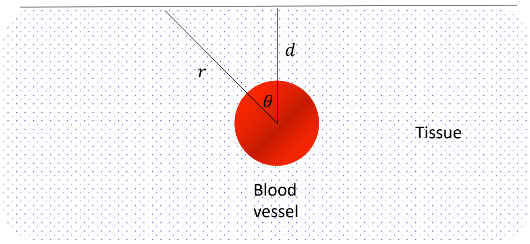

Figure 3.2: Geometry used for theoretical calculation. The circle represents the cross section of blood vessel with parameters: D_{in}, W_1, k_1, μ_a^{in}, $\mu_s'^{in}$; The area outside the circle represents the static scattering media, i.e. tissue with parameters: D_{out}, W_0, k_0, μ_a^{out}, $\mu_s'^{out}$. We adopt cylindrical coordinates and define the center of the vessel as the origin.

$$[\nabla^2 + k^2]G_1(\vec{r},\tau) = -\frac{S(\vec{r})}{D} \tag{3.7}$$

in which

$$k = jW(\tau) \tag{3.8}$$

Since the scattering parameters are different inside and outside the blood vessel, two sets of parameters are used. The parameters inside the blood vessel are represented using subscript 1, i.e. $k_1 = jW_1(\tau)$. The parameters outside the blood vessel are represented using subscript 0, i.e. $k_0 = jW_0(\tau)$.

$$W_1 = \sqrt{\frac{1}{D_{in}}[\mu_a^{in} + \frac{1}{3}\mu_s k_\lambda^2 \langle \Delta r^2(\tau) \rangle]} \tag{3.9}$$

$$W_0 = \sqrt{\frac{\mu_a^{out}}{D_{out}}} \tag{3.10}$$

To solve equation (3.7), we need to first find the mean squared displacement $\langle \Delta r^2(\tau) \rangle$. The mean square displacement for RBCs includes Brownian, shear induced diffusion and convective motion. We can represent the position variation of RBCs over a given time interval as[Belau et al., 2017]:

$$\langle \Delta r^2(\tau) \rangle = 6D_\alpha \tau + \bar{V}^2 \tau^2 \tag{3.11}$$

where the first term in equation (3.11) is caused by Brownian and shear induced diffusions and the second term by convection. For RBCs, the diffusion by Brownian motions is much smaller than the shear induced diffusion [Wu et al., 1990]. The flow of RBCs inside arteries can be modeled by a laminar flow and the diffusion coefficient can be represented as [Owen and Roberts, 2007]

$$D_\alpha = \alpha_s \left| \frac{\partial v_{RBC}}{\partial r} \right| = \frac{4}{3} \alpha_s \frac{V_{max}}{a} \tag{3.12}$$

α_s is a parameter describing the interaction strength among blood cells due to shear and its value has been measured experimentally [Goldsmith and Marlow, 1979, Funck et al., 2018, Nanne et al., 2010, Higgins et al., 2009, Biasetti et al., 2014, Tang et al., 2018]. The radial dependent shear rate is usually replaced by its average value due to the fact that multiple scattering will lead to an ensemble averaging across all radial locations . For tissue blood perfusion, the slow flow speed and small blood vessel diameter make the diffusive motion the dominant effect compared to the convective motion [Sakadžić et al., 2017]. The situation is reversed, however, for main arteries and our phantom model where the vessel inner diameter is of millimeter size and the blood flow speed is several centimeters per second[Gabe et al., 1969]. In such cases, the convective motion becomes the dominant effect. Hence in our analysis, we have ignored the diffusion contribution and included only the convective flow contribution in equation (3.11).

We can then write the general solution of the correlation function in equation (3.7) as follows,

$$G_1(\vec{r},\tau) = G_1^{in}(\vec{r},\tau) + G_1^{sc}(\vec{r},\tau) \tag{3.13}$$

The first term is the inhomogeneous solution and the second term is the homogeneous solution for equation (3.7) in the absence of the source. The diffusion equation under a given boundary condition can be solved in polar coordinates and the method of separation of variables. For an approximate analytic solution, we kept only the zeroth order term since all higher order terms are insignificant compared with the zeroth order term. A continuity boundary condition is applied at the cylinder interface between the blood vessel and the surrounding tissue. The air-tissue surface is ignored for simplicity in the solution. After solving the differential equation with some approximations based on the numerical value of actual tissue and blood cell scattering properties, the normalized correlation function g_1 can be written in the form of equation (3.14), inspired from the Fermi-Dirac function in semiconductor physics (i.e. by performing the transformations: $\ln(\tau) = \varepsilon, \ln(T_F) = E_F$,equation (3.14) is similar to the Fermi-Dirac function).

$$g_1(r,a,\theta,\tau) = \frac{1 - g_1(r,a,\theta,\infty)}{1 + \frac{\tau}{T_F}} + g_1(r,a,\theta,\infty) \tag{3.14}$$

$$\frac{1}{T_F} \approx Vnk_0\sqrt{\frac{\mu_s'^{in}}{3\mu_a^{in}}} \tag{3.15}$$

where V is the flow velocity of blood, n is the refractive index of blood, k_0 is the wavevector of 784 *nm* light in vacuum, $\mu_s'^{in}$ is the reduced scattering coefficient of blood (m^{-1}), and μ_a^{in} is the absorption coefficient of blood (m^{-1}). If we define T_F as the characteristic decorrelation time, and $1/T_F$ as the characteristic decorrelation rate, we obtain the key relation that the characteristic decorrelation rate is only a function of flow speed and blood optical parameters, as shown in equation (3.15). In equation (3.14), $g_1(r,a,\theta,\infty)$ is the asymptotic value of g_1 when τ approaches infinity, and its value is a function of detector position and blood vessel diameter. In the later chapters, I would show detailed derivation and solve equation (3.7) numerically, we have validated the approximations that led to the analytic solution for g_1 in equation (3.14) and most importantly, the linear relation between $1/T_F$ and the blood flow velocity. We have also shown that the decorrelation time for 2D and 3D analyses is nearly the same. The detailed mathematical derivations as well as the numerical computations for the diffused light model will be described in a separate publication.

From the approximated relation in equation (3.15), we find that the characteristic decorrelation rate is proportional to the flow speed. The proportional constant has a square root dependence on the ratio between the scattering coefficient and the absorption coefficient. This is intuitive since scattering events cause dephasing, and light absorption would terminate the scattering process.

Chapter 3 is based on a reprint of Zhang, A.C., Lo, Y.H., 2020. Non-invasive optical Measurement of arterial blood flow speed. *Biomedical Optics Express (under peer review).*The dissertation author was the primary author of this material.

Chapter 4

Photon Transport in Static Random Scattering Media

In following chapters, I will go through the details physics mentioned in the previous chapter. In this chapter, the discussion will be focused on the light transport in a static random media. In order to describe and quantify the behaviour of photon propagation in random media, people usually take two approaches to model light propagation in a strongly scattered biological medium. In one approach, we start with the wave equation and introduce the scattering and absorption characteristics along the optical path. Despite its rigor in the mathematical formulation, to make the result useful, approximations have to be made to make the problem solvable. Twersky's theory and Dyson's equation fall into this category [Ishimaru, 1978]. In another approach, we can formulate the problem in a transport equation that deals with photon energy transport. These two methods eventually give rise to the same result. In this thesis, the second approach is taken because of its relative simplicity.

4.1 Derivation of Radiative transfer equation (RTE)

The following is based on a phenomenological approach that is based the transport of energy through media that contains particles [Ishimaru, 1978][Wang and Wu, 2012].This equation is the fundamental equation that captures all the physical phenomena when the photon propagates through a random media exhibiting the classical behavior of absorption and scattering. Typically, a full transport equation would not have a analytical solution that provides physical insight except at some cases where the transport equation can be simplified. One of the cases is when there are few scatterers in the media, and if the scatters are also mainly absorbing, this would lead to the famous Beer-Lambert law. However, this approximation would break down when the media is scattering dominate and when the scattering particles have a high density. But luckly, at this end of the extremety, the transport equation can be simplified using the diffusion approximation. In most biological tissues, the photon transport can be characterized by the diffusion equation. In order to provide a clear physical understanding of the problem, this chapter will outline the basic idea behind the radiative transport equation and subsequently the diffusion approximation.

4.1.1 Definition of Physical Quantity

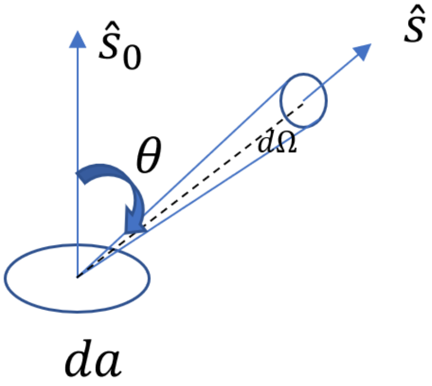

Figure 4.1: Directional vector, da represents the differential area, $\hat{s}_0$ is the normal vector

Specific Intensity $I(\vec{r},\hat{s})$, Unit: $Wm^{-2}sr^{-1}$

Specific Intensity comes with the unit of Watt per area per unit solid angle, also known as radiance or brightness[Wang and Wu, 2012].

The amount of power flowing through the differential area da, within a solid angle of $d\Omega$ at the direction of unit vector $\hat{s}_0$ as in fig 4.1 is:

$$dP = I(\vec{r},\hat{s})\hat{s}' \cdot \hat{s}\; da\; d\Omega \tag{4.1}$$

in which, $\hat{s}' \cdot \hat{s}$ is the dot product of the two unit vectors, which is, $\hat{s}' \cdot \hat{s} = \cos\theta$ as indicated in fig 4.1:

Average Intensity: $U(\vec{r})$**, unit:**W/m^2

The average intensity is obtained by integrating the specific intensity over the entire 4π solid angle.

$$U(\vec{r}) = \int_{4\pi} I(\vec{r},\hat{s})\; d\Omega \tag{4.2}$$

Energy flux: $\vec{F}(\vec{r})$**, unit:** W/m^2

$$\vec{F}(\vec{r}) = \int_{4\pi} I(\vec{r},\hat{s})\hat{s} d\Omega \tag{4.3}$$

This could be considered as the vector counterpart of average intensity.

Scattering Cross Section of a single particle: σ_s, unit, m^2

Consider a incident wave as a linearly polarized plane wave with electric field characterized as follows[Ishimaru, 1978]:

$$\vec{E}_{s'}(\vec{r}) = \vec{e}_{s'}\ \exp(i\vec{k}\cdot\vec{r}) \tag{4.4}$$

$\vec{e}_i$ is the unit vector in the direction of polarization of the incident plane wave, $\vec{s'}$ is the direction of propagation of the incident plane wave. Note the amplitude of the incident wave is normalized to one(V/m). The far field scattered electric field by a single particle is given by the following:

$$\vec{E}_s(\vec{r}) = \vec{f}(\hat{s},\hat{s}')\frac{e^{ikR}}{R} \tag{4.5}$$

Under the far-field (Fraunhofer) approximation, the scattered field is approximated by a spherical wave, provided $R >> D^2/\lambda$.

$\vec{f}(\hat{s},\hat{s}')$ is the amplitude, phase and polarization of the scattered wave in the far field in the direction of $\hat{s}$ when the particle is illuminated by a plane wave propagating in the direction $\hat{s'}$ with unit amplitude and is the called the scattering amplitude.

Before we define the scattering cross section, let's write the time averaged Poyting vector of the incident wave and scattered wave respectively:

$$\vec{S}_{s'} = \frac{1}{2}\vec{E}_{s'}\times\vec{H}^*_{s'} = \frac{|\vec{E}_{s'}|^2}{2\eta_0}\hat{s'} \tag{4.6}$$

$$\vec{S}_s = \frac{1}{2}\vec{E}_s\times\vec{H}^*_s = \frac{|\vec{E}_s|^2}{2\eta_0}\hat{s} \tag{4.7}$$

Poyting vector is the energy flux and has the unit of W/m^2

Now, let's define the differential scattering cross section:

$$|\vec{S}_s|\ dA = |\vec{S}_{s'}|\ d\sigma \tag{4.8}$$

in which, $|S_{s'}|$ and $|S_s|$ are just the magnitude of Poyting Vector of incident and scattered wave. dA is the differential surface area of a sphere, $dA = R^2\ d\Omega$.

Physically, for the above equation, it means that the amount of power that is scattered into a surface area of dA is caused by the incident flux scatter with a cross section of area $d\sigma$.

$$d\sigma = \frac{|\vec{S}_s|\ dA}{|\vec{S}_{s'}|} = \frac{|\vec{S}_s| R^2\ d\Omega}{|\vec{S}_{s'}|} \tag{4.9}$$

Combing equation (4.6) to (4.9), it's very easy to see:

$$d\sigma = |\vec{f}(\hat{s}, \hat{s}')|^2\ d\Omega \tag{4.10}$$

Or:

$$\frac{d\sigma}{d\Omega} = |\vec{f}(\hat{s}, \hat{s}')|^2 \tag{4.11}$$

And, $d\sigma$ is called the differential cross section since it has a unit of m^2.

So here is the physical meaning: $d\sigma$ is the area that captures the amount of incoming flux that would be scattered into a solid angle of $d\Omega$. Since $d\Omega$ is unitless, sometimes people also call $\frac{d\sigma}{d\Omega}$ the differential cross section or can be interpreted as differential cross section per unit solid angle.

If we integrate the differential scattering cross section over 4π solid angle:

$$\int_{4\pi} \frac{d\sigma}{d\Omega} d\Omega = \int_{4\pi} |\vec{f}(\hat{s},\hat{s}')|^2 \, d\Omega' = \sigma_s \tag{4.12}$$

σ_s is the total scattering cross section.

Usually, for convenience, since the scattering is angle dependent, we could define a "normalized" differential scattering cross section, $p(\hat{s},\hat{s}')$ or sometimes called 'phase function', of which has its origin in astronomy represents lunar phase and has nothing to do with the phase of an EM wave.

$$1 = \int_{4\pi} p(\hat{s},\hat{s}') \, d\Omega' \tag{4.13}$$

Or in other words:

$$\sigma_s = \sigma_s \int_{4\pi} p(\hat{s},\hat{s}') \, d\Omega' = \int_{4\pi} |\vec{f}(\hat{s},\hat{s}')|^2 \, d\Omega' \tag{4.14}$$

Scattering Anisotropy, unitless

$$g = \int_{4\pi} \hat{s}\cdot\hat{s}' \; p(\hat{s},\hat{s}') \, d\Omega' \tag{4.15}$$

Here is how it can be understood, it's the mean cosine of the scattering angle. In other words, it is the difference between forward scattering($\hat{s}\cdot\hat{s}' > 0$) and backward scattering($\hat{s}\cdot\hat{s}' < 0$). If $g = 0$, it would mean the the forward scattering equals to the backward scattering and the scattering is isotropic since in that case, $p(\hat{s},\hat{s}')$ will be constant[Ishimaru, 1978].

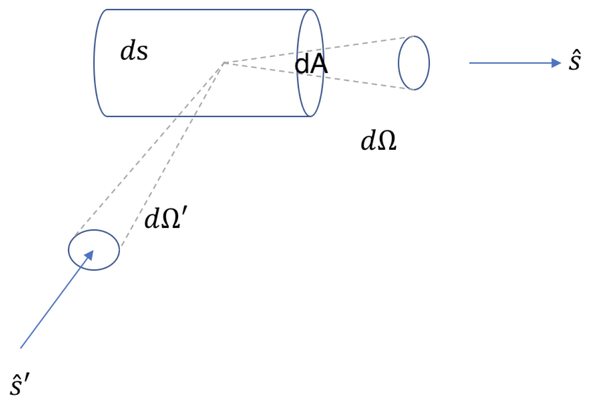

Figure 4.2: Cylindrical differential volume with a cross section area of dA with a normal direction of $\hat{s}$ and length of ds in the direction of $\hat{s}$ [Ishimaru, 1978]

Total cross section of a single particle: σ_t

Now, similarly we include the effect of absorption, define the absorption cross section as σ_a, so the total cross section of both scattering and absorption σ_a is defined as:

$$\sigma_t = \sigma_a + \sigma_s \tag{4.16}$$

If part of the energy is absorbed by the particle, we know it won't contribute to the scattering profile.

4.1.2 Equation of Transfer

Consider a specific intensity that is incident on a cylindrical differential volume with a cross section area of dA with a normal direction of $\hat{s}$ and length of ds in the direction of $\hat{s}$ as shown in the figure below fig. 4.2.

Let's consider the change of power (unit:W) inside the elementary volume(left), it would be equal to the total loss of power of every single particle either due to absorption or scattering(exited the volume):

$$dP_1 = -\rho \, ds \, dA \, d\Omega(\sigma_a + \sigma_s) \, I = -\rho \, ds \, dA \, d\Omega \, \sigma_t \, I \tag{4.17}$$

The particle concentration inside the volume is ρ has a unit of number per unit volume. Equation (4.17) physically means: the specific intensity at direction $\hat{s}$ is reduced due to absorption and scattering of the particles in the volume.

Now, let's consider the contribution of incident specific intensity from other directions outside the differential volume element. Assuming there is another incident intensity from direction $\hat{s}'$ scattered by a particle in the volume, we need to know the scattered intensity to the direction $\hat{s}$ as in fig 4.2. Still, consider the power differential, and recall equation (4.9) and (4.10), the magnitude of Poynting vector(W/m^2) and definition of scattering amplitude, rewrite them as follows:

$$|\vec{S}_s|R^2 = |\vec{S}_{s'}||\vec{f}(\hat{s},\hat{s}')|^2 = I(\vec{r},\hat{s}')|\vec{f}(\hat{s},\hat{s}')|^2 d\Omega' \tag{4.18}$$

The above equation is the power scattered to direction $\hat{s}$ due to one single particle from a incident angle of $d\Omega'$, if we account for all particles in the elementary volume and account for 4π incident solid angle $d\Omega'$ that scatters into a solid angle of $d\Omega$ (Please notice the distinction)

$$dP_2 = \rho \, dA \, ds \, d\Omega \int_{4\pi} |\vec{f}(\hat{s},\hat{s}')|^2 I(\vec{r},\hat{s}') \, d\Omega' \tag{4.19}$$

Using equation (4.14),

$$dP_2 = \sigma_s \rho \, dA \, ds \int_{4\pi} p(\hat{s},\hat{s}') I(\vec{r},\hat{s}') \, d\Omega' \tag{4.20}$$

If there exists source $S(\vec{r},\hat{s})$, $Wm^{-3}sr^{-1}$ in the volume:

$$dP_3 = S(\vec{r},\hat{s})\ dA\ ds\ d\Omega \tag{4.21}$$

Sum up all the power, the total differential power would be[Wang and Wu, 2012, Ishimaru, 1978]:

$$dP = dP_1 + dP_2 + dP_3 = dI(\vec{r},\hat{s})\ dA\ ds\ d\Omega \tag{4.22}$$

Plug in and we would have the equation of transfer, dA and $d\Omega$ exists on both side of the equation and will be cancelled, another way to see this is that the specific intensity has a unit of $Wm^{-2}sr^{-1}$.

$$\frac{dI(\vec{r},\hat{s})}{ds} = -\rho\ \sigma_t I(\vec{r},\hat{s}) + \rho\sigma_s \int_{4\pi} p(\hat{s},\hat{s}')I(\vec{r},\hat{s}')\ d\Omega' + S(\vec{r},\hat{s}) \tag{4.23}$$

The above equation is the time-independent radiative transfer equation(RTE), the first term on the RHS represents power loss due to single scattering or absorption, the second term represents external contribution and the last term is the ”generation term” representing the source.

4.2 Diffusion approximation

It is very difficult to solve the complete transfer equation. However,the equation could become easier to handle under a few scenarios. One of the cases that we are interested is when the particle density in the media become very large that the incident photon has almost completely lost it’s memory of the propagation direction. We could resort to the approximation technique called Diffusion approximation. There are a few different ways to get the diffusion approximation, the following is the easiest although lack of mathematical rigor. After the light went through a series of scattering, the photon lost it's original direction of propagation. So, at a certain point along propagation direction, the light intensity distribution in the scattering media will be isotropic, i.e. the light has equal probability of propagating forward and backward, or toward any direction. However, that will mean that there will be no net power propagation which apparently contradicts what we experience. So there should be slightly more power in the propagation direction. For the intensity distribution, we could approximate the intensity by the following[Ishimaru, 1978]:

$$I(\vec{r},\hat{s}) \simeq \frac{1}{4\pi}U(\vec{r}) + c\vec{F}(\vec{r})\cdot\hat{s} \tag{4.24}$$

In order to see the approximation clearly, the major steps and results are presented in this subsection first. The detailed derivation is placed in the following sections.
It can be found out that $c = \frac{3}{4\pi}$, so the specific intensity can be written as:

$$I(\vec{r},\hat{s}) \simeq \frac{1}{4\pi}U(\vec{r}) + \frac{3}{4\pi}\vec{F}(\vec{r})\cdot\hat{s} \tag{4.25}$$

Step 1 is to plug the above equation (4.25) into the RTE (4.23) and the RTE would become:

$$\nabla\cdot\vec{F}(\vec{r}) = -\rho\sigma_a U(\vec{r}) + S(\vec{r}) \tag{4.26}$$

Note the above source function $S(\vec{r})$ is only position dependent.

Then, Step 2 is to multiple the RTE (4.23) with $\hat{s}$ and integrate over 4π solid angle yields the following, i.e. the vectorial RTE:

$$\frac{1}{3}\nabla U(\vec{r})+\rho[\sigma_a+\sigma_s(1-g)]\vec{F}(\vec{r})=0 \tag{4.27}$$

We define the following parameter, scattering coefficient and scattering mean free path:

$$\mu_s=\rho\sigma_s=\frac{1}{l_s} \tag{4.28}$$

Reduced scattering coefficient which acounts for the anisotropy of the light scattering. If light scatters in all directions, then reduced scattering coefficient and scattering coefficient will be the same.

$$\mu_s'=\rho\sigma_s(1-g)=\frac{1}{l_s'} \tag{4.29}$$

in which g is the mean cosine phase function defined previously.

Absorption coefficient and absorption mean free path:

$$\mu_a=\rho\sigma_a=\frac{1}{l_a} \tag{4.30}$$

The extinction coefficient is:

$$\mu_t=\mu_s+\mu_a=\frac{1}{l_t} \tag{4.31}$$

And finally, the transport coefficient and reduced transport mean free path:

$$\mu_{tr}=\mu_s'+\mu_a=\frac{1}{l_{tr}} \tag{4.32}$$

Define photon diffusion coefficient is defined as[Graaff and Ten Bosch, 2000]:

$$D = \frac{1}{3u'_{tr}} \tag{4.33}$$

Rewrite equation (4.26) and (4.27) using the above definition:

$$\nabla \cdot \vec{F}(\vec{r}) = -\mu_a U(\vec{r}) + S(\vec{r}) \tag{4.34}$$

$$\nabla U(\vec{r}) + \frac{1}{D}\vec{F}(\vec{r}) = 0 \tag{4.35}$$

The light speed c in diffusivity is dropped for simplicity, so the diffusivity would have a unit of m instead of m^2/s.

With the above definition, combine equation (4.34) and (4.35), we will get the photon diffusion equation:

$$[D\nabla^2 - \mu_a]U(\vec{r}) = -S(\vec{r}) \tag{4.36}$$

The physical meaning of the diffusion approximation can be interpreted as follows: the time-independent radiative transfer equation(RTE) has 5 variables(x, y, z, θ, ϕ),with the diffusion approximation, the light intensity distribution can be described by a diffusion equation which only depends on the average intensity which is position dependent only.

Chapter 5

Photon Transport in Dynamic Random Scattering Media

In the previous chapter, I outlined how to describe the photon transport in a scattering media when the scatterers' relative position is constant. But to serve our purpose of finding the blood flow speed, it is still far from sufficient. In his chapter, we shall see how we could transfer the techniques used in the previous chapter to a scattering system where all or part of the scatterers would change its location overtime. In our case, we will be dealing with the problem of moving blood cells. To describe with such a system, typically we will be dealing with the autocorrelation function. Typically, what we measure is photon current, and what we mathematically calculate is the correlation function of the electrical field. The two is typically related by the Siegert relation which will be described in detail here with mathematical rigor.

First, I will start from the electrical field correlation of the simplest case of single scattering by moving particles[Berne and Pecora, 2000].

5.1 Single scattering

The scattered field detected by the detector is $E(t)$, $\vec{r}_i$ is the position vector of i th particle at time t, N denotes the N fields scattered by all the N particles.

$$E(t) = \sum_{i=1}^{N} E_0 \exp[i\vec{q} \cdot \vec{r}_i(t)] \tag{5.1}$$

in which, $\vec{q}$ is the momentum transfer of the scattering and can be illustrated as follows:

$$\vec{q} = k(\hat{s} - \hat{s}') \tag{5.2}$$

We define $G_1^s(\tau)$ as the un-normalized autocorrelation function,

$$G_1^s(\tau) = \langle E(t)E^*(t+\tau)\rangle \tag{5.3}$$

in which, $\langle\rangle$ represents the ensemble averaging.

Similarly, the normalized field autocorrelation function can be written as[Berne and Pecora, 2000],

$$\begin{aligned} g_1^s(\tau) = \frac{G_1^s(\tau)}{G_1^s(0)} &= \frac{\langle E(t)E^*(t+\tau)\rangle}{\langle E(t)E^*(t)\rangle} \\ &= \frac{\langle \sum_{i=1}^{N} E_0 \exp[i\vec{q} \cdot \vec{r}_i(t)] \sum_{j=1}^{N} E_0 \exp[-i\vec{q} \cdot \vec{r}_j(t+\tau)]\rangle}{\langle \sum_{i=1}^{N} E_0 \exp[i\vec{q} \cdot \vec{r}_i(t)] \sum_{j=1}^{N} E_0 \exp[-i\vec{q} \cdot \vec{r}_j(t)]\rangle} \end{aligned} \tag{5.4}$$

$$G_1^s(\tau) = \langle \sum_{i=1}^{N} \sum_{j=1}^{N} |E_0|^2 \exp(i\vec{q} \cdot [\vec{r}_i(t) - \vec{r}_j(t+\tau)])\rangle \tag{5.5}$$

Purely from physical argument, for any particle other than itself, the ensemble average of the correlation function will be zero, i.e. the off diagonal terms will all be zero (Ladder approximation)[Akkermans and Montambaux, 2007]. So the above equation can be simplified by only retaining the $i = j$ terms, i.e. the correlation of each particle itself. Also, the product of the two series is reduced to only one series since there are only N particles not N^2 particles.

$$G_1^s(\tau) = \langle \sum_{i=1}^{N} |E_0|^2 \exp(i\vec{q} \cdot [\vec{r}_i(t) - \vec{r}_i(t+\tau)]) \rangle \tag{5.6}$$

Furthermore, each particle is statistially identical, the above series can be further simplified as:

$$G_1^s(\tau) = N\langle |E_0|^2 \exp(i\vec{q} \cdot [\vec{r}_i(t) - \vec{r}_i(t+\tau)]) \rangle \tag{5.7}$$

If the number of scatters in the scattering volume during the measurement time scale is assumed to be constant, $|E_0|$ can be assumed to be a constant, although it would be follow poisson distribution in a sufficiently long time scale. This way, the magnitude and phase can be decoupled as follows:

$$G_1^s(\tau) = N\langle |E_0|^2 \rangle \langle \exp(i\vec{q} \cdot [\vec{r}_i(t) - \vec{r}_i(t+\tau)]) \rangle \tag{5.8}$$

Then, the normalized field correlation can be written as:

$$g_1^s(\tau) = \langle \exp(-i\phi(\tau)) \rangle \tag{5.9}$$

in which,(the sign flipped as well for next step)

$$\phi(\tau) = \vec{q} \cdot \Delta\vec{r}_i(\tau) = \vec{q} \cdot [\vec{r}_i(t+\tau) - \vec{r}_i(t)] \tag{5.10}$$

In $g_1(\tau)$, using the moment generating function to the second order:

$$\begin{aligned} g_1^s(\tau) &= \langle \exp(-i\phi(\tau)) \rangle \\ &= 1 - i\langle \phi(\tau) \rangle - \frac{\langle \phi^2(\tau) \rangle}{2} + ... \end{aligned} \tag{5.11}$$

If $\phi(\tau)$ is small and assumed to be zero mean Gaussian random variable, and using the property of taylor series:

$$g_1^s(\tau) = 1 - \frac{\langle \phi^2(\tau) \rangle}{2} \approx \exp\left(- \frac{\langle \phi^2(\tau) \rangle}{2} \right) \tag{5.12}$$

Averaging over the scattering angle, the above equation can be written as:

$$\begin{aligned} g_1^s(\tau) &= \exp\left(- \frac{\langle |\vec{q} \cdot [\Delta\vec{r}_i(\tau)]|^2 \rangle}{2} \right) \\ g_1^s(\tau) &= \exp\left(- \frac{1}{6} q^2 \langle \Delta r_i^2(\tau) \rangle \right) \end{aligned} \tag{5.13}$$

5.1.1 Off diagonal term, Ladder Approximation

Mathematically, a more satisfying way of getting this result can be achieved by doing the following steps[Akkermans and Montambaux, 2007]:

$$
\begin{aligned}
G_1^s(\tau) &= \langle \sum_{i=1}^{N}\sum_{j=1}^{N} |E_0|^2 \exp(i\vec{q}\cdot[\vec{r}_i(t)-\vec{r}_j(t+\tau)])\rangle \\
&= \langle \sum_{i=1}^{N} E_0 \exp[i\vec{q}\cdot\vec{r}_i(t)] \sum_{j=1}^{N} E_0 \exp[-i\vec{q}\cdot\vec{r}_j(t+\tau)]\rangle \\
&\overset{i\neq j}{=} \langle \sum_{i=1}^{N} E_0 \exp[i\vec{q}\cdot\vec{r}_i(t)]\rangle\langle \sum_{j=1}^{N} E_0 \exp[-i\vec{q}\cdot\vec{r}_j(t+\tau)]\rangle \\
&= N|E_0|^2\langle \exp[i\vec{q}\cdot\vec{r}_i(t)]\rangle\langle \exp[-i\vec{q}\cdot\vec{r}_j(t+\tau)]\rangle
\end{aligned} \tag{5.14}
$$

To calculate the ensemble average, we can write it in integral form and using the density of states:

$$
\lim_{V=\infty} V\langle \exp[-i\vec{q}\cdot\vec{r}_i(t)]\rangle = \lim_{V=\infty}\int_V d^3r \exp[i\vec{q}\cdot\vec{r}_i(t)] = \delta(\vec{q}) \tag{5.15}
$$

which means, as long as there is momentum transfer, the off diagonal term will be zero.

5.2 Correlation transfer equation (CTE)

From the previous chapter, we have obtained the correlation function for single scattering as in equation (5.13). This single scattering function can be incorporated into the radiative transfer equation, yielding the so-called correlation transfer equation which is the dynamic counter part of the static radiative transfer equation [Boas and Yodh, 1997]:

$$
\frac{dG_1(\vec{r},\hat{s},\tau)}{ds} = -\rho\sigma_t G_1(\vec{r},\hat{s},\tau) \;+\; \rho\sigma_s \int_{4\pi} p(\hat{s},\hat{s}')\;\; g_1^s(\hat{s},\hat{s}',\tau) G_1(\vec{r},\hat{s},\tau)\, d\Omega' + S(\vec{r},\hat{s}) \tag{5.16}
$$

Similarly, the diffusion approximation can also be applied to obtain the correlation diffusion equation which is again the counterpart of the static diffusion equation described previously.

Equation (5.16) is the correlation diffusion equation. The diffusion equation can then be solved with appropriate boundary conditions to be compared with experimental results.

$$[D\nabla^2 - \mu_a - \frac{1}{3}\mu_s' k_0^2 \langle \Delta r^2(\tau) \rangle] G_1(\vec{r}, \tau) = -S(\vec{r}) \tag{5.17}$$

where n is the refactive index of scattering media, k_0 is the wavevector in vacuum, μ_s' is the reduced scattering coefficient which is the scattering coefficient modified due to scattering anisotropy. For isotropic scattering, the scattering coefficient would be the same reduced scattering coefficient.

5.3 Intensity correlation

In the previous discussions, we have been talking about the field correlation. However, what we measure through the photodetector is not electrical field directly, but photocurrent. In order to relate the measurement to theoretical calculation, we will first introduce the Siegert relation and then come up with the expression that relates the electrical field to photocurrent. This is seemingly straightforward, however, it actually involves many non-trivial steps.

5.3.1 Isserlis' Theorem / Wick's Theorem

We first need to introduce the Isserlis' Theorem/ Wick's Theorem to relate the second order correlation to the first order correlation[Isserlis, 1916].

If X_i is a zero mean Gaussian Random Variable, then, for the fourth order moment can be written as:

$$\langle X_1 X_2 X_3 X_4 \rangle = \langle X_1 X_2 \rangle \langle X_3 X_4 \rangle + \langle X_1 X_3 \rangle \langle X_2 X_4 \rangle + \langle X_1 X_4 \rangle \langle X_2 X_3 \rangle \tag{5.18}$$

This is basically reflecting the fact that a Gaussian random variable can be fully characterized by it's second order moment.

5.3.2 Siegert Relation

Recall:

$$E(t) = \sum_{i=1}^{N} E_0 \exp[i\vec{q} \cdot \vec{r}_i(t)] \tag{5.19}$$

in which, $\vec{q}$ is the momentum transfer of the scattering.

$$\vec{q} = k(\hat{s} - \hat{s}') \tag{5.20}$$

When N is big, using central limit theorem, E(t) will become Gaussian.

For a photodetector, the photocurrent is proportional to the optical power impinging on the device which is proportional to $|E(t)|^2$, if we use lower case $i(t)$ representing the photocurrent, the autocorrelation of the photocurrent will be proportional to the autocorrelation of the field squared.

$$\langle i(t)i(t+\tau)\rangle \propto \langle |E(t)|^2 |E(t+\tau)|^2 \rangle \tag{5.21}$$

And we can define:

$$G_2(\tau) = \langle |E(t)|^2 |E(t+\tau)|^2 \rangle \tag{5.22}$$

in which, G_2 represents the second order correlation of the field.

And the normalized version can be written as follows and note that it needs to be normalized to its the individual intensity:

$$g_2(\tau) = \frac{\langle |E(t)|^2 |E(t+\tau)|^2 \rangle}{\langle |E(t)|^2 \rangle^2} \tag{5.23}$$

recall the first order correlation we defined previously:

$$G_1(\tau) = \langle E(t)E^*(t+\tau) \rangle \tag{5.24}$$

And the normalized version:

$$g_1(\tau) = \frac{\langle E(t)E^*(t+\tau) \rangle}{\langle E(t)E^*(t) \rangle} \tag{5.25}$$

With the above definition, we rewrite the G_2 into the product of complex conjugate form and use Wick's theorem:

$$\begin{aligned} G_2(\tau) =& \langle |E(t)|^2 |E(t+\tau)|^2 \rangle \\ =& \langle E(t)E^*(t)E(t+\tau)E^*(t+\tau) \rangle \\ =& \langle E(t)E^*(t) \rangle \langle E(t+\tau)E^*(t+\tau) \rangle + \langle E(t)E(t+\tau) \rangle \langle E^*(t)E^*(t+\tau) \rangle \\ &+ \langle E(t)E^*(t+\tau) \rangle \langle E^*(t)E(t+\tau) \rangle \end{aligned} \tag{5.26}$$

In the above equation, the first term has the meaning of intensity squared(differ by a impedance constant):

$$\langle E(t)E^*(t) \rangle \langle E(t+\tau)E^*(t+\tau) \rangle = |G_1(0)|^2 \tag{5.27}$$

The third term:

$$\langle E(t)E^*(t+\tau) \rangle \langle E^*(t)E(t+\tau) \rangle = |G_1(\tau)|^2 \tag{5.28}$$

To calculate the second term, we write the first ensemble average in second term in the integral form, similar to the previous derivation, we only consider the diagonal terms[Lang, 2004]:

$$\begin{aligned}
\langle E(t)E(t+\tau)\rangle &= N\langle|E_0|^2\rangle\langle\exp(i\vec{q}\cdot[\vec{r}_i(t)+\vec{r}_i(t+\tau)])\rangle \\
&= N\langle|E_0|^2\rangle\langle\exp(i\vec{q}\cdot[\vec{r}_0+\vec{r}_\tau])\rangle \\
&= N\langle|E_0|^2\rangle\int d^3r_0\int d^3r_\tau P(\vec{r}_0)P_c(\vec{r}_\tau,\tau|\vec{r}_0,0)\exp(i\vec{q}\cdot[\vec{r}_0+\vec{r}_\tau]) \\
&= N\langle|E_0|^2\rangle\int d^3r_0\int d^3r_\tau P(\vec{r}_0)P_c(\vec{r}_0-\vec{r}_\tau,\tau)\exp(i\vec{q}\cdot[\vec{r}_0+\vec{r}_\tau]) \\
&= \frac{1}{8V}\int d(\vec{r}_0+\vec{r}_\tau)\exp(i\vec{q}\cdot[\vec{r}_0+\vec{r}_\tau])\int d(\vec{r}_0-\vec{r}_\tau)P_c(\vec{r}_0-\vec{r}_\tau,\tau) \\
&\propto \delta(\vec{q})
\end{aligned} \tag{5.29}$$

In the above equation, P and P_c is the pdf and conditional pdf. And it involves a coordinate transformation $(\vec{r}_0,\vec{r}_\tau)$ to $(\vec{r}_0-\vec{r}_\tau,\vec{r}_0-\vec{r}_\tau)$ and $\frac{1}{8}$ is the Jacobian[Lang, 2004].

Therefore, the second term in G_2 is zero.

$$G_2(\tau) = |G_1(0)|^2+|G_1(\tau)|^2 \tag{5.30}$$

And this is commonly known as the Siegert relation which relates the first order correlation to the second order correlation[Berne and Pecora, 2000].

5.3.3 Photocurrent Correlation

Previously, we only look at one single detection point or effectively one coherent area. For our detection system,assume there are N coherent areas or spatial modes that will be collected by the detector. Again, we will use lower case i for detector current. The total detector current is $i(t)$, and it's a superposition of all the current of individual coherent areas[Berne and Pecora, 2000].

$$i(t) = \sum_{k=1}^{N} i_k(t) \tag{5.31}$$

The current can be written in terms of the average current i_a and the fluctuating part. $\langle\rangle$ denotes the time average instead of ensemble average.

$$i_k(t) = \langle i_a \rangle + \delta i_k(t) \tag{5.32}$$

Looking at the correlation function of current:

$$\begin{aligned} \langle i(t)i(t+\tau)\rangle &= \left\langle \sum_{k=1}^{N}\sum_{k'=1}^{N} \left[\langle i_a\rangle + \delta i_k(t)\right]\left[\langle i_a\rangle + \delta i_{k'}(t+\tau)\right] \right\rangle + \left\langle i_s(0) i_s(\tau)\right\rangle \\ &= N^2\langle i_a\rangle^2 + N\langle \delta i(t)\delta i(t+\tau)\rangle + \left\langle i_s(0)i_s(\tau)\right\rangle \end{aligned} \tag{5.33}$$

$$\frac{\langle i(t)i(t+\tau)\rangle}{\langle i(t)\rangle^2} = \frac{\langle i(t)i(t+\tau)\rangle}{N^2\langle i\rangle^2} = 1 + \frac{1}{N}\frac{\langle \delta i(t)\delta i(t+\tau)\rangle}{\langle i_a\rangle^2} + \frac{\langle i_s(0)i_s(\tau)\rangle}{N^2\langle i_a\rangle^2} \tag{5.34}$$

For the above equation, the numerator of the second term is just the covariance of photocurrent at time t and $t+\tau$, and from Siegert relation:

$$\langle \delta i_a(t)\delta i_a(t+\tau)\rangle = G_2(\tau) - |G_1(0)|^2 = |G_1(\tau)|^2 \tag{5.35}$$

$$\langle i_a\rangle^2 = |G_1(0)|^2 \tag{5.36}$$

The shotnoise correlation can be found out to be:

$$\langle i_s(0) i_s(\tau)\rangle = Ne\langle i_a\rangle \delta(\tau) \tag{5.37}$$

Then, the normalized current correlation function can be found out to be[Berne and Pecora, 2000]:

$$\frac{\langle i(t) i(t+\tau)\rangle}{\langle i(t)\rangle^2} = 1 + \frac{1}{N}|g_1(\tau)|^2 + \frac{e\delta(t)}{\langle i(t)\rangle} \tag{5.38}$$

Equation (5.38) is the equation that we will use to connect the first order field correlation to the second order photocurrent correlation. The number of spatial modes is typically unknown, but since the electrical field correlation will normalize to one, N will simply be a normalization constant.

5.4 Mean square displacement

We obtained expression for single scattering correlation function in 4.13, we still need to deal with the mean square displacement in equation (4.13). For blood cells flowing in blood vessel, the motion the blood cells experience can typicall be catagorized into two type: diffusive and convective. For the diffusive motion, let's look at the one dimensional case[Frenkel and Smit, 2001]:

$$\langle \Delta x^2(\tau)\rangle = \frac{1}{N}\sum_{i=1}^{N} |x_i(t+\tau) - x_i(t)|^2 \tag{5.39}$$

Without lose of generality, we can set $t = 0$:

$$\langle \Delta x^2(\tau) \rangle = \frac{1}{N} \sum_{i=1}^{N} |x_i(\tau) - x_i(0)|^2 \tag{5.40}$$

For a particle under diffusive motion can be represented by the particle diffusion equation of its probability distribution function:

$$\frac{\partial P(x,\tau)}{\partial \tau} = D \frac{\partial^2}{\partial x^2} P(x,\tau) \tag{5.41}$$

In the above equation $P(x,\tau)$ is the conditional probability of finding the particle at position x and time delay τ given a starting location of x^0.

Taking the spatial Fourier transform:

$$\frac{\partial P(k,\tau)}{\partial \tau} = -Dk^2 P(k,\tau) \tag{5.42}$$

The above equation has the following solution:

$$P(k,\tau) = P(k,\tau = 0) e^{-Dk^2\tau} \tag{5.43}$$

The initial condition in real space domain can be written as:

$$P(x,\tau = 0) = \delta(x - x^0) \tag{5.44}$$

in which x^0 is the starting location.

Using the Fourier transform for the initial condition:

$$P(k,\tau=0)=\frac{1}{\sqrt{2\pi}}\int_{-\infty}^{\infty}\delta(x-x^0)e^{-ikx}dx=\frac{e^{-ikx^0}}{\sqrt{2\pi}} \tag{5.45}$$

Then:

$$P(k,\tau)=\frac{e^{-ikx^0}}{\sqrt{2\pi}}e^{-Dk^2\tau} \tag{5.46}$$

Taking the inverse Fourier transform:

$$\begin{aligned} P(x,\tau) &= \frac{1}{2\pi}\int_{\infty}^{\infty}e^{-ikx^0}e^{-Dk^2\tau}e^{ikx}dk \\ &= \frac{1}{2\pi}\int_{\infty}^{\infty}e^{-Dk^2\tau+ik(x-x^0)}dk \\ &= \frac{1}{2\pi}e^{-D\tau(\frac{x-x^0}{2D\tau})^2}\frac{1}{\sqrt{D\tau}}\int_{\infty}^{\infty}e^{-[\sqrt{D\tau}(k-\frac{i(x-x^0)}{2D\tau})]^2}d[\sqrt{D\tau}(k-\frac{i(x-x^0)}{2D\tau})] \\ &= \frac{1}{2\pi}e^{-D\tau(\frac{(x-x^0)}{2D\tau})^2}\frac{1}{\sqrt{D\tau}}\sqrt{\pi} \\ &= \frac{1}{\sqrt{4\pi D\tau}}\exp\left[-\frac{(x-x^0)^2}{4D\tau}\right] \end{aligned} \tag{5.47}$$

Obviously, this is the Gaussian distribution, the variance:

$$\langle\Delta x^2(\tau)\rangle=\sigma^2=2D\tau \tag{5.48}$$

In 3 dimensional space, each dimension is statistically independent:

$$\begin{aligned}\langle \Delta r^2(\tau) \rangle &= \langle \Delta x^2(\tau) + \Delta y^2(\tau) + \Delta z^2(\tau) \rangle \\ &= \langle \Delta x^2(\tau) \rangle + \langle \Delta y^2(\tau) \rangle + \langle \Delta z^2(\tau) \rangle \\ &= 6D\tau\end{aligned} \tag{5.49}$$

For convective motion:

$$\Delta r(\tau) = V\tau \tag{5.50}$$

For simplicity, assuming there is no velocity fluctuation,

$$\langle \Delta r^2(\tau) \rangle = \langle V^2 \rangle \tau^2 = \bar{V}^2 \tau^2 \tag{5.51}$$

in which, $\bar{V}$ is the average flow velocity.

So, the total mean square displacement can be written as[Boas et al., 2016]:

$$\langle \Delta r^2(\tau) \rangle = 6D_\alpha \tau + \bar{V}^2 \tau^2 \tag{5.52}$$

In the previous section, we came up with the expression of the mean square displacement, however, in a system of mixed physical mechanisms, sometime, it would be important to identify the dominant mechanism and simply the problem. The diffusion of red blood cells in the vessel can be caused by either the Brownian motion or the shear force. Experimentally, we demonstrated that the second term is the dominate term and will further discuss this matter in the discussion chapter.

Chapter 6

Analytical solution

In order to analytically solve the problem. I attempted to make the following assumption, which physically may not be accuracy, but would capture the essential part of the physics.

Rewrite equation (5.17) in the standard form of Helmholtz equation:

$$[\nabla^2 + k^2] G_1(\vec{r}, \tau) = -\frac{S(\vec{r})}{D} \tag{6.1}$$

in which

$$k = jW(\tau) \tag{6.2}$$

Later on we will see that the imaginary number would change the regular bessel function to a modified bessel function and it's linear combinations. It's solution will not exhibit oscilation behaviour but will be an exponential function.

The total field would be a linear combination of the incident field and the scattered field, denoted as G_1^i and G_1^s. Let's first look at the scattered field.

$$G_1(\vec{r}, \tau) = G_1^{in}(\vec{r}, \tau) + G_1^{sc}(\vec{r}, \tau) \tag{6.3}$$

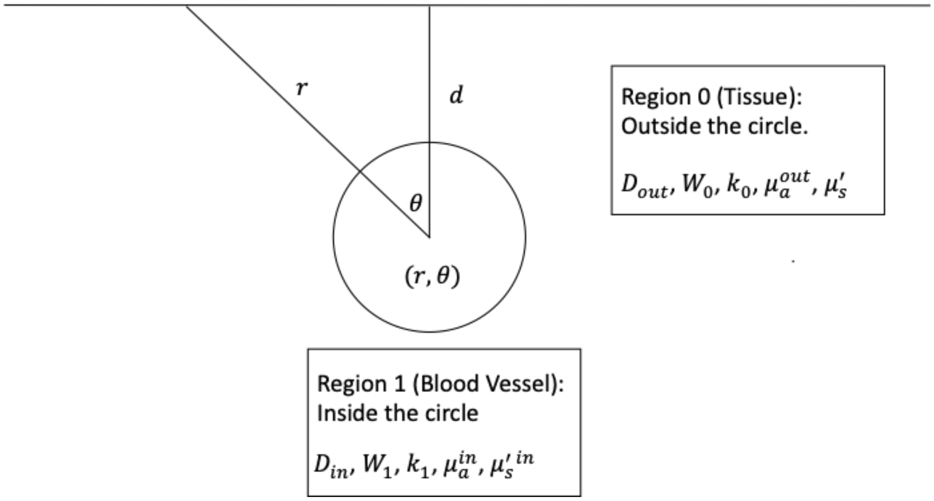

Figure 6.1: This figure is an illustration of the geometry used for numerical calculation using a plane illumination from the top surface. The coordinate system in this figure is polar coordinate, the center $r = 0$ is located at the center of the blood vessel. The region inside the circle represents the blood vessel, the area outside the circle represents the tissue which is semi-infinite.

6.1 Scattered field, Homogeneous solution

And the scattered field would follow the homogeneous form of equation (6.1):

$$[\nabla^2 + k^2] G_1^{sc}(\vec{r}, \tau) = 0 \tag{6.4}$$

As illustrated in figure 6.1, we choose the *x*-axis as the cylinder direction and we assume the cylinder length is infinite. And equation (6.4) becomes a 2d helmholtz equation, and can be expressed in polar coordinates(y-z plane) utilizing the symmetry property of the cylinder.

The solution can be obtained using the separation of variable[Morse and Feshbach, 1954]:

$$G_1^{sc} = \psi_1(r)\psi_2(\theta) \tag{6.5}$$

And this r is the radial component under the new coordinate system which is a different from the $\vec{r}$ in the previous equations. The laplacian under polar coordinates can be written as:

$$\nabla^2 G_1^{sc} = \frac{1}{r}\frac{\partial}{\partial r}\left(r\frac{\partial f}{\partial r}\right) + \frac{1}{r^2}\frac{\partial^2 G_1^{sc}}{\partial \theta^2} \tag{6.6}$$

Substituting back into equation (6.4):

$$\frac{1}{r}\frac{\partial}{\partial r}\left\{r\frac{\partial}{\partial r}[\psi_1(r)\psi_2(\theta)]\right\} + \frac{1}{r^2}\frac{\partial^2[\psi_1(r)\psi_2(\theta)]}{\partial \theta^2} + k^2\psi_1(r)\psi_2(\theta) = 0 \tag{6.7}$$

After re-arranging the terms, the above equation can be written as:

$$\frac{r^2}{\psi_1(r)}\frac{d^2\psi_1}{dr^2} + \frac{r}{\psi_1(r)}\frac{d\psi_1}{dr} + k^2r^2 = -\frac{1}{\psi_2(\theta)}\frac{d^2\psi_2(\theta)}{d\theta^2} \tag{6.8}$$

Use separation of variable for equation (6.8), the LHS is only a function of r and RHS is only a function of θ. Define a constant m:

$$\frac{1}{\psi_2(\theta)}\frac{d^2\psi_2(\theta)}{d\theta^2} = -m^2 \tag{6.9}$$

$$\frac{r^2}{\psi_1(r)}\frac{d^2\psi_1}{dr^2} + \frac{r}{\psi_1(r)}\frac{d\psi_1}{dr} + k^2r^2 = m^2 \tag{6.10}$$

The solution for equation (6.9) is:

$$\psi_2(\theta) = e^{jm\theta} \tag{6.11}$$

Applying the periodical condition, i.e. $\psi_2(\theta) = \psi_2(\theta + 2\pi)$. So m will has to be an integer.

Equation (6.10) can be written as:

$$r^2\frac{d^2\psi_1(r)}{dr^2}+r\frac{d\psi_1(r)}{dr}+(k^2r^2-n^2)\psi_1(r)=0 \tag{6.12}$$

The solution to the above equation can be written in the form of Bessel functions:

$$\psi_1(r)=A_mJ_m(kr)+B_mY_m(kr) \tag{6.13}$$

In which, J_m and Y_m is the Bessel function of the first kind of order m and Bessel function of the second kind of order m. And A_m, B_m are constants depending on the boundary condition. Equation (6.13) can also be written as the combination of Hankel functions:

$$\psi_1(r)=C_mH_m^{(1)}(kr)+D_mH_m^{(2)}(kr) \tag{6.14}$$

in which, the Hankel functions are a combination of Bessel functions:

$$H_m^{(1)}(kr)=J_m(kr)+jY_m(kr) \tag{6.15}$$

which is called the Hankel function of the first kind of order m.

$$H_m^{(2)}(kr)=J_m(kr)-jY_m(kr) \tag{6.16}$$

which is called the Hankel function of the second kind of order m. And the constants have the following relation: $A_m=C_m+D_m$, $B_m=j(C_m-D_m)$

Combine the solution and all the possible values of m, the scattered field can be written as:

$$G_1^{sc}(r,\theta,\tau) = \sum_{m=-\infty}^{m=+\infty} e^{jm\theta}[A_m J_m(kr) + B_m Y_m(kr)] \tag{6.17}$$

Or in the form of Hankel function:

$$G_1^{sc}(r,\theta,\tau) = \sum_{m=-\infty}^{m=+\infty} e^{jm\theta}[C_m H_m^{(1)}(kr) + D_m H_m^{(2)}(kr)] \tag{6.18}$$

The above equation can be simplified due to a physical constraint of the scalar wave satisfying helmholtz equation proposed by German Physicist Sommerfeld. It basically means, the scalar wave must radiates its energy to the infinity, not the other way, no energy may radiate coming from infinity which can be mathematically expressed as the Sommerfeld Far field condition[Sommerfeld, 1949]:

$$\lim_{r\longrightarrow\infty} \sqrt{r}(\frac{\partial}{\partial r} - jk)G_1^{sc} = 0 \tag{6.19}$$

The asymptotic expression of the two Hankel functions when the argument (kr) goes to infinity can be written as [Abramowitz et al., 1988]:

$$H_m^{(1)}(kr) = \sqrt{\frac{2}{\pi kr}} e^{j(kr-\frac{1}{2}m\pi-\frac{\pi}{4})} \tag{6.20}$$

$$H_m^{(2)}(kr) = \sqrt{\frac{2}{\pi kr}} e^{-j(kr-\frac{1}{2}m\pi-\frac{\pi}{4})} \tag{6.21}$$

Using Sommerfeld condition as in equation (6.19), with a simple derivative, we can easily find that the Hankel function of the second kind does not satisfy the Sommerfeld far field condition. In other words, in equation (6.18), coefficient D_m has to be zero.

So, the scattered field can be simplified as:

$$G_1^{sc}(r,\theta,\tau) = \sum_{m=-\infty}^{m=+\infty} e^{jm\theta}[C_m H_m^{(1)}(kr)] \tag{6.22}$$

Now, since the k inside and outside the cylinder is different: k_1 which would represent the moving scatters and k_0 which is the static scatters outside the vessel. Let's assume the vessel/cylinder radius is a. So $k = k_0$ when $r > a$ and $k = k_1$ when $r < a$.

6.2 Plane Wave illumination

Assume the cylinder is deep enough so that the source only exist outside of the cylinder. Inside the cylinder, there only exists scattered field, outside of the cylinder, the total scalar field is a linear combination of incident field and scattered field. For the incident field, there are two choices, one is to choose a point source and the other is just to choose a simple plane wave. In my opinion, either choice should lead to satisfactory and similar results for our problem. It is because, our tube diameter is in the same order the transport mean free path, of which the scalar wave can be considered as a plane wave and our interest is the normalized correlation function which does not depend on the absolute intensity of the incident field. The quantity of interest is the decorrelation rate,from the experiment result, we could know that the quantity of interest would not depend on the choice of incident field. For here, let's first go with plane wave as incident field.

The plane wave illumination is assuming an uniform illumination of plane wave on top of the surface. As light scatters when the photon enters the medium, the source term would be the un-scattered photon.

We choose the direction of wave propagation as Z-axis. A plane wave can be written as the following form [Colton and Kress, 2019] using the Jacobi–Anger expansion:

$$e^{ikr\cos(\theta)} = \sum_{m=-\infty}^{m=+\infty} j^m J_m(kr) e^{jm\theta} \tag{6.23}$$

$S(\vec{r})$ will be replaced by $S_0 \exp[jk_t(d-z)] = S_0 \exp(jk_t d) \exp(-jk_t r\cos(\theta))$, in which $k_t = j\mu_t$, in which μ_t is the total scattering cross section, d is the depth of the vessel from the surface of tissue where the plane wave incident from and S_0 is the source intensity.
In order to find the inhomogeneous solution, let

$$\begin{aligned} G_1^{in}(r,\theta) &= AS_0 \exp[jk_t(d-z)] \\ &= AS_0 \exp(-\mu_t d) \exp(\mu_t z) \end{aligned} \tag{6.24}$$

And A is unknown, substitute the above equation into the following equation(diffusion equation):

$$[\nabla^2 + k^2] G_1(\vec{r},\tau) = -\frac{S(\vec{r})}{D} \tag{6.25}$$

Since it's the diffusion equation for the outside medium, the above equation can be written as:

$$[\nabla^2 - \frac{\mu_a^{out}}{D_{out}}] G_1(\vec{r},\tau) = -\frac{S(\vec{r})}{D_{out}} \tag{6.26}$$

A can be found out to be:

$$A = \frac{1}{\mu_a - \mu_t^2 D_{out}} \tag{6.27}$$

The inhomogeneous solution can then be written as:

$$\begin{aligned} G_1^{in}(r,\theta) &= \frac{S_0 \exp(-\mu_t d)}{\mu_a - \mu_t^2 D_{out}} \exp(\mu_t z) \\ &= B \exp(\mu_t z) \\ &= B \sum_{m=-\infty}^{m=+\infty} j^m J_m(-k_t r) e^{jm\theta} \end{aligned} \tag{6.28}$$

The total solution can be written as:

$$G_{1,out}(r,\theta,\tau) = \sum_{m=-\infty}^{m=+\infty} B j^m J_m(-k_t r) + C_m H_m^{(1)}(k_0 r)] e^{jm\theta} \tag{6.29}$$

For the field inside the vessel/cylinder, we use equation 53 instead of the Hankel function. Immediately, we can see that $B_m = 0$ as the Bessel function of second kind, Y_m diverges when r approaching 0. So the scattered wave inside the cylinder is:

$$G_{1,in}(r,\theta,\tau) = \sum_{m=-\infty}^{m=+\infty} e^{jm\theta} A_m J_m(k_1 r) \tag{6.30}$$

6.2.1 Boundary condition

The boundary condition requires the photon density or the correlation function to be continuous at the cylinder boundary and also the flux to be continuous normal to the boundary and it can be expressed as follows[Boas et al., 1994, Bourlier et al., 2013]:

$$G_{1,in}(a,\theta,\tau) = G_{1,out}(a,\theta,\tau) \tag{6.31}$$

And:

$$D_{in}\frac{\partial G_{1,in}(r,\theta,\tau)}{\partial r}\bigg|_{r=a} = D_{out}\frac{\partial G_{1,out}(r,\theta,\tau)}{\partial r}\bigg|_{r=a} \tag{6.32}$$

The above two boundary conditions can be written as:

$$\sum_{m=-\infty}^{m=+\infty} e^{jm\theta}A_mJ_m(k_1a) = \sum_{m=-\infty}^{m=+\infty}[Bj^mJ_m(-k_ta)+C_mH_m^{(1)}(k_0a)]e^{jm\theta} \tag{6.33}$$

And,

$$D_{in}k_1\sum_{m=-\infty}^{m=+\infty} e^{jm\theta}A_mJ'_m(k_1a) = D_{out}\sum_{m=-\infty}^{m=+\infty}[-Bk_tj^mJ'_m(-k_ta)+k_0C_mH'^{(1)}_m(k_0a)]e^{jm\theta} \tag{6.34}$$

The above relation is valid for all m and θ, and thus, it can be reduced to:

$$A_mJ_m(k_1a) = Bj^mJ_m(-k_ta)+C_mH_m^{(1)}(k_0a) \tag{6.35}$$

$$D_{in}k_1A_mJ'_m(k_1a) = -D_{out}Bk_tj^mJ'_m(-k_ta)+D_{out}k_0C_mH'^{(1)}_m(k_0a) \tag{6.36}$$

From the above two equations, A_m and C_m can be solved as:

$$A_m = Bj^m \frac{D_{out}k_0J_m(-k_ta)H_m^{\prime(1)}(k_0a) + D_{out}k_tJ_m^{\prime}(-k_ta)H_m^{(1)}(k_0a)}{D_{out}k_0J_m(k_1a)H_m^{\prime(1)}(k_0a) - D_{in}k_1J_m^{\prime}(k_1a)H_m^{(1)}(k_0a)} \tag{6.37}$$

$$C_m = Bj^m \frac{D_{in}k_1J_m^{\prime}(k_1a)J_m(-k_ta) + D_{out}k_tJ_m(k_1a)J_m^{\prime}(-k_ta)}{D_{out}k_0J_m(k_1a)H_m^{\prime(1)}(k_0a) - D_{in}k_1J_m^{\prime}(k_1a)H_m^{(1)}(k_0a)} \tag{6.38}$$

For our interest, since the term of the incident field is not τ dependent, we can only look at the the scattered field outside the cylinder:

$$G_{1,out}^s(r,\theta,\tau) = \sum_{m=-\infty}^{m=+\infty} C_mH_m^{(1)}(k_0r)e^{jm\theta} \tag{6.39}$$

Substitute in C_m:

$$G_{1,out}^s(r,\theta,\tau) = \sum_{m=-\infty}^{m=+\infty} Bj^m \frac{D_{in}k_1J_m^{\prime}(k_1a)J_m(-k_ta) + D_{out}k_tJ_m(k_1a)J_m^{\prime}(-k_ta)}{D_{out}k_0J_m(k_1a)H_m^{\prime(1)}(k_0a) - D_{in}k_1J_m^{\prime}(k_1a)H_m^{(1)}(k_0a)}H_m^{(1)}(k_0r)e^{jm\theta} \tag{6.40}$$

6.2.2 Solution Simplification

The above equation can be simplified using the following recurrence relation:

$$f_{-n}(x) = (-1)^n f_n(x) \tag{6.41}$$

Rewrite equation (6.29):

$$
\begin{aligned}
G^{s}_{1,out}(r,\theta,\tau) &= \sum_{m=-\infty}^{m=+\infty} B j^{m} \frac{D_{in}k_1 J'_m(k_1a)J_m(-k_ta) + D_{out}k_t J_m(k_1a)J'_m(-k_ta)}{D_{out}k_0 J_m(k_1a)H'^{(1)}_m(k_0a) - D_{in}k_1 J'_m(k_1a)H^{(1)}_m(k_0a)} H^{(1)}_m(k_0r)e^{jm\theta} \\
&= B\frac{D_{in}k_1 J'_0(k_1a)J_0(-k_ta) + D_{out}k_t J_0(k_1a)J'_0(-k_ta)}{D_{out}k_0 J_0(k_1a)H'^{(1)}_0(k_0a) - D_{in}k_1 J'_0(k_1a)H^{(1)}_0(k_0a)} H^{(1)}_0(k_0r) \\
&+ B\sum_{m=1}^{m=+\infty} j^{m} \frac{D_{in}k_1 J'_m(k_1a)J_m(-k_ta) + D_{out}k_t J_m(k_1a)J'_m(-k_ta)}{D_{out}k_0 J_m(k_1a)H'^{(1)}_m(k_0a) - D_{in}k_1 J'_m(k_1a)H^{(1)}_m(k_0a)} H^{(1)}_m(k_0r) \\
&[e^{jm\theta} + (-1)^m e^{-jm\theta}]
\end{aligned}
\tag{6.42}
$$

The derivative can be replaced by the reccurence relation as follows:

$$f'_m(x) = \frac{m}{x} f_m(x) - f_{m+1}(x) \tag{6.43}$$

In which, the function f could be $J_m(x)$, $H^{(1)}_m(x)$

In particular, when $m = 0$:

$$f'_0(x) = -f_1(x) \tag{6.44}$$

equation (6.42) can then be written as:

$$
\begin{aligned}
&\frac{G^{s}_{1,out}(r,\theta,\tau)}{B} = \frac{D_{in}k_1J'_0(k_1a)J_0(-k_ta)+D_{out}k_tJ_0(k_1a)J'_0(-k_ta)}{D_{out}k_0J_0(k_1a)H'^{(1)}_0(k_0a)-D_{in}k_1J'_0(k_1a)H^{(1)}_0(k_0a)}H^{(1)}_0(k_0r)\\
&+\sum_{m=1}^{m=+\infty} j^m\frac{D_{in}k_1J'_m(k_1a)J_m(-k_ta)+D_{out}k_tJ_m(k_1a)J'_m(-k_ta)}{D_{out}k_0J_m(k_1a)H'^{(1)}_m(k_0a)-D_{in}k_1J'_m(k_1a)H^{(1)}_m(k_0a)}H^{(1)}_m(k_0r)\\
&[e^{jm\theta}+(-1)^m e^{-jm\theta}]\\
&=\frac{-D_{in}k_1J_1(k_1a)J_0(-k_ta)-D_{out}k_tJ_0(k_1a)J_1(-k_ta)}{-D_{out}k_0J_0(k_1a)H^{(1)}_1(k_0a)+D_{in}k_1J_1(k_1a)H^{(1)}_0(k_0a)}H^{(1)}_0(k_0r)\\
&+\sum_{m=1}^{m=+\infty} j^m\frac{D_{in}k_1[\frac{m}{k_1a}J_m(k_1a)-J_{m+1}(k_1a)]J_m(k_0a)+D_{out}k_tJ_m(k_1a)[\frac{m}{-k_ta}J_m(-k_ta)-J_{m+1}(-k_ta)]}{D_{out}k_0J_m(k_1a)[\frac{m}{k_0a}H^{(1)}_m(k_0a)-H^{(1)}_{m+1}(k_0a)]-D_{in}k_1[\frac{m}{k_1a}J_m(k_1a)-J_{m+1}(k_1a)]H^{(1)}_m(k_0a)}\\
&H^{(1)}_m(k_0r)[e^{jm\theta}+(-1)^m e^{-jm\theta}]
\end{aligned}
\tag{6.45}
$$

From the above equation, we can see that only the zeroth order and even order will be non-zero. Also, due to the small value of the argument, after computing the remaining even series, the 2nd order will already be 5-6 order magnitude lower than the zeroth order. So In the remaining part, we will only retain the zeroth order.

k_0 and k_1 are pure imaginary, and $k_0 = jW_0$, and $k_1 = jW_1(\tau)$, we will need the following modified bessel function which would show no oscillations. Again, I changed the upper case K to W to avoid confusion between modified bessel function of the second kind.

$$J_m(jx) = j^m I_m(x) \tag{6.46}$$

and:

$$H^{(1)}_m(jx) = \frac{2}{\pi}j^{-m-1}K_m(x) \tag{6.47}$$

The zeroth order term can be then written as:

$$\begin{aligned}
&\frac{D_{in}k_1J_0'(k_1a)J_0(-k_ta)+D_{out}k_tJ_0(k_1a)J_0'(-k_ta)}{D_{out}k_0J_0(k_1a)H_0'^{(1)}(k_0a)-D_{in}k_1J_0'(k_1a)H_0^{(1)}(k_0a)}H_0^{(1)}(k_0r)\\
=&\frac{-D_{in}k_1J_1(k_1a)J_0(-k_ta)-D_{out}k_tJ_0(k_1a)J_1(-k_ta)}{-D_{out}k_0J_0(k_1a)H_1^{(1)}(k_0a)+D_{in}k_1J_1(k_1a)H_0^{(1)}(k_0a)}H_0^{(1)}(k_0r)\\
=&\frac{D_{in}W_1I_1(W_1a)I_0(-\mu_ta)+D_{out}\mu_tI_0(W_1a)I_1(-\mu_ta)}{-D_{out}W_0I_0(W_1a)K_1(W_0a)-D_{in}W_1I_1(W_1a)K_0(W_0a)}K_0(W_0r)
\end{aligned} \tag{6.48}$$

So the scattered correlation function containing only the zeroth order will be:

$$G^s_{1,out}(r,\theta,\tau)=B\frac{D_{in}W_1I_1(W_1a)I_0(-\mu_ta)+D_{out}\mu_tI_0(W_1a)I_1(-\mu_ta)}{-D_{out}W_0I_0(W_1a)K_1(W_0a)-D_{in}W_1I_1(W_1a)K_0(W_0a)}K_0(W_0r) \tag{6.49}$$

The total measured field will be:

$$G_{1,out}(r,\theta,\tau)=B\exp(\mu_tz)+B\frac{D_{in}W_1I_1(W_1a)I_0(-\mu_ta)+D_{out}\mu_tI_0(W_1a)I_1(-\mu_ta)}{-D_{out}W_0I_0(W_1a)K_1(W_0a)-D_{in}W_1I_1(W_1a)K_0(W_0a)}K_0(W_0r) \tag{6.50}$$

We can make one approximation to simplify the above equation, in the numerator, typically, the first term will be order magnitude larger than the second term. Therefore, in order to understand the underlining physics better, we will drop the second term and the above equation becomes:

$$\begin{aligned}
G_{1,out}(r,\theta,\tau) &= B\exp(\mu_t z) + B\frac{D_{in}W_1 I_1(W_1 a)I_0(-\mu_t a)}{-D_{out}W_0 I_0(W_1 a)K_1(W_0 a) - D_{in}W_1 I_1(W_1 a)K_0(W_0 a)}K_0(W_0 r) \\
&= B\exp(\mu_t z) + B\frac{D_{in}I_0(-\mu_t a)}{-D_{out}\frac{W_0 I_0(W_1 a)}{W_1 I_1(W_1 a)}K_1(W_0 a) - D_{in}K_0(W_0 a)}K_0(W_0 r) \\
&\approx B\exp(\mu_t z) - B\frac{D_{in}I_0(-\mu_t a)}{D_{out}\frac{1}{W_1 a} + D_{in}K_0(W_0 a)}K_0(W_0 r) \\
&= \frac{S_0}{\mu_a - \mu_t^2 D_{out}}\left[1 - \frac{\exp(-\mu_t d)D_{in}I_0(-\mu_t a)}{D_{out}\frac{1}{W_1 a} + D_{in}K_0(W_0 a)}K_0(W_0 r)\right]
\end{aligned} \tag{6.51}$$

In which,

$$W_1(\tau) = \sqrt{\frac{1}{D_{in}}[\mu_a^{in} + \frac{1}{3}\mu_s' k_\lambda^2 \langle \Delta r^2(\tau)\rangle]} \tag{6.52}$$

$$W_0 = \sqrt{\frac{\mu_a^{out}}{D_{out}}} \tag{6.53}$$

For motion caused by convective flow, the above equation could be rewritten as:

$$W_1(\tau) = \sqrt{\frac{1}{D_{in}}[\mu_a^{in} + \frac{1}{3}\mu_s' k_\lambda^2 V^2 \tau^2]} = \sqrt{c + b\tau^2} \tag{6.54}$$

Define the following τ independent function to simplify the equation

$$f_1 = \exp(-\mu_t d)D_{in}I_0(-\mu_t a)K_0(W_0 r) \tag{6.55}$$

$$f_2 = D_{in}K_0(W_0 a) \tag{6.56}$$

Then, the normalized correlation function can be written as:

$$g_1(r,\theta,\tau) = \frac{1 - \frac{f_1}{\frac{D_{out}}{W_1(\tau)a} + f_2}}{1 - \frac{f_1}{\frac{D_{out}}{W_1(\tau=0)a} + f_2}} \tag{6.57}$$

The above equation can be written in the form of:

$$g_1(r,a,\theta,\tau) = \frac{1 - g_1(r,a,\theta,\infty)}{1 + \tau/T} + g_1(r,a,\theta,\infty) \tag{6.58}$$

It can be found out that:

$$g_1(r,a,\theta,\infty) = \left[1 - \frac{f_1}{f_2}\right]\left[1 - \frac{f_1}{\frac{D_{out}}{a\sqrt{\frac{\mu_a^{in}}{D_{in}}}} + f_2}\right]^{-1} \tag{6.59}$$

$$\begin{aligned} T_F &= \frac{\tau(a\sqrt{c}f_2 + D_{out})}{af_2(\sqrt{b\tau^2 + c} - \sqrt{c})} \\ &\approx \frac{(a\sqrt{c}f_2 + D_{out})}{af_2\sqrt{b}} \\ &\approx \sqrt{\frac{c}{b}} \\ &= \frac{1}{V}\sqrt{\frac{3\mu_a^{in}}{\mu_s^{in}k_\lambda^2}} \end{aligned} \tag{6.60}$$

$$\frac{1}{T_F} \approx Vk_\lambda\sqrt{\frac{\mu_s^{in}}{3\mu_a^{in}}} \tag{6.61}$$

And k_λ is the wave vector value at wavelength λ.

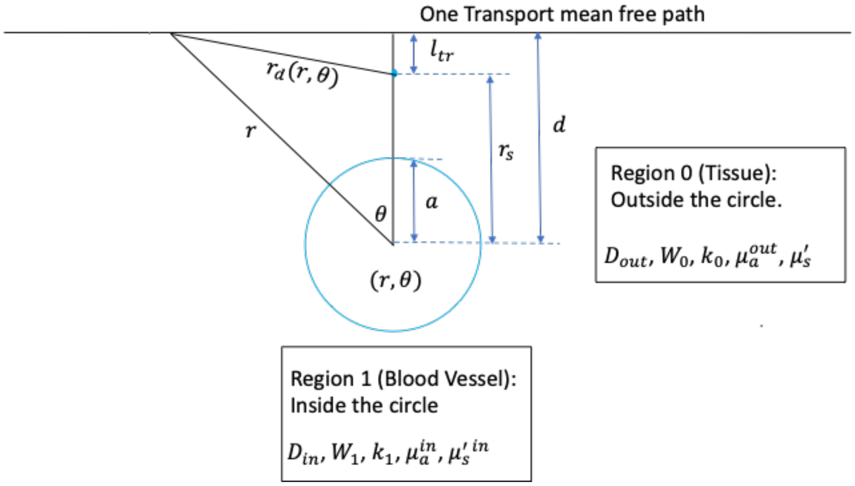

Figure 6.2: Geometry for point source calculation, the point source is inside the media at a depth of one transport mean free path.

6.3 Point Source Approximation

In the previous chapter, we analytically solved the Helmholtz equation with a incident plane wave and obtained encouraging and intuitive results. In this chapter, we would like to explore a different source profile typically used in diffuse correlation spectroscopy. If we shrink the plane wave into a pencil beam, i.e. infinitely narrow laser beam. This laser beam can then be approximated by a point source that is embedded in the scattering media at a depth of one transport mean free path. As we previously discussed, the transport mean free path is a length that the photon will lose its propagation direction and the propagation will become isotropic[Haskell et al., 1994]. For this reason, a pencil beam with sufficient scattering can equivalently be treated as a point source.

6.4 Point Source illumination

The illumination profile in the real experiment is neither a plane wave or a point source, but in between. As seen from the previous chapter, an important result from the Fermi function interpretation is that the measured decorrelation rate is independent of the source geometry, detector position and vessel diameter. In this chapter, we will prove that for point source illumination, this is also the case. The quantity used in this chapter can be referred to figure 6.2 The green's function of the 2D Helmholtz equation can be written as[Bourlier et al., 2013]:

$$\begin{aligned} g_{2D}(\vec{r}, \vec{r}_s) &= \frac{j}{4} H_0^{(1)}(k\|\vec{r} - \vec{r}_s\|) \\ &= \frac{j}{4} H_0^{(1)}\left[k\sqrt{(y-y')^2 + (z-z')^2}\right] \\ &= \frac{j}{4} H_0^{(1)}[kr_d(r, \theta)] \end{aligned} \tag{6.62}$$

And the L2-norm can be calculated as:

$$r_d(r, \theta) = \|\vec{r} - \vec{r}_s\| = \sqrt{r^2 + r_s^2 - 2rr_s \cos\theta} \tag{6.63}$$

Recall the scattered field solution can be written as:

$$G_1^s(r, \theta, \tau) = \sum_{m=-\infty}^{m=+\infty} e^{jm\theta}[C_m H_m^{(1)}(kr)] \tag{6.64}$$

The total correlation function outside the cylinder is:

$$G_{1,out}(r, \theta, \tau) = \frac{S_0}{D_{out}} \frac{j}{4} H_0^{(1)}(k_0 r_d) + \sum_{m=-\infty}^{m=+\infty} e^{jm\theta}[C_m H_m^{(1)}(k_0 r)] \tag{6.65}$$

The scattered wave inside the cylinder is the same as equation 61, written here as:

$$G_{1,in}(r, \theta, \tau) = \sum_{m=-\infty}^{m=+\infty} e^{jm\theta} A_m J_m(k_1 r) \tag{6.66}$$

6.4.1 Boundary condition

The boundary condition can be written here as[Boas et al., 1994, Bourlier et al., 2013]:

$$G_{1,in}(a,\theta,\tau) = G_{1,out}(a,\theta,\tau) \tag{6.67}$$

And:

$$D_{in}\left.\frac{\partial G_{1,in}(r,\theta,\tau)}{\partial r}\right|_{r=a} = D_{out}\left.\frac{\partial G_{1,out}(r,\theta,\tau)}{\partial r}\right|_{r=a} \tag{6.68}$$

For the first boundary condition:

$$\sum_{m=-\infty}^{m=+\infty} e^{jm\theta} A_m J_m(k_1 a) = \frac{S_0}{D_{out}}\frac{j}{4}H_0^{(1)}(k_0 r_{as}) + \sum_{m=-\infty}^{m=+\infty} e^{jm\theta}[C_m H_m^{(1)}(k_0 a)] \tag{6.69}$$

in which:

$$r_{as} = r_d(a,\theta) \tag{6.70}$$

For the second boundary condition,there are two ways to do this, noting the fact that r_d is L2 norm of the difference vector of source and detector, technically, r_d is a function of detection point r and θ. The differential operator should operate on this source term.

The second boundary condition can be written as:

$$\begin{aligned} & D_{in} k_1 \sum_{m=-\infty}^{m=+\infty} e^{jm\theta} A_m J'_m(k_1 a) \\ & = -D_{out}\frac{S_0}{D_{out}}\frac{jk_0}{4}\left.\frac{H_1^{(1)}(k_0\|\vec{r}-\vec{r}_s\|)}{\|\vec{r}-\vec{r}_s\|}(\vec{r}-\vec{r}_s)\cdot\hat{n}\right|_{r=a} + D_{out} k_0 \sum_{m=-\infty}^{m=+\infty} e^{jm\theta}[C_m H_m^{\prime(1)}(k_0 a)] \end{aligned} \tag{6.71}$$

The surface normal unit vector $\hat{n}$ will be $\hat{r}$. And the L2-norm can be calculated as:

$$r_d(r,\theta) = \|\vec{r} - \vec{r}_s\| = \sqrt{r^2 + r_s^2 - 2rr_s\cos\theta} \tag{6.72}$$

Since the source is located Then the first term on the RHS can be written as:

$$\begin{aligned} & -D_{out}\frac{S_0}{D_{out}}\frac{jk_0}{4}\frac{H_1^{(1)}(k_0\|\vec{r}-\vec{r}_s\|)}{\|\vec{r}-\vec{r}_s\|}(\vec{r}-\vec{r}_s)\cdot\hat{n}\Bigg|_{r=a} \\ & = -D_{out}\frac{S_0}{D_{out}}\frac{jk_0}{4}\frac{H_1^{(1)}[k_0r_{as}]}{r_{as}}(a - r_s\cos\theta) \\ & = SS \end{aligned} \tag{6.73}$$

For simplicity, equation (6.73) is defined as *SS*.

θ_s is defined as the angle between the detection position vector and the source position vector. If the source is located on z-axis, then θ_s will be the same as θ, as illustrated in figure.... Then, the boundary condition can be written as:

$$D_{in}k_1\sum_{m=-\infty}^{m=+\infty} e^{jm\theta}A_mJ'_m(k_1a) = SS + D_{out}k_0\sum_{m=-\infty}^{m=+\infty} e^{jm\theta}[C_mH_m^{'(1)}(k_0a)] \tag{6.74}$$

Again, this is true for all θ and m, the two boundary condition can be written as:

$$e^{jm\theta}A_mJ_m(k_1a) = \frac{S_0}{D_{out}}\frac{j}{4}H_0^{(1)}(k_0r_{as}) + e^{jm\theta}C_mH_m^{(1)}(k_0a) \tag{6.75}$$

$$D_{in}k_1e^{jm\theta}A_mJ'_m(k_1a) = SS + D_{out}k_0e^{jm\theta}C_mH_m^{'(1)}(k_0a) \tag{6.76}$$

C_m and A_m can be solved as:

$$C_m = \frac{J_m(k_1 a) \times SS - \frac{S_0}{D_{out}} \frac{j}{4} H_0^{(1)}(k_0 r_{as}) D_{in} k_1 J'_m(k_1 a)}{e^{jm\theta} H_m^{(1)}(k_0 a) D_{in} k_1 J'_m(k_1 a) - e^{jm\theta} J_m(k_1 a) D_{out} k_0 H_m^{'(1)}(k_0 a)} \tag{6.77}$$

The total correlation function outside the cylinder is:

$$\begin{aligned} G_{1,out}(r,\theta,\tau) = {} & \frac{S_0}{D_{out}} \frac{j}{4} H_0^{(1)}(k_0 r_d) \\ & + \sum_{m=-\infty}^{m=+\infty} \frac{J_m(k_1 a) \times SS - \frac{S_0}{D_{out}} \frac{j}{4} H_0^{(1)}(k_0 r_{as}) D_{in} k_1 J'_m(k_1 a)}{H_m^{(1)}(k_0 a) D_{in} k_1 J'_m(k_1 a) - J_m(k_1 a) D_{out} k_0 H_m^{'(1)}(k_0 a)} H_m^{(1)}(k_0 r) \end{aligned} \tag{6.78}$$

6.4.2 Solution Simplification

Using the recurrence relation:

$$f_{-n}(x) = (-1)^n f_n(x) \tag{6.79}$$

$$\begin{aligned} G_{1,out}(r,\theta,\tau) = {} & \frac{S_0}{D_{out}} \frac{j}{4} H_0^{(1)}(k_0 r_d) \\ & + \frac{J_0(k_1 a) \times SS - \frac{S_0}{D_{out}} \frac{j}{4} H_0^{(1)}(k_0 r_{as}) D_{in} k_1 J'_0(k_1 a)}{H_0^{(1)}(k_0 a) D_{in} k_1 J'_0(k_1 a) - J_0(k_1 a) D_{out} k_0 H_0^{'(1)}(k_0 a)} H_0^{(1)}(k_0 r) \\ & + \sum_{m=2,4,6\ldots}^{m=+\infty} \frac{J_m(k_1 a) \times SS - \frac{S_0}{D_{out}} \frac{j}{4} H_0^{(1)}(k_0 r_{as}) D_{in} k_1 J'_m(k_1 a)}{H_m^{(1)}(k_0 a) D_{in} k_1 J'_m(k_1 a) - J_m(k_1 a) D_{out} k_0 H_m^{'(1)}(k_0 a)} H_m^{(1)}(k_0 r) \end{aligned} \tag{6.80}$$

Taking out the zeroth order term since all the higher order term is much smaller:

Again, with the following relation:

$$f'_0(x) = -f_1(x) \tag{6.81}$$

$$
\begin{aligned}
&G_{1,out}(r,\theta,\tau)\\
&=\frac{S_0}{D_{out}}\frac{j}{4}H_0^{(1)}(k_0r_d)+\frac{J_0(k_1a)\times SS-\frac{S_0}{D_{out}}\frac{j}{4}H_0^{(1)}(k_0r_{as})D_{in}k_1J_0'(k_1a)}{H_0^{(1)}(k_0a)D_{in}k_1J_0'(k_1a)-J_0(k_1a)D_{out}k_0H_0^{'(1)}(k_0a)}H_0^{(1)}(k_0r)\\
=&\frac{S_0}{D_{out}}\frac{j}{4}H_0^{(1)}(k_0r_d)\\
&+\frac{J_0(k_1a)\times SS+\frac{S_0}{D_{out}}\frac{j}{4}H_0^{(1)}(k_0r_{as})D_{in}k_1J_1(k_1a)}{-H_0^{(1)}(k_0a)D_{in}k_1J_1(k_1a)+J_0(k_1a)D_{out}k_0H_1^{(1)}(k_0a)}H_0^{(1)}(k_0r)
\end{aligned}
\tag{6.82}
$$

k_0 and k_1 are pure imaginary, and $k_0 = jW_0$, and $k_1 = jW_1(\tau)$.

$$
J_m(jx) = j^m I_m(x) \tag{6.83}
$$

and:

$$
H_m^{(1)}(jx) = \frac{2}{\pi} j^{-m-1} K_m(x) \tag{6.84}
$$

$$
\begin{aligned}
G_{1,out}(r,\theta,\tau) &= \frac{S_0}{D_{out}}\frac{j}{4}H_0^{(1)}(k_0 r_d)+\\
&\frac{J_0(k_1 a)[-D_{out}\frac{S_0}{D_{out}}\frac{jk_0}{4}\frac{H_1^{(1)}(k_0 r_{as})}{r_{as}}(a-r_s\cos\theta_s)]+\frac{S_0}{D_{out}}\frac{j}{4}H_0^{(1)}(k_0 r_{as})D_{in}k_1 J_1(k_1 a)}{-H_0^{(1)}(k_0 a)D_{in}k_1 J_1(k_1 a)+J_0(k_1 a)D_{out}k_0 H_1^{(1)}(k_0 a)}H_0^{(1)}(k_0 r)\\
&= \frac{S_0}{D_{out}}\frac{j}{4}[\frac{2}{\pi}j^{-1}K_0(W_0 r_d)]+\\
&\frac{I_0(W_0 a)[-D_{out}\frac{S_0}{D_{out}}\frac{-W_0}{4}\frac{\frac{2}{\pi}j^{-2}K_1(W_0 r_{as})}{r_{as}}(a-r_s\cos\theta_s)]+\frac{S_0}{D_{out}}\frac{j}{4}[\frac{2}{\pi}j^{-1}K_0(W_0 r_{as})]D_{in}jW_1[jI_1(W_1 a)]}{-[\frac{2}{\pi}j^{-1}K_0(W_0 a)]D_{in}jW_1 jI_1(W_1 a)+I_0(W_1 a)D_{out}jW_0[\frac{2}{\pi}j^{-2}K_1(W_0 a)]}\\
&\frac{2}{\pi}j^{-1}K_0(W_0 r)\\
&= \frac{S_0}{2\pi D_{out}}K_0(W_0 r_d)\\
&+\frac{I_0(W_0 a)[-D_{out}\frac{S_0}{2\pi D_{out}}\frac{W_0(a-r_s\cos\theta_s)}{r_{as}}K_1(W_0 r_{as})]-\frac{S_0}{2\pi D_{out}}D_{in}W_1 I_1(W_1 a)K_0(W_0 r_{as})}{D_{in}W_1 I_1(W_1 a)K_0(W_0 a)+D_{out}W_0 I_0(W_1 a)K_1(W_0 a)}K_0(W_0 r)\\
&= \frac{S_0}{2\pi D_{out}}\Bigg[K_0(W_0 r_d)\\
&-\frac{\frac{(a-r_s\cos\theta_s)}{r_{as}}D_{out}W_0 I_0(W_0 a)K_1(W_0 r_{as})+D_{in}W_1 I_1(W_1 a)K_0(W_0 r_{as})}{D_{in}W_1 I_1(W_1 a)K_0(W_0 a)+D_{out}W_0 I_0(W_1 a)K_1(W_0 a)}K_0(W_0 r)\Bigg]
\end{aligned}
\tag{6.85}
$$

when the source and detector are both at z-axis:

$$a-r_s\cos\theta = r_{as} \tag{6.86}$$

$$
\begin{aligned}
G_{1,out}(r,\theta,\tau) = \frac{S_0}{2\pi D_{out}}\Bigg[&K_0(W_0 r_d)\\
&-\frac{D_{out}W_0 I_0(W_0 a)K_1(W_0 r_{as})+D_{in}W_1 I_1(W_1 a)K_0(W_0 r_{as})}{D_{in}W_1 I_1(W_1 a)K_0(W_0 a)+D_{out}W_0 I_0(W_1 a)K_1(W_0 a)}K_0(W_0 r)\Bigg]
\end{aligned}
\tag{6.87}
$$

in order to simplify the solution using their respective asymptotic expression, when the argument is small, the asymptotic relation can be written as follows (We will leave K_0 modified bessel function as is since it won't help to use the asymptotic form):

$$I_0 \approx 1 \tag{6.88}$$

$$I_1 \approx \frac{x}{2} \tag{6.89}$$

$$K_1 \approx \frac{1}{x} \tag{6.90}$$

When the argument is large($\tau = \infty$), since this would only affect W_1, the asymptotic expression can be written as follows:

$$I_0 \approx I_1 \approx \frac{e^x}{\sqrt{2\pi x}} \tag{6.91}$$

In other words:

$$\frac{I_0}{I_1} \approx 1 \tag{6.92}$$

On the numerator, one approximation can be made, again, the first term is much smaller than the second term. Plus the approximation of the bessel functions.

$$
\begin{aligned}
&G_{1,out}(r,\theta,\tau)\\
&= \frac{S_0}{2\pi D_{out}}\left[K_0(W_0 r_d) - \frac{D_{out}W_0 I_0(W_0 a)K_1(W_0 r_{as}) + D_{in}W_1 I_1(W_1 a)K_0(W_0 r_{as})}{D_{in}W_1 I_1(W_1 a)K_0(W_0 a) + D_{out}W_0 I_0(W_1 a)K_1(W_0 a)}K_0(W_0 r)\right]\\
&\approx \frac{S_0}{2\pi D_{out}}\left[K_0(W_0 r_d) - \frac{D_{in}K_0(W_0 r_{as})}{D_{out}W_0\frac{I_0(W_1 a)}{W_1 I_1(W_1 a)}K_1(W_0 a) + D_{in}K_0(W_0 a)}K_0(W_0 r)\right]\\
&\approx \frac{S_0}{2\pi D_{out}}\left[K_0(W_0 r_d) - \frac{D_{in}K_0(W_0 r_{as})}{D_{out}\frac{W_0}{W_1}K_1(W_0 a) + D_{in}K_0(W_0 a)}K_0(W_0 r)\right]\\
&\approx \frac{S_0}{2\pi D_{out}}\left[K_0(W_0 r_d) - \frac{D_{in}K_0(W_0 r_{as})}{D_{out}\frac{1}{W_1(\tau)a} + D_{in}K_0(W_0 a)}K_0(W_0 r)\right]\\
&= \frac{S_0 K_0(W_0 r_d)}{2\pi D_{out}}\left[1 - \frac{D_{in}K_0(W_0 r_{as})}{D_{out}\frac{1}{W_1(\tau)a} + D_{in}K_0(W_0 a)}\frac{K_0(W_0 r)}{K_0(W_0 r_d)}\right]
\end{aligned}
\tag{6.93}
$$

in which,

$$
W_1(\tau) = \sqrt{\frac{1}{D_{in}}[\mu_a^{in} + \frac{1}{3}\mu_s' k_\lambda^2 \langle \Delta r^2(\tau)\rangle]}
\tag{6.94}
$$

Similar to the definition in the plane wave case to isolate the τ dependent term and define the following:

$$
f_1 = D_{in}K_0(W_0 r_{as})\frac{K_0(W_0 r)}{K_0(W_0 r_d)}
\tag{6.95}
$$

$$
f_2 = D_{in}K_0(W_0 a)
\tag{6.96}
$$

The normalized correlation function can be written as:

$$
\begin{aligned}
g_{1,out}(r,\theta,\tau) &= \frac{G_{1,out}(r,\theta,\tau)}{G_{1,out}(r,\theta,\tau=0)} \\
&= \frac{1-\frac{f_1}{\frac{D_{out}}{W_1(\tau)a}+f_2}}{1-\frac{f_1}{\frac{D_{out}}{W_1(\tau=0)a}+f_2}}
\end{aligned}
\tag{6.97}
$$

The above equation can be written in the form of:

$$
g_1(r,a,\theta,\tau) = \frac{1-g_1(r,a,\theta,\infty)}{1+\tau/T} + g_1(r,a,\theta,\infty)
\tag{6.98}
$$

It can be found out that:

$$
g_1(r,a,\theta,\infty) = \left[1-\frac{f_1}{f_2}\right]\left[1-\frac{f_1}{\frac{D_{out}}{a\sqrt{\frac{\mu_a^{in}}{D_{in}}}}+f_2}\right]^{-1}
\tag{6.99}
$$

$$
\begin{aligned}
T_F &= \frac{\tau(a\sqrt{c}f_2+D_{out})}{af_2(\sqrt{b\tau^2+c}-\sqrt{c})} \\
&\approx \frac{(a\sqrt{c}f_2+D_{out})}{af_2\sqrt{b}} \\
&\approx \sqrt{\frac{c}{b}} \\
&= \frac{1}{V}\sqrt{\frac{3\mu_a^{in}}{\mu_s^{in}k_\lambda^2}}
\end{aligned}
\tag{6.100}
$$

$$
\frac{1}{T_F} \approx Vk_\lambda\sqrt{\frac{\mu_s^{in}}{3\mu_a^{in}}}
\tag{6.101}
$$

And k_λ is the wave vector value at wavelength λ.

The final few equations are exactly the same as the plane wave case, except for the difference in f_1. This is lead to the same expression for the characteristic time.

6.5 Conclusion

In conclusion, this chapter we analytically solved the Helmholtz equation for two different source illumination profile. The results show that the decorrelation rate is not related to the illumination profile. The effect of different illumination profile, detector location, vessel diameter is all lumped into function f_1 which is not what we are interested in.

Chapter 6 is based on a reprint of Zhang, A.C., Lo,Y.H.,2020. Theoretical Analysis of non-invasive measurement of arterial blood flow speed. IEEE Journal of Selected Topics in Quantum Electronics. The dissertation author was the primary author of this material.

Chapter 7

Numerical Simulation: Finite Element method (FEM)

In the previous chapters, we developed the theory of photon transport described by the radiative transfer equation. For scattering dominant scattering media, the radiative equation can be simplified using the diffusion approximation which describes the photon density distribution using a diffusion equation. When the scatterers are dynamic, the radiative transfer equation can be changed into the correlation transfer equation. and the diffusion equation can be changed to incorporate the dynamic scattering part. We analytically solved a semi-infinite 2D problem with a blood vessel buried inside the scattering media (tissue) as shown in figure 7.1 with plane wave incident on the top surface. And we also analytically solved the same geometry but with an embedded point source as illustrated in figure 7.2. The plane wave and the point source illustrate the two extremes of the beam profile. In the analytical calculation, we have ignored the air-tissue boundary to simplify the solution and only the blood-tissue boundary. Furthermore, we made a series of the approximations to come up with the expression which contains clear physical meaning. The result is then compared with the experimental results. For a 3D analytical solution, it would be even more involved than it has already been for the case of 2D.

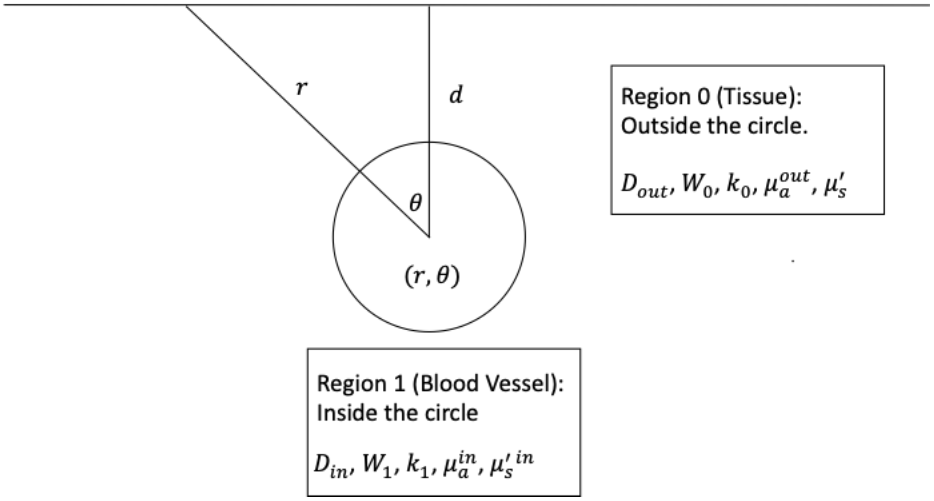

Figure 7.1: illustration of the 2D geometry with plane wave illumination, region 1 represents the blood vessel and region 0 represents the tissue

Alternatively, the diffusion equation can be solved numerically using the finite element method. In the simulation, we could consider the external boundary condition and simulate in 3D without making any additional approximations other the diffusion approximation itself. With finite element method(FEM), we would be able to validate the accuracies of the our analytical solution. However, the power of FEM method is usually diminished by it's lack of clear physical insight of the solution and cannot provide practical estimation of a measurement, in our case, the flow speed.

In the following sections, the simulation will be done using Comsol Multiphysics.

7.1 2D Simulation

In this section, I will present the simulation in a 2 dimensional geometry. Different from problem setup in the analytical approach, the blood vessel will be confined within a ”box” geometry as shown in 7.3.

The module I use in the simulation is the mathematical module as we are solving the diffusion

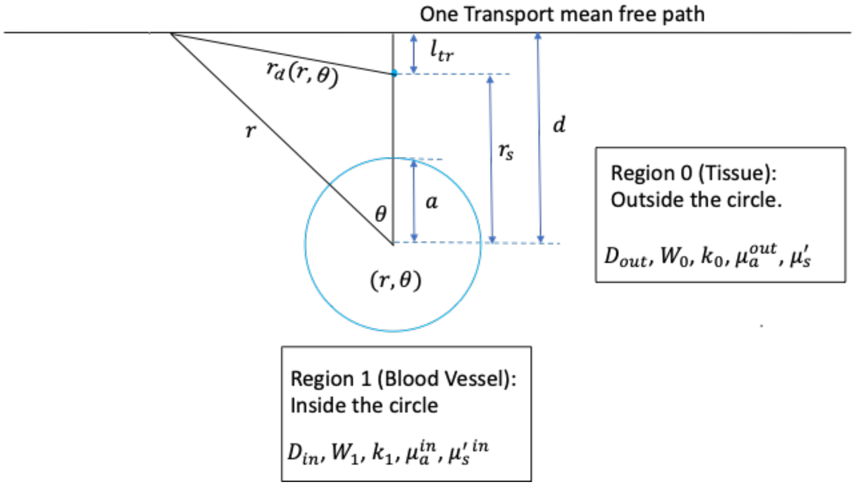

Figure 7.2: Illustration of the illumination profile using point source approximation, the point source is located at one transport mean free path below the surface

equation.

7.1.1 Collimated Incident Beam

For a collimated incident beam, the trangular mesh used in the simulation is shown in figure 7.4.

For the boundary condition of air-tissue interface, recall equation (**??**) which is rewritten here:

$$U(\vec{r}) - 2D\nabla U(\vec{r}) \cdot \hat{n} = 0 \tag{7.1}$$

This is a robin type boundary condition, which contains the derivative and its value at the boundary. As shown in figure 7.5, the 4 external boundary that is labeled as 1,2,3,4 are the boundaries using the robin boundary condition. The internal boundary condition, 5,6,7,8 is automatically handled by comsol using the continuity boundary condition. For the internal boundary condition, we have previously discussed analytically, essentially, it requires the photon density and photon flux both to be continuous at the interface.

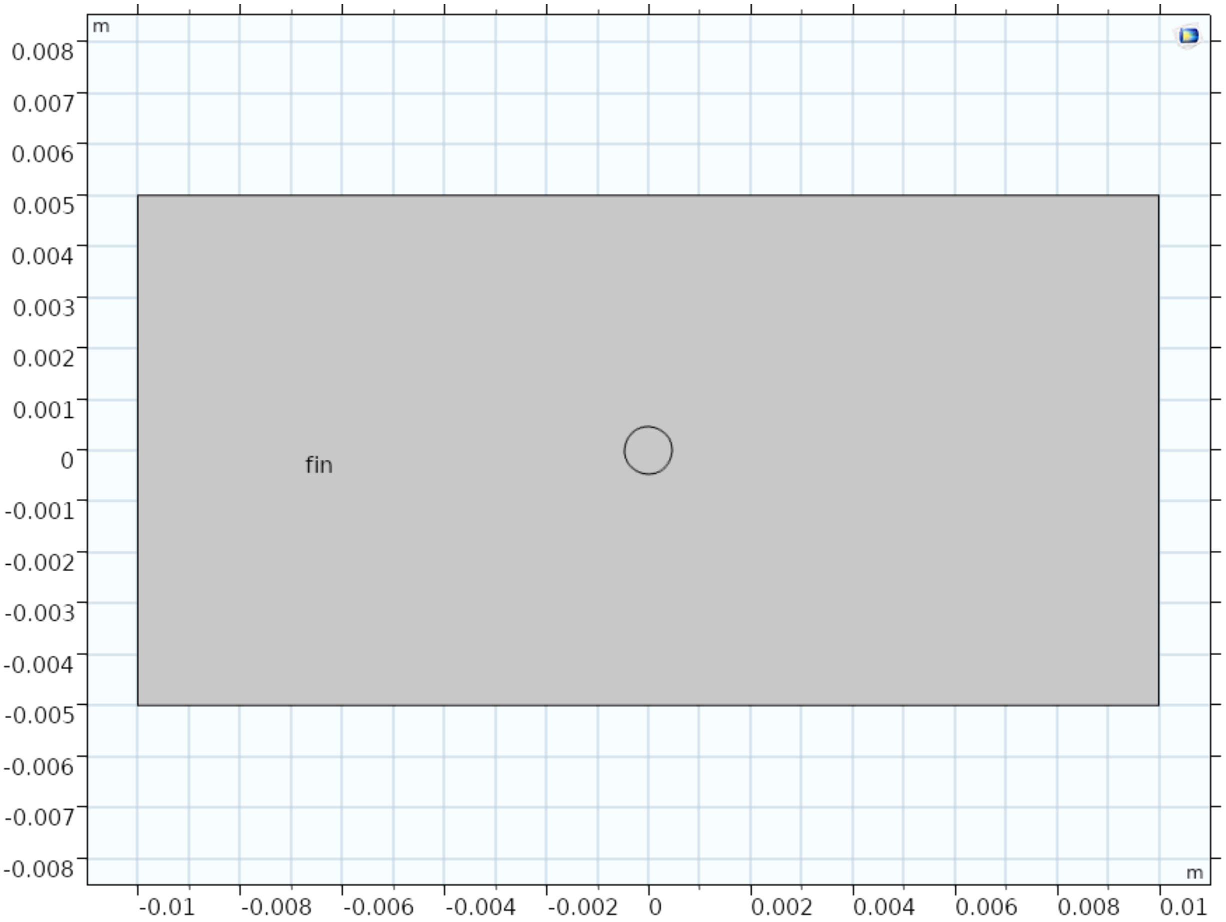

Figure 7.3: 2D Simulation Geometry, the center circle represents the blood vessel, and the area outside represents the tissue

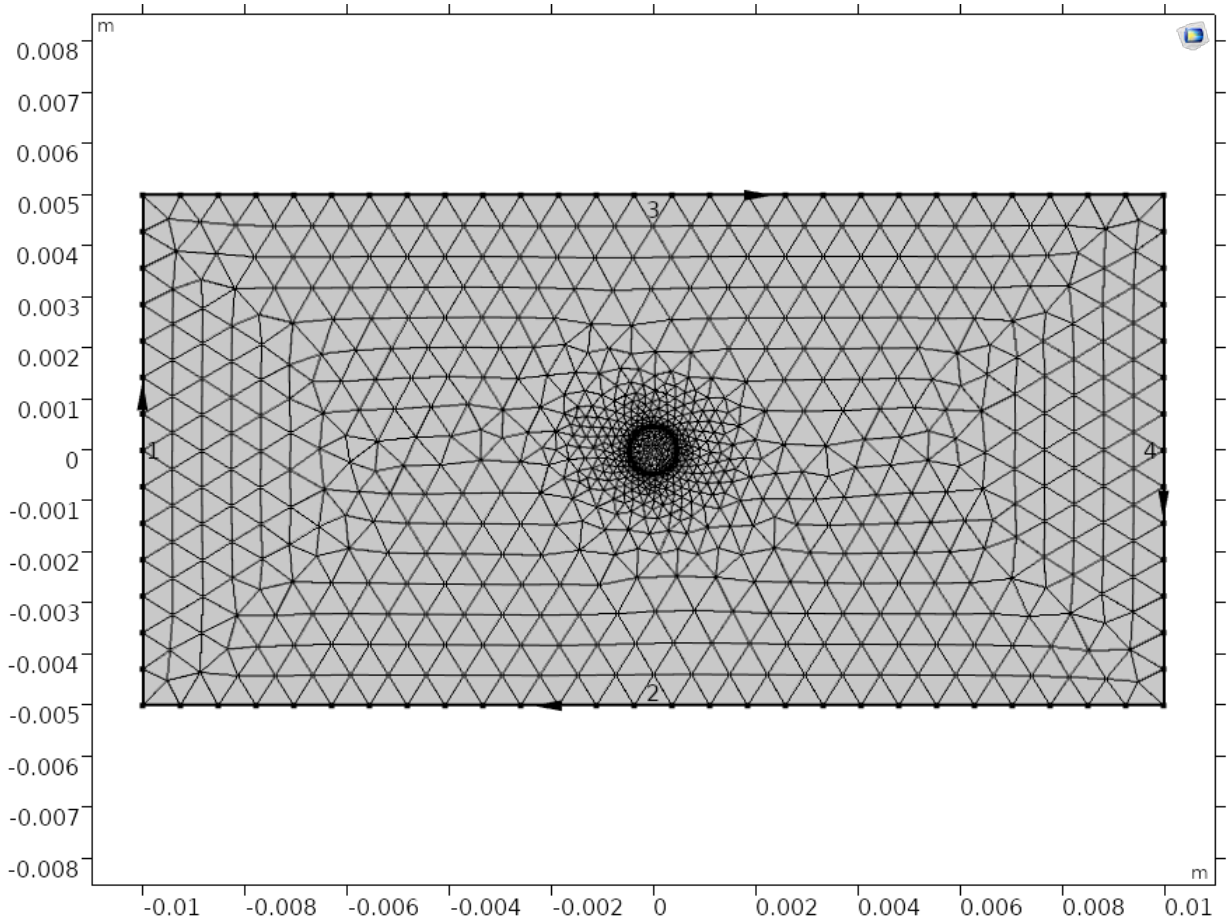

Figure 7.4: 2D Trangular mesh for plane wave illumination and the mesh is chosen such that there are sufficient resolution at the boundary

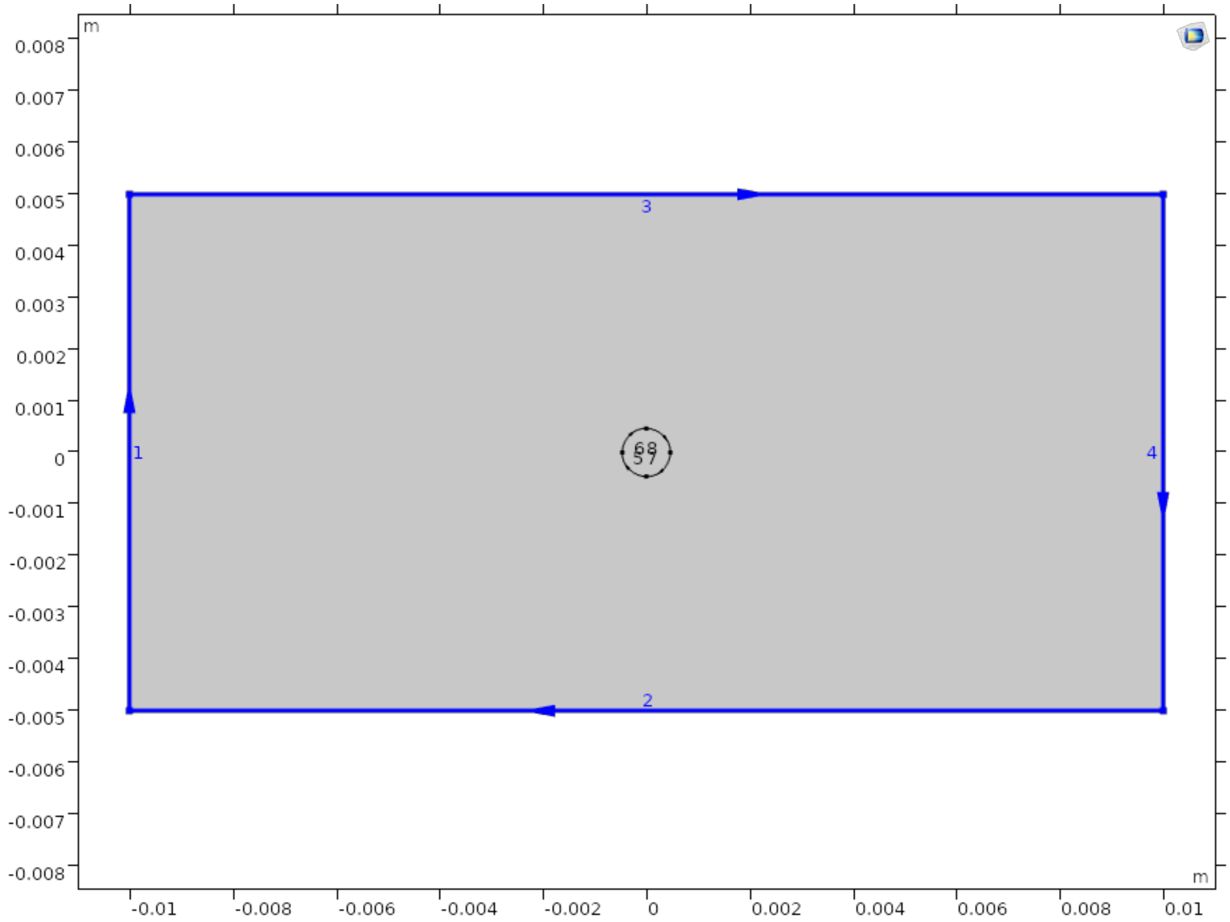

Figure 7.5: Boundary condition for 2D structure. 1,2,3,4 represents the external boundary, 5,6,7,8 represents the internal boundary

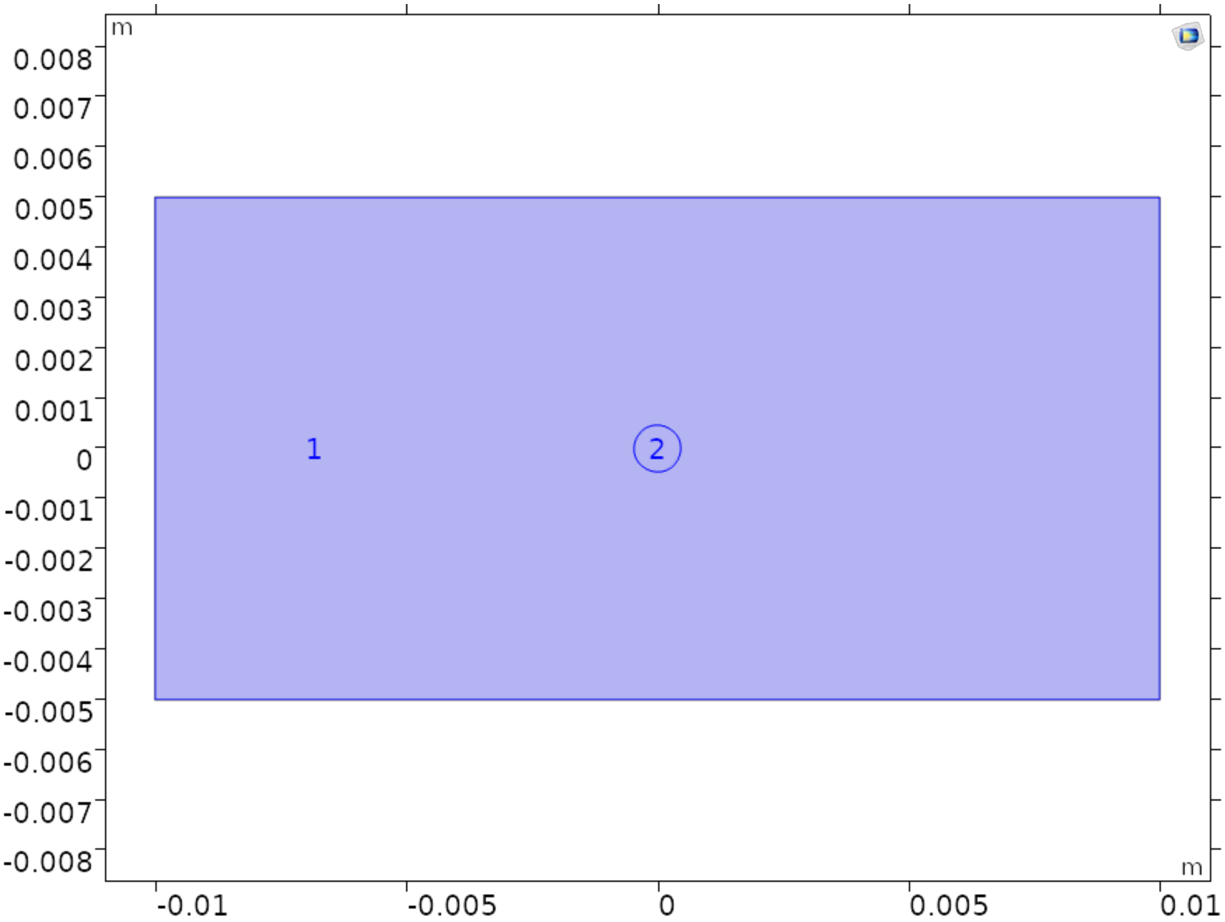

Figure 7.6: Two sets of Helmholtz equations are solved, region 1 represents the tissue, region 2 represents the blood vessel.

Two sets of Helmholtz equations are solved with different parameters in region 1(tissue) and region 2(blood vessel) as shown in figure 7.6. Specifically, in region 1, the Helmholtz equation is solved:

$$[\nabla^2 + k_1^2]G_1(\vec{r}, \tau) = -\frac{S(\vec{r})}{D} \tag{7.2}$$

in which

$$k_1 = jW_1(\tau) \tag{7.3}$$

$$W_1(\tau) = \sqrt{\frac{1}{D_{in}}[\mu_a^{in} + \frac{1}{3}\mu_s' k_\lambda^2 \langle \Delta r^2(\tau) \rangle]} \tag{7.4}$$

And in region 2, inside the vessel, the following Helmholtz equation is solved:

$$[\nabla^2 + k_2^2]G_1(\vec{r},\tau) = -\frac{S(\vec{r})}{D} \tag{7.5}$$

in which

$$k_2 = jW_2(\tau) \tag{7.6}$$

$$W_2 = \sqrt{\frac{\mu_a^{out}}{D_{out}}} \tag{7.7}$$

As previously mentioned, as the speed of light is much faster than the movement of particles, all the equation we solve is the steady state version of the transport equation and diffusion equation. In the simulation, time delay τ is considered as a parameter to the equation. In order to see the results at different time delay, many iterations of the equation need to be solved.

Figure 7.7 is showing the photon intensity distribution at $\tau = 0$. The source is a collimated beam with a gaussian profile impinging from the top surface, the FWHM is set to be $3.2mm$.

With the simulation condition listed above, for a detection point in figure 7.8, we could plot the electrical field correlation function in figure for different flow speed.

7.1.2 Point Source illumination

For a similar setup as the case of plane wave, with the difference in the trangular mesh setup as can be seen from figure 7.10.

Similar to the detection point shown on figure 7.8, the electrical field autocorrelation can be plotted in figure 7.11:

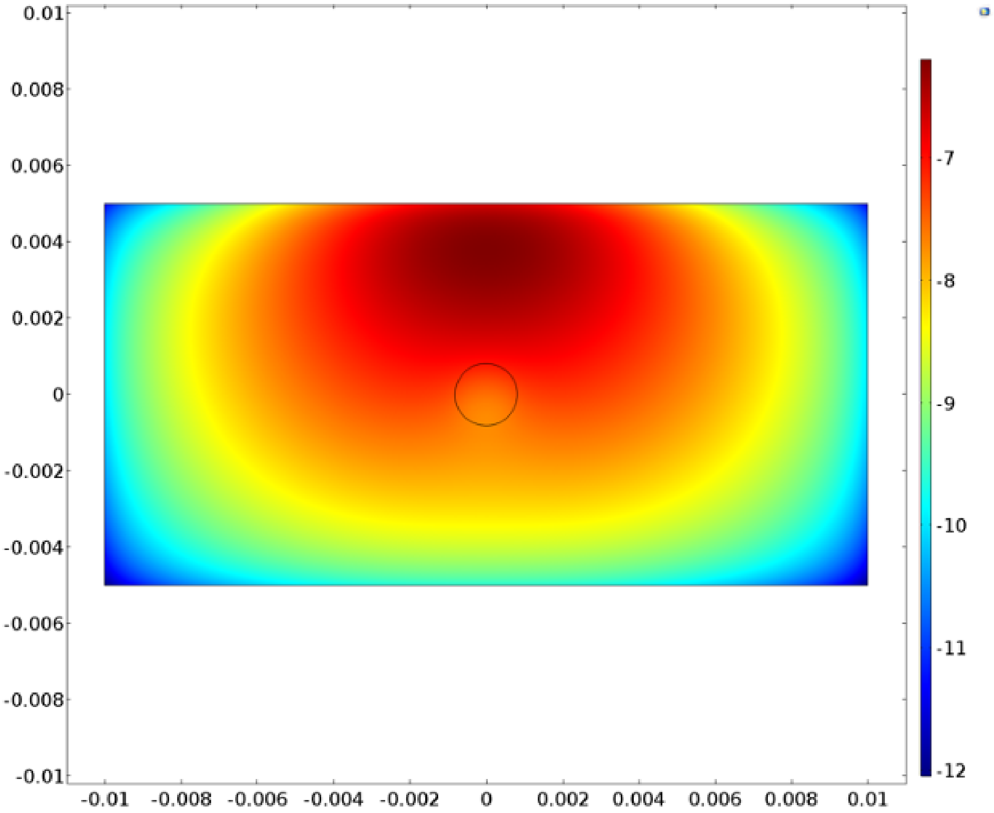

Figure 7.7: Photon density color map at $\tau = 0$. The source is a collimated beam with a gaussian profile impinging from the top surface, the FWHM is set to be 3.2*mm*.

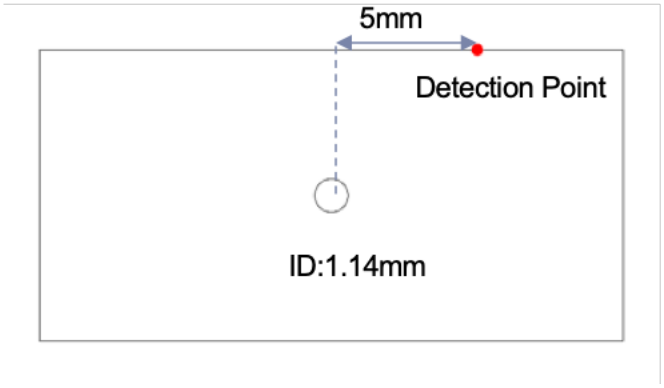

Figure 7.8: Location of the point detection, this applies to both the 2D and 3D simulation

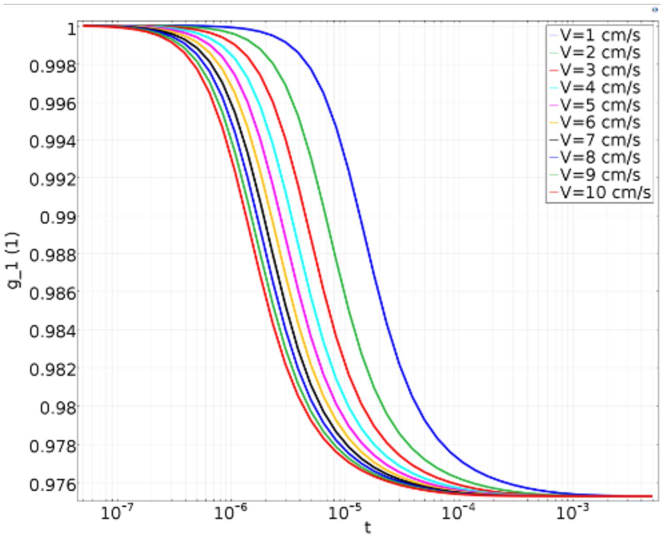

Figure 7.9: g_1 plot, for a 2D geometry, with a collimated beam with gaussian profile impinging the surface, the detection point is chosen 5mm away from the center of the top surface.

7.2 3D Simulation

7.2.1 Collimated incident beam

In additional to the 2D geometry, a more realistic 3D structure is also simulated. Figure 7.12 shows the geometry used in the Comsol simulation. And figure 7.13 shows the 3D trangular mesh used under plane wave illumination. And figure 7.14 is the X-Y view of Photo density distribution in the 3D geometry with a circular Gaussian beam illumination with FWHM of 3.2mm illuminating from the top surface. This is the initial state of photon distribution in the medium ($\tau \approx 0$).

And figure 7.15 is the Y-Z view of Photo density distribution in the 3D geometry with a circular Gaussian beam illumination with FWHM of 3.2mm illuminating from the top surface(X-Y surface). This is the initial state of photon distribution in the medium ($\tau \approx 0$).

And the simulated electrical field correlation is shown in figure 7.16. And this is for a detection point illustrated by 7.8 at plane of $x = 0$ as shown in figure 7.15.

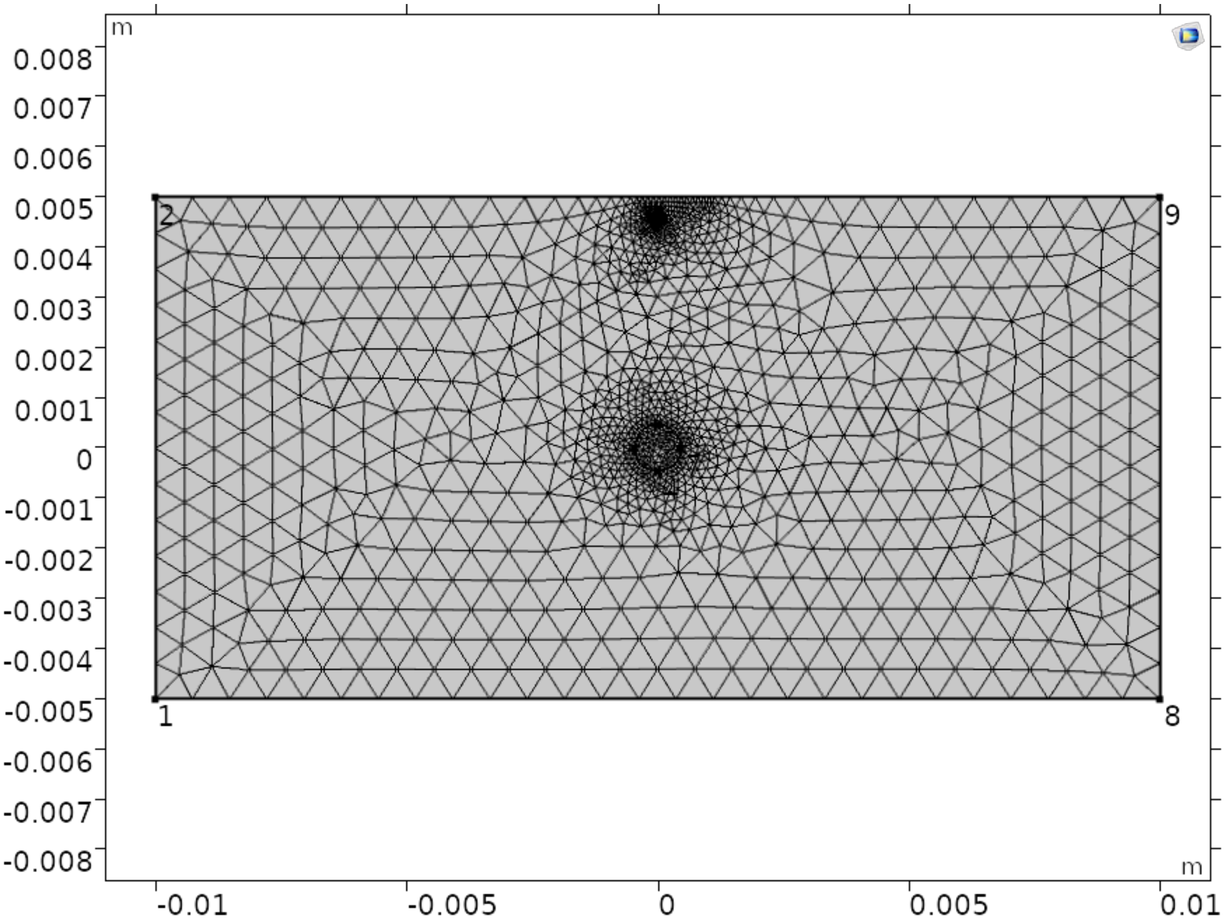

Figure 7.10: Trangular mesh setup for point source illumination and the mesh is chosen such that there are sufficient resolution at the point source and the boundary

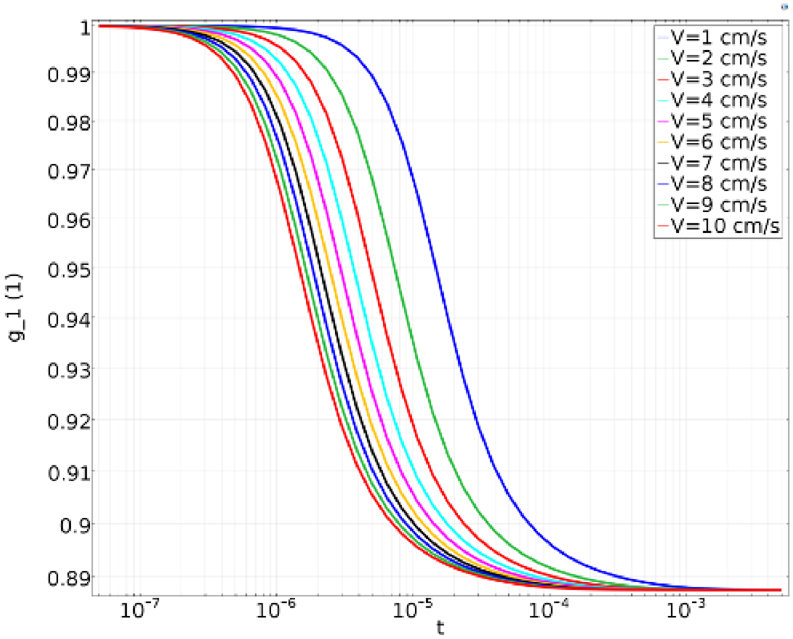

Figure 7.11: g_1 plot of 2D simulation with point source illumination for different flow speed.

7.2.2 Point Source illumination

Similar to the 2D simulation, using the point source approximation, an equivalent point source is placed inside the medium with a depth of one transport mean free path. The 3D mesh with inclusion of a point source is illustrated in figure 7.17. The photon density plots in X-Y view can be illustrated in figure 7.18, the Y-Z view can be illustrated in figure 7.19. And the simulated electrical field correlation is shown in figure 7.16. And this is for a detection point illustrated by 7.8 at plane of $x = 0$ as shown in figure 7.15.

Chapter 7 is based on a reprint of Zhang, A.C., Lo,Y.H.,2020. Theoretical Analysis of non-invasive measurement of arterial blood flow speed. IEEE Journal of Selected Topics in Quantum Electronics. The dissertation author was the primary author of this material.

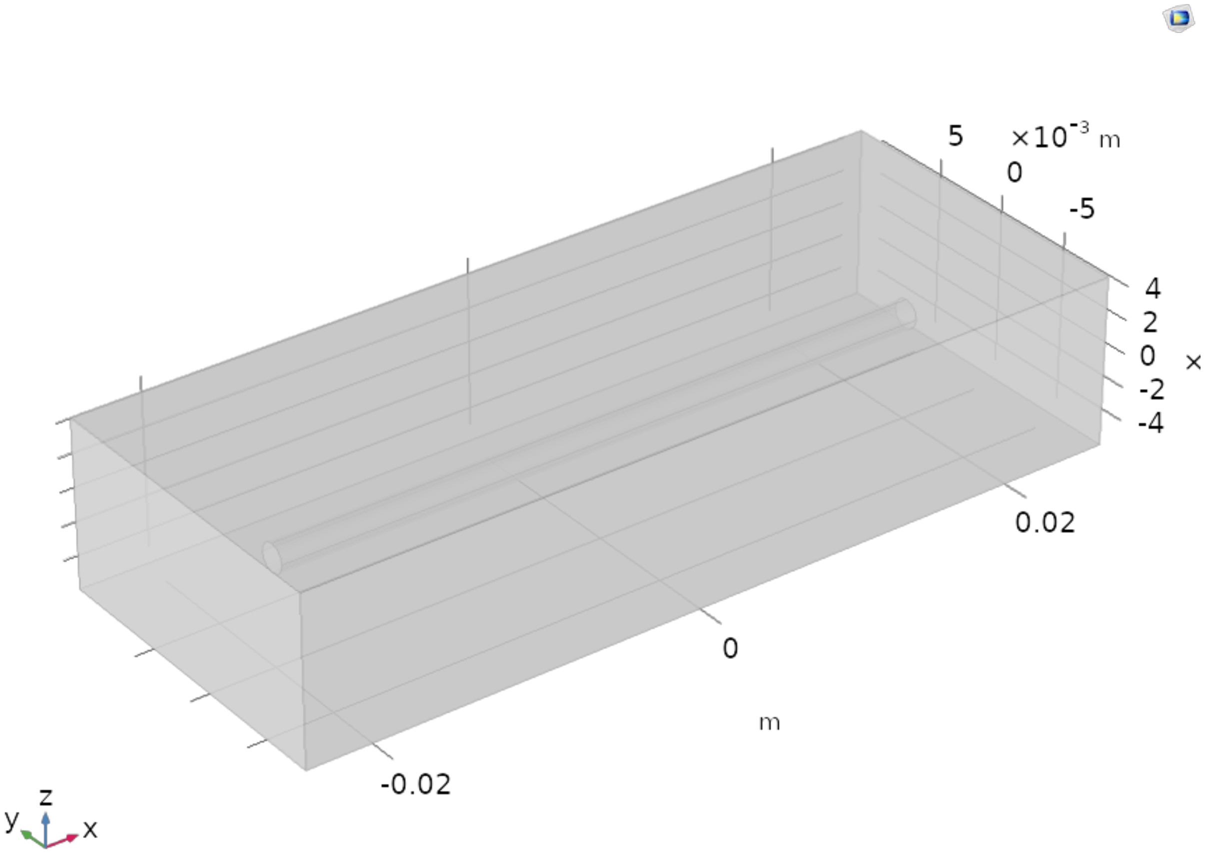

Figure 7.12: 3D geometry used for Comsol simulation, the glass tube embedded represents the blood vessel.

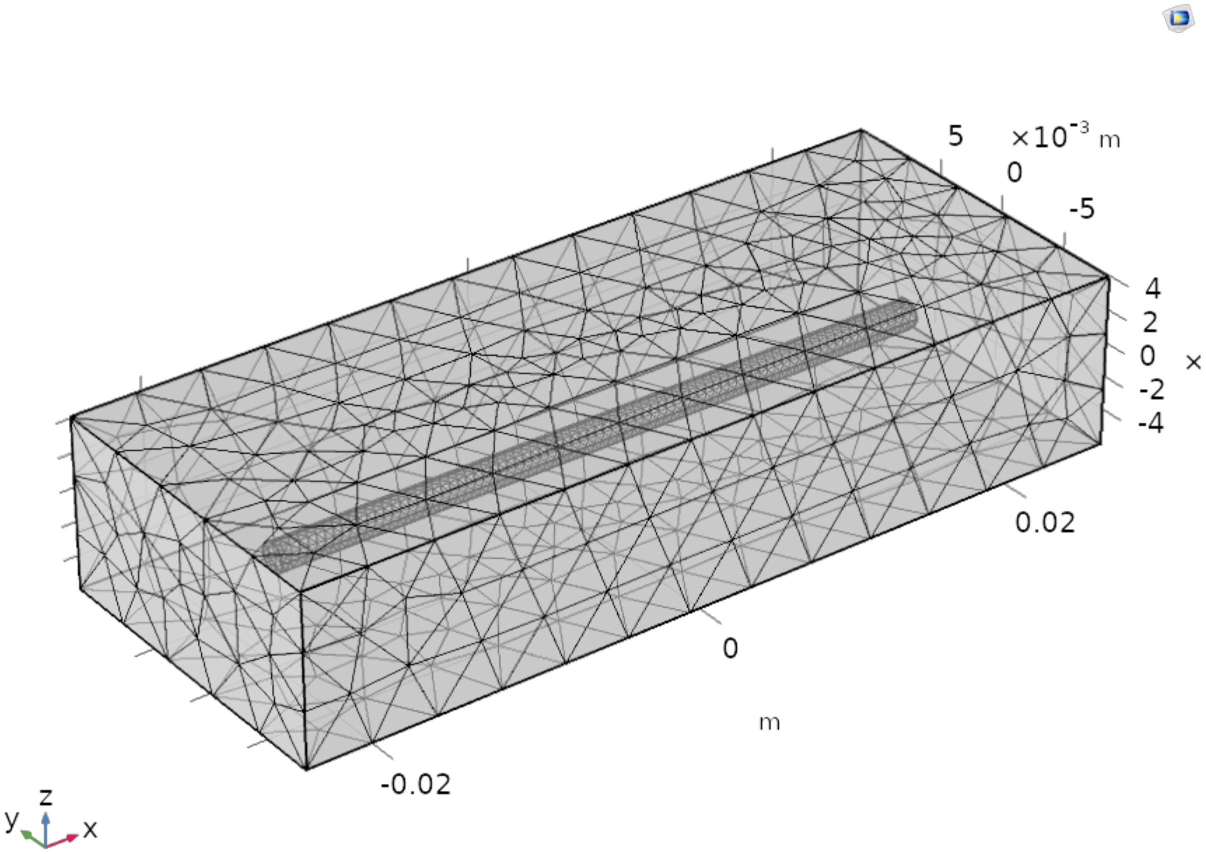

Figure 7.13: 3D trangular mesh usd under plane wave illumination and the mesh is chosen such that there are sufficient resolution at the interface.

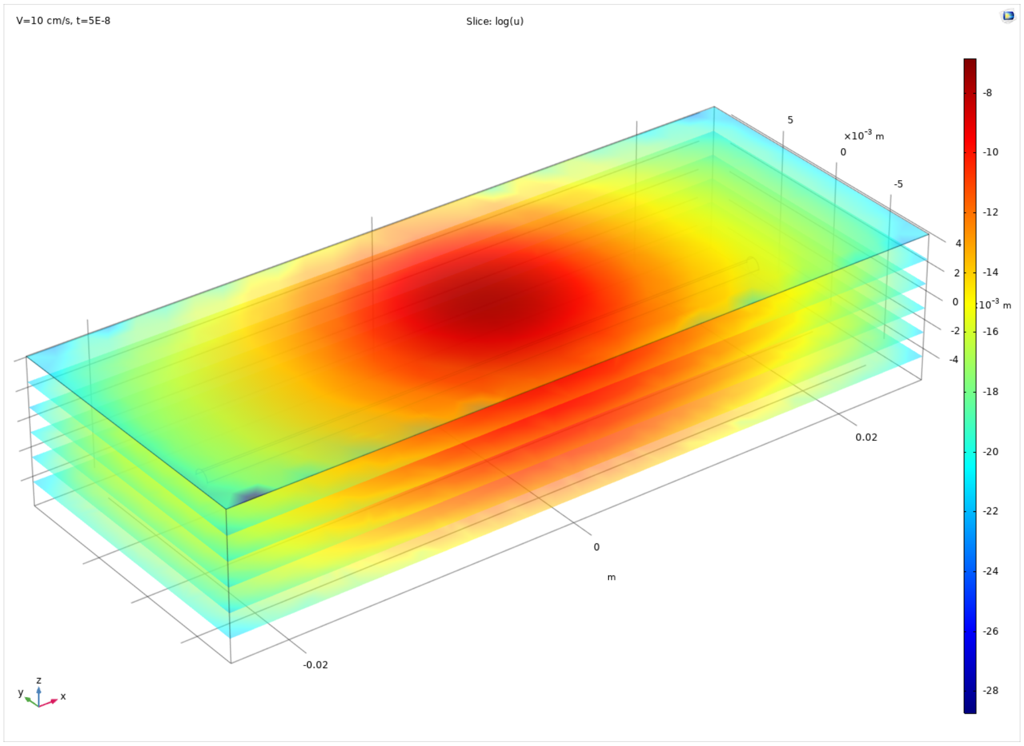

Figure 7.14: X-Y view of Photo density distribution in the 3D geometry with a circular Gaussian beam illumination with FWHM of 3.2mm illuminating from the top surface. This is the initial state of photon distribution in the medium ($\tau \approx 0$).

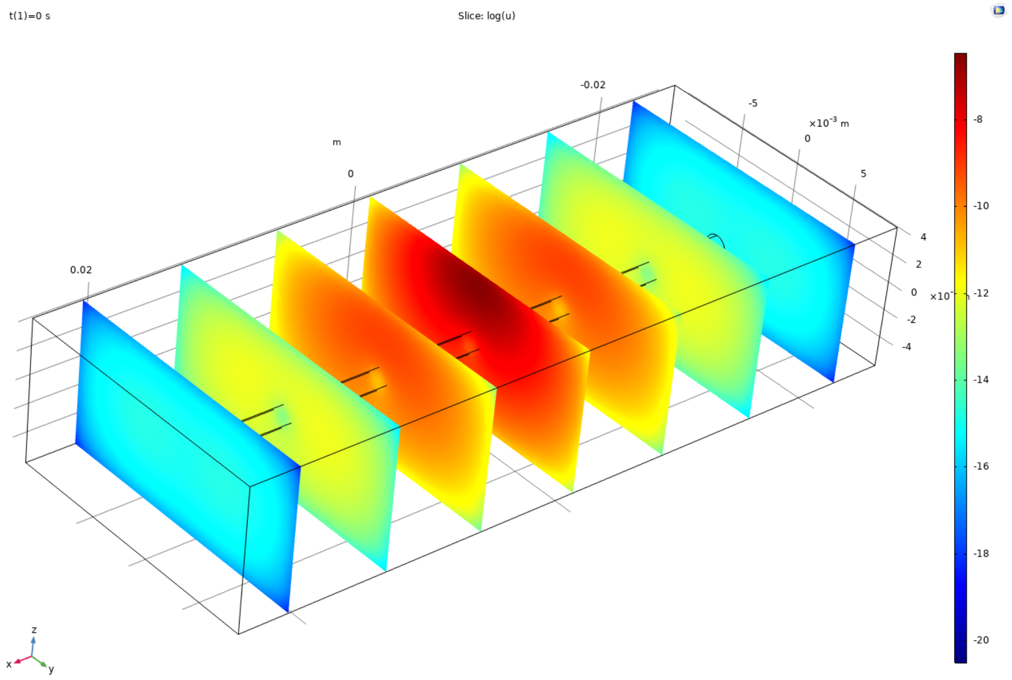

Figure 7.15: Y-Z plane slices of field distribution using a Gaussian beam illumination with FWHM of 3.2mm.

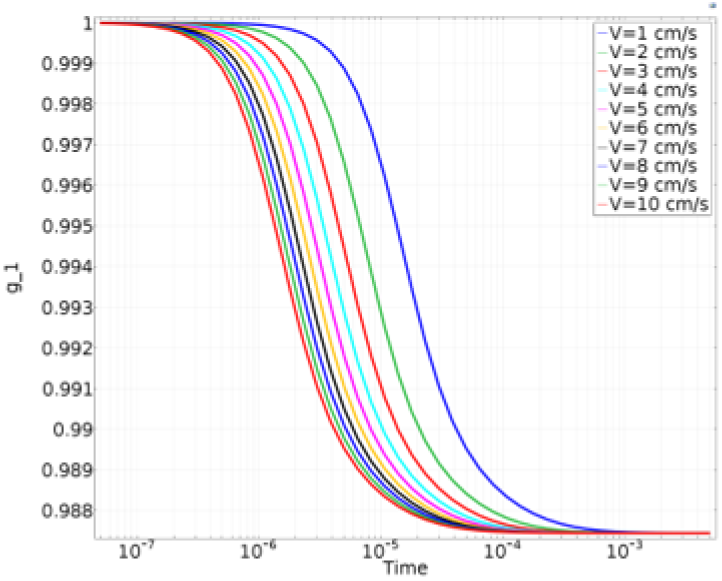

Figure 7.16: g_1 plot for 3D simulation using collimated beam with a circular Gaussian beam profile with a FWHM of 3.2mm.

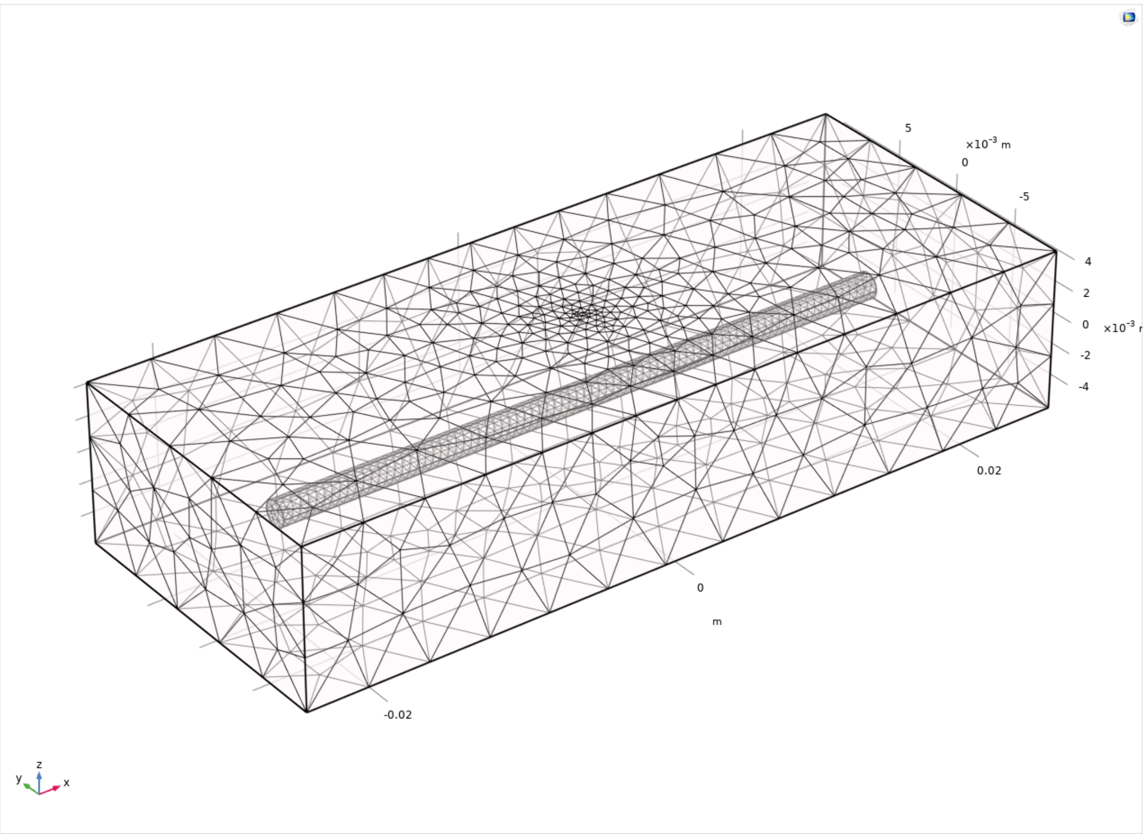

Figure 7.17: Compared to the mesh used in the plane illumination, the 3D mesh for point source illumination is constructed so that sufficient precision is considered close to the point source.

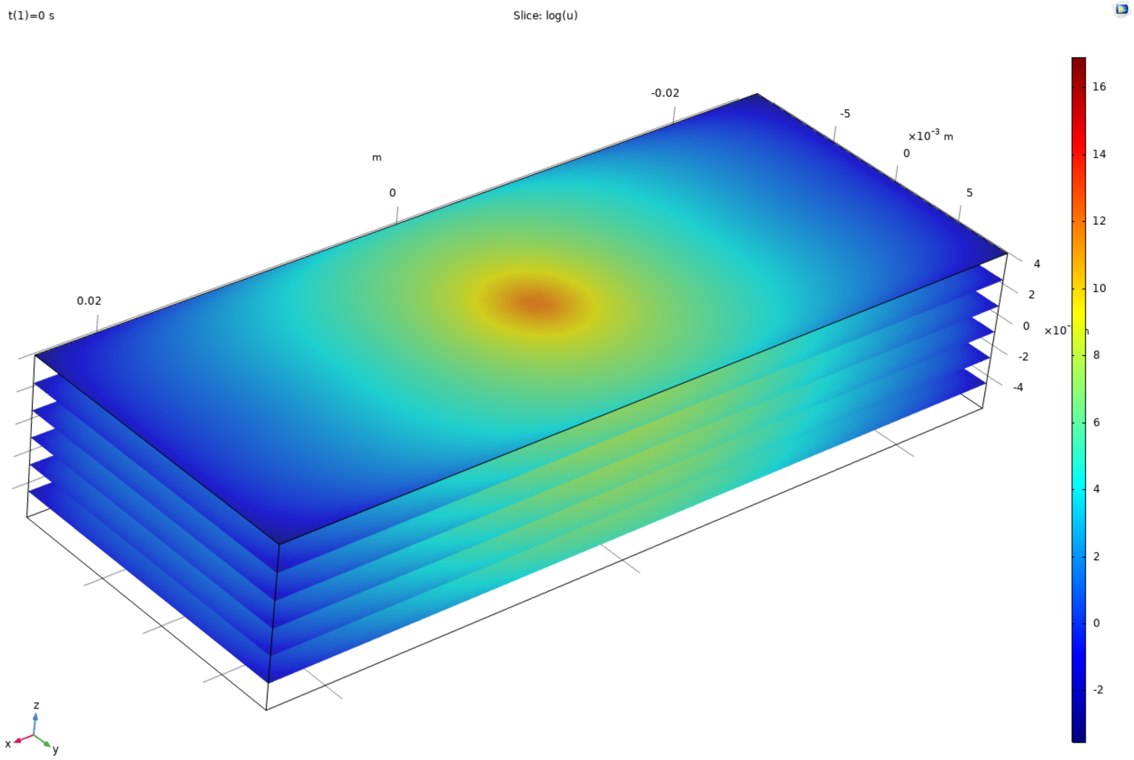

Figure 7.18: X-Y view of photon density distribution for point source illumination at $\tau = 0$

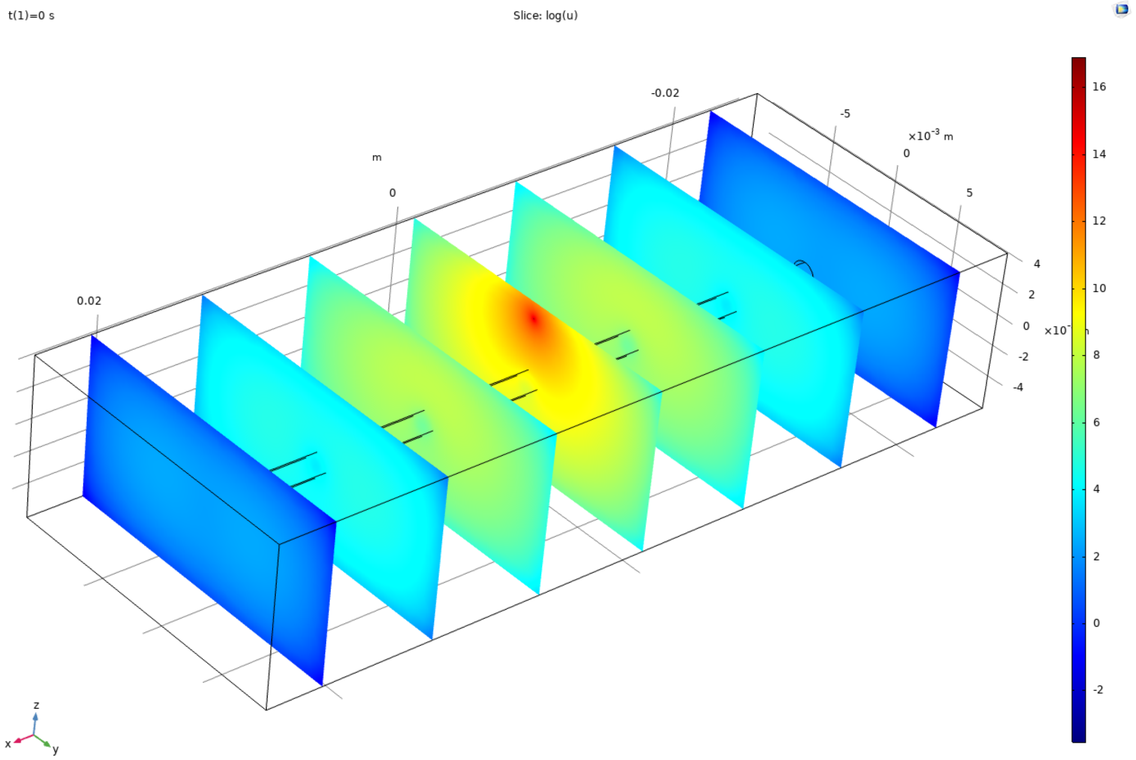

Figure 7.19: Y-Z view of photon density distribution for point source illumination at $\tau = 0$

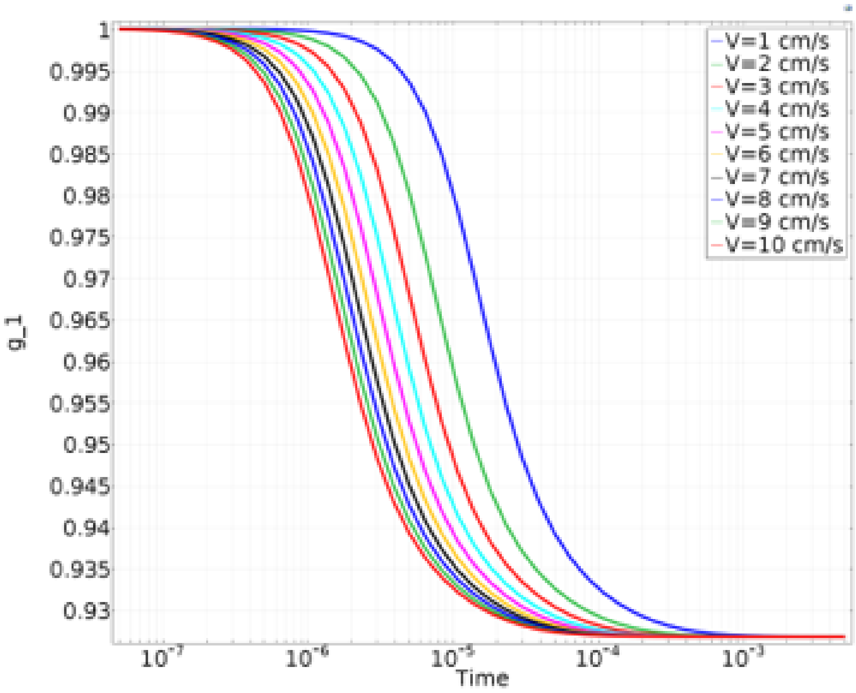

Figure 7.20: g_1 plot for an equivalent point source illumination for different flow speed

Chapter 8

Further Discussion

8.1 Dominant Force for the De-correlation Process

As we previous demonstrated, there are two type of forces as indicated in the following equation:

$$\langle \Delta r^2(\tau) \rangle = 6D_\alpha \tau + \bar{V}^2 \tau^2 \tag{8.1}$$

In the previous discussions, we have concluded that in the range of flow rate, and size of the vessel diameter, the second term will be dominant. This comes from the fact that the de-correlation rate is proportional to the flow rate and is not a function of blood vessel diameter. In other words, if we plot the de-correlation rate versus flow speed for all different diameter sizes, if the de-correlation rate is also dependent on the vessel diameter, the curves would not be collapsed into one curve. Experimentally, we could see from figure 8.1. The experimental data can be represented by the expression derived previously:

$$\frac{1}{T_F} \approx V k_\lambda \sqrt{\frac{\mu_s^{in}}{3\mu_a^{in}}} \tag{8.2}$$

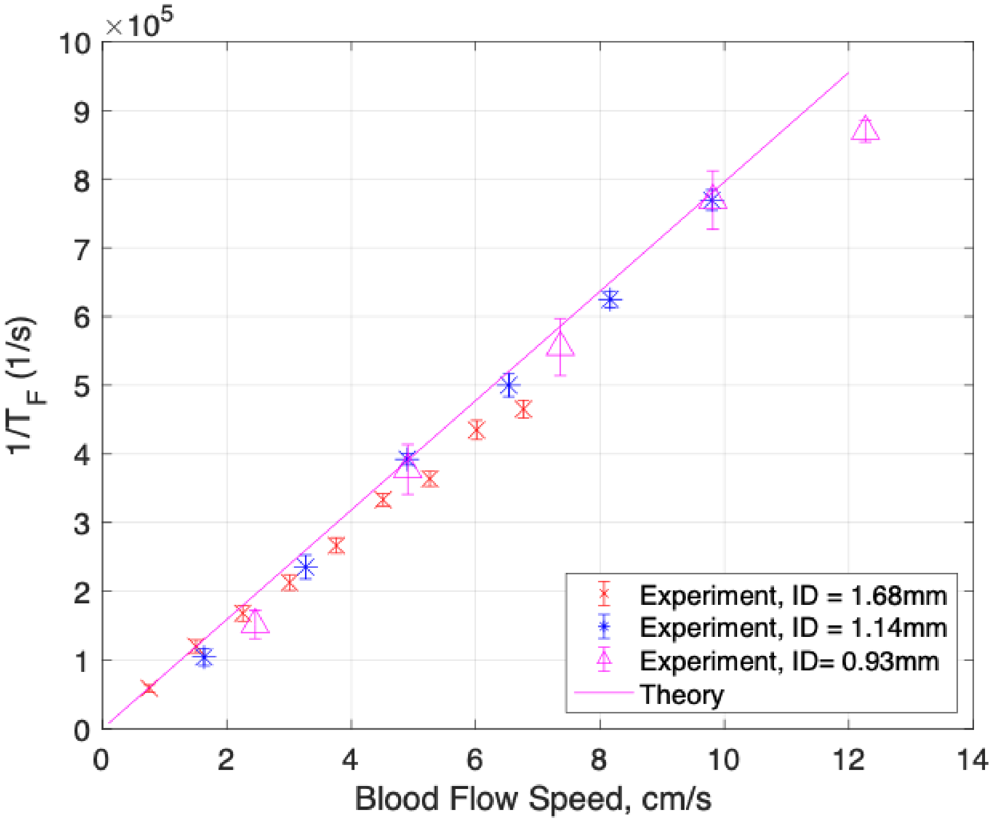

Figure 8.1: The De-correlation rate Versus speed plot for different tube diameters, the theoretical fitting is followed by equation 8.2. The 3 curves collapsed into one curve indicating the proposed hypothesis.

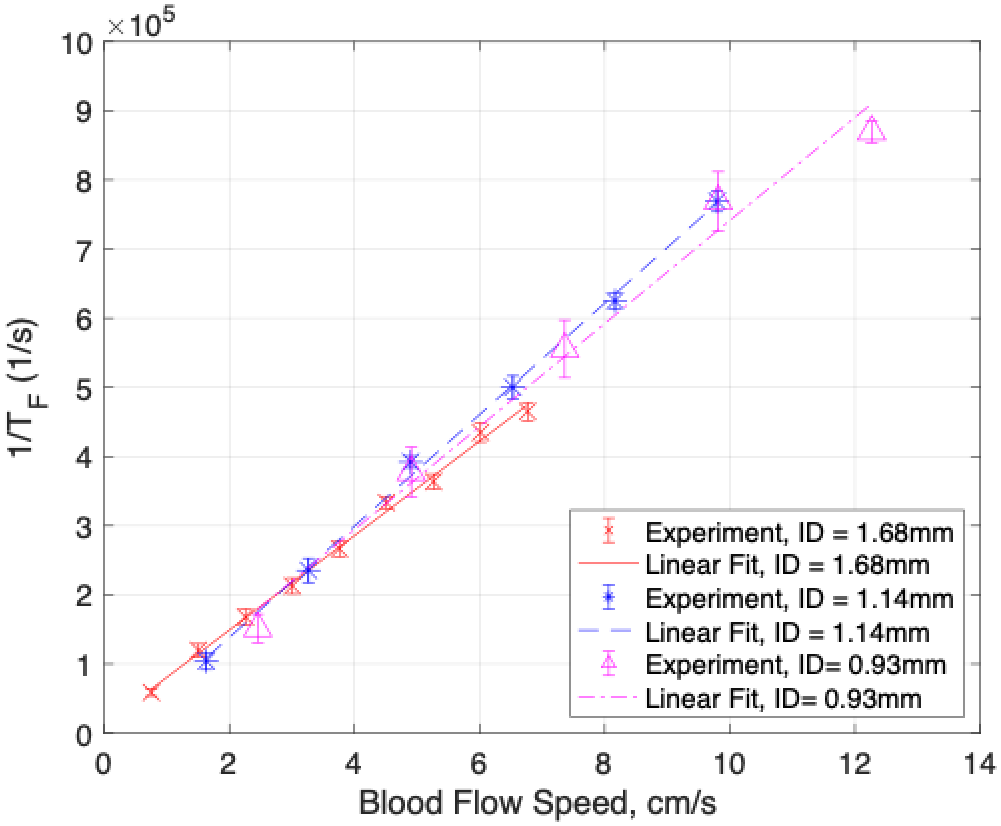

Figure 8.2: Experimentally measured de-correlation rate Versus flow speed in different vessel diameters

To further illustrate this point, in figure8.2 ,the de-correlation rate versus flow speed is plotted to be compared with figure 8.3, where the de-correlation rate versus shear rate is plotted. Clearly, from the experiment, we can verify our hypothesis. The first term,i.e. the diffusion term is usually dominate in slower flow and for smaller vessels.

8.2 Inflection point and it's derivative

In the beginning of the thesis, we defined the inflection point as the characteristic time as shown in figure 8.4. However, it looks like that the inflection point is actually not so obvious from the plot. In this section, I will demonstrate a way to clearly find the inflection point. For the g_1 plot, if taking the derivative, we can clearly see the inflection point. In figure, we

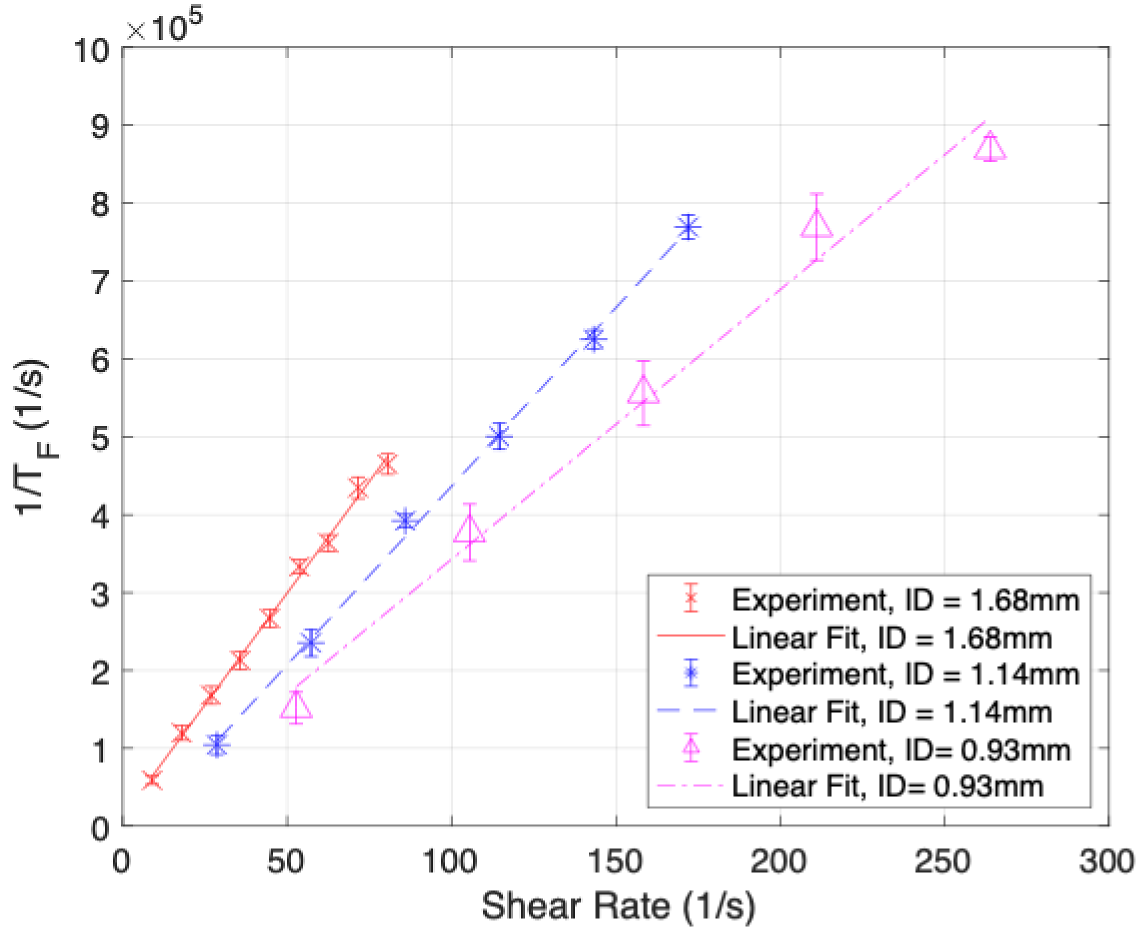

Figure 8.3: Experimentally measured de-correlation rate Versus shear rate in different vessel diameters

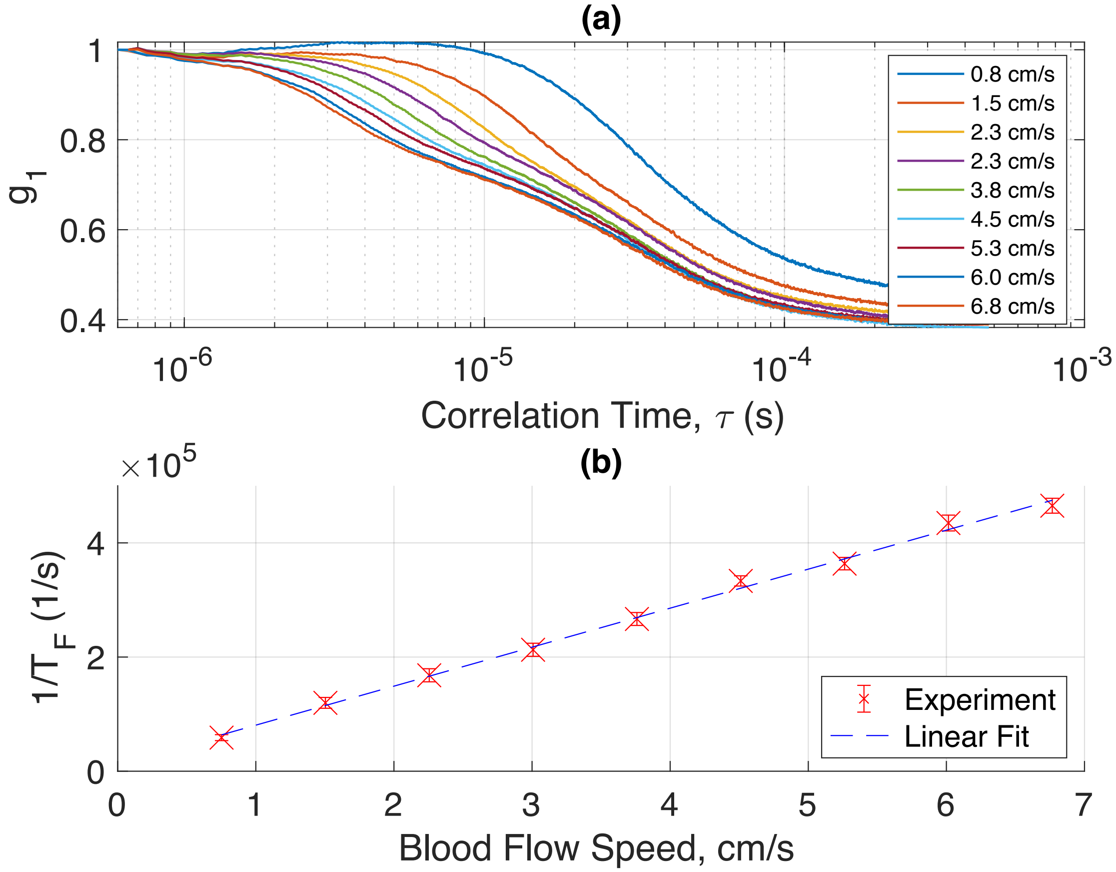

Figure 8.4: figure (a) g_1 plot for tube diameter of 1.68mm, figure (b) is a linear fit of calculated blood flow speed

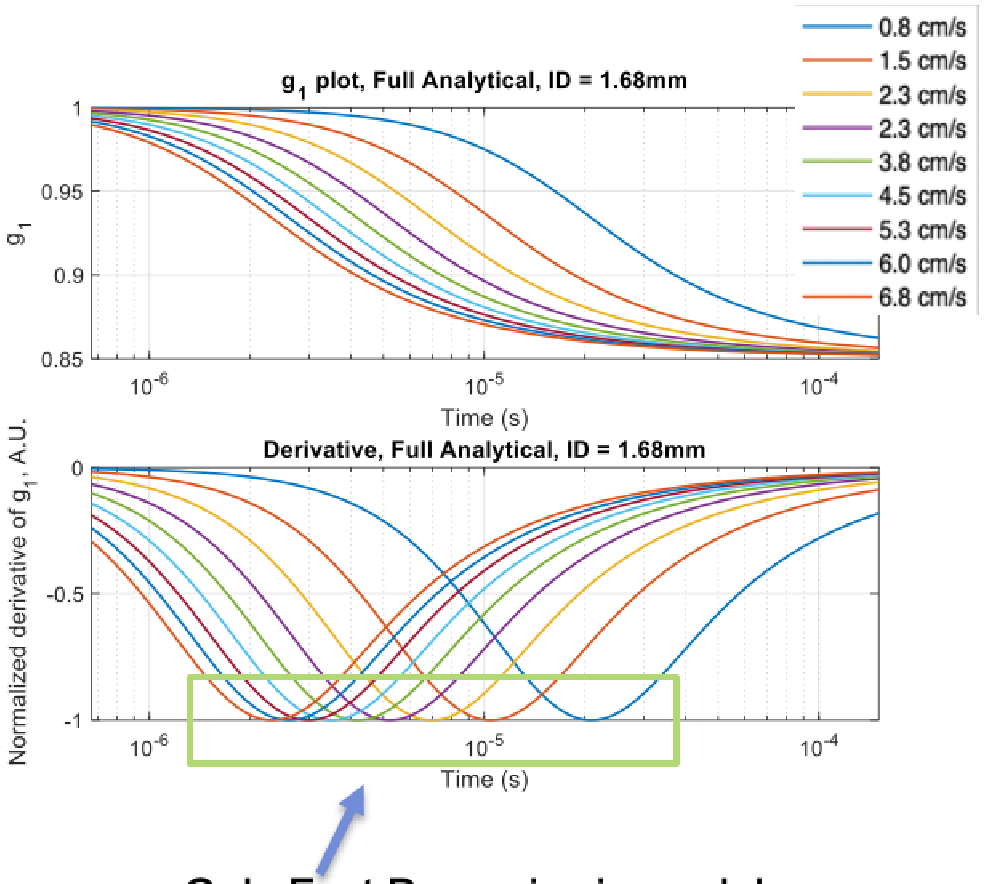

Only Fast Dynamics in model

Figure 8.5: The calculated normalized field correlation and its derivative, only the fast dynamics, i.e. the convective flow is included in the model.

demonstrate the theoretical field correlation curves g_1 using the following equation (8.3) as previously derived in chapter 6.

$$G^{s}_{1,out}(r,\theta,\tau) = \sum_{m=-\infty}^{m=+\infty} B j^{m} \frac{D_{in}k_1 J'_m(k_1 a) J_m(-k_t a) + D_{out} k_t J_m(k_1 a) J'_m(-k_t a)}{D_{out} k_0 J_m(k_1 a) H'^{(1)}_m(k_0 a) - D_{in} k_1 J'_m(k_1 a) H^{(1)}_m(k_0 a)} H^{(1)}_m(k_0 r) e^{jm\theta} \tag{8.3}$$

The calculated normalized field correlation and its derivative can be illustrated as in figure 8.5. The experimentally measured normalized field correlation and its derivative can be illustrated as in figure 8.6. Although the g_1 curve looks different from the theoretical curve, but if we focus

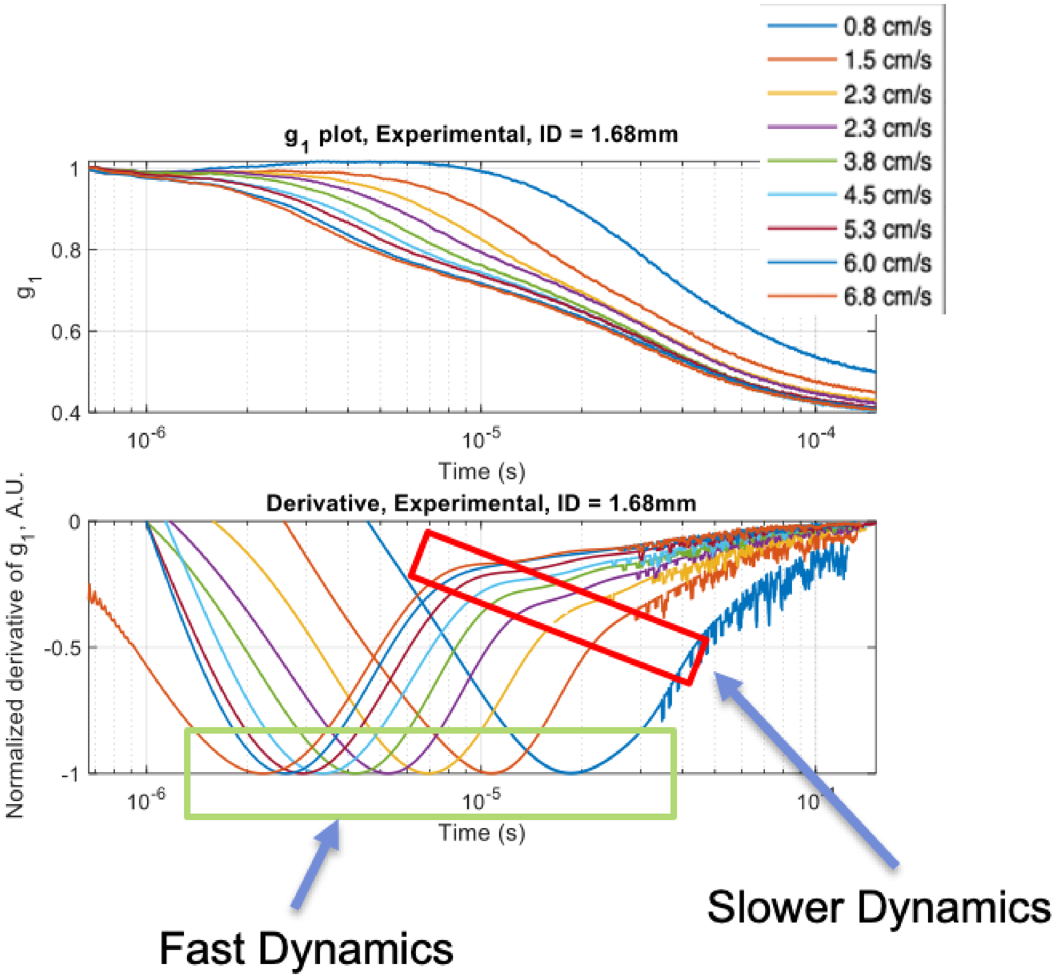

Figure 8.6: Comparison of the fast flow dynamics and slow flow dynamics. The fast dynamics is the convection flow and flower dynamics is caused by the diffusion motion.

only on the fast dynamics, we could see that the correlation time is almost identical. For the experiment, we also observed a slower dynamics which could be caused by the diffusive motion of blood cells. In this speed range, the two modes of motion are separated in time. We could simply focus on the fast flow dynamics.

Chapter 8 is based on a reprint of Zhang, A.C., Lo,Y.H.,2020. Theoretical Analysis of non-invasive measurement of arterial blood flow speed. IEEE Journal of Selected Topics in Quantum Electronics. The dissertation author was the primary author of this material.

Chapter 9

Conclusion

In this work, we demonstrated a simple technique to directly measure the blood flow speed in main arteries based on the diffused light model. The device uses a single fiber bundle, a diode laser, and a photoreceiver. The concept is demonstrated with a phantom that uses intralipid hydrogel to model the biological tissue and an embedded glass tube with flowing human blood to model the blood vessel. The correlation function of the measured photocurrent was used to find the electrical field correlation function via the Siegert Relation. Interestingly the measured electric field correlation function $g_1(\tau)$ and $\ln(T_F)$ shows a relation similar to the Fermi-Dirac function, allowing us to define the $ln(\tau)$, equivalent to the "Fermi energy" occurring at the first inflection point of $g_1(\tau)$. Surprisingly, the value $1/T_F$, which we call characteristic decorrelation rate, is found to be linearly proportional to the blood speed and is independent of the diameter of the tube diameter over the size and speed ranges for major arteries. This striking property can be explained by an approximate analytic solution for the diffused light equation in the regime where the convective flow would dominate the decorrelation. This discovery is highly significant because, for the first time, we can use a simple device to directly measure the blood speed in major arteries without any prior knowledge or assumption about the geometry or mechanical properties of the blood vessels. A non-invasive method of measuring arterial blood speed produces important information about health conditions. Although the device and setup can be further optimized (e.g. adding different light wavelengths) and the physical model can be expanded to acquire more information from the measurements, the work has paved its way to a new promising modality for measurements of blood supplies to vital organs.

Chapter 9 is based on a reprint of Zhang, A.C., Lo, Y.H., 2020. Non-invasive optical Measurement of arterial blood flow speed. *Biomedical Optics Express (under peer review)*. The dissertation author was the primary author of this material.

Nomenclature

α_s	Diffusion Cross Section for Blood Cells	$10^{-12} m^2$
β	Coherence factor, related only to collection optics	$unitless$
η	impedance	Ω
λ_0	Wavelength of the incident CW coherent source	$785\,nm$
μ'_{tr}	Reduced transport coefficient	m^{-1}
μ_a	Absorption coefficient	m^{-1}
μ_a^{in}	Absorption coefficient inside the cylinder, blood	$1/m$
μ_a^{out}	Absorption coefficient outside the cylinder, tissue	$1/m$
μ_s	Scattering coefficient	m^{-1}
μ'_s	Reduced scattering coefficient	m^{-1}
$\Psi(t)$	Wave function of the scalar field	$\sqrt{W}/m$
ρ	Number Density	$\#/m^3$
σ_a	Absorption cross section	m^2
σ_s	Scattering cross section	m^2

σ_t	Total cross section, absorption + scattering	m^2
θ	Angle of incident relative to z-axis	rad
$\vec{r}$	Position Vector referenced to the origin of the coordinate system	m
$\vec{r}_s$	Position vector of the virtual point source referenced to the origin of the coordinate system	m
a	Radius of the cylinder	m
D',D,D_γ	Photon Diffusion Coefficient	m
D_b	Diffusivity for Blood Cells	m^2/s
D_{in}	Photon diffusion coefficient for inside the cylinder,blood	m
D_{out}	Photon diffusion coefficient for outside the cylinder,tissue	m
ds	Elementary Volume	m^3
$E(t)$	Complex amplitude of the electrical field	V/m
g	Mean cosine phase function/ scattering anisotropy	$unitless$
G_1	Unnormalized Wave function Correlation	Wm^{-2}
g_1	Normalized Wave function/E-field correlation	$unitless$
g_1^s	Normalized Wave function correlation for single scattering	$unitless$
$G_1^s(\vec{r},\tau)$	Scattered correlation function	Wm^{-2}
$g_2(\tau)$	Normalized intensity correlation	$unitless$
I	Specific Intensity	$Wm^{-2}sr^{-1}$

$k(\tau)$	”Wave vector” of the correlation field, purely imaginary, representing de-correlation due to absorption and particle motion	$1/m$
k_0	”Wave vector” of the correlation field outside the cylinder, tissue	$1/m$
k_1	”Wave vector” of the correlation field inside the cylinder, blood	$1/m$
l'_{tr}	Reduced transport mean free path	m
l_s	Scattering mean free path	m
n	Refractive index of blood	$unitless$
r	radial distance from the center of polar coordinates, the center of the vessel	m
r_d	Distance between the virtual point source and detection point	m
$S(\vec{r})$	Source strength	Wm^{-3}
$S(\vec{r},\hat{s})$	Source strength	$Wm^{-3}Sr^{-1}$
U	Average intensity	Wm^{-2}
V_{max}	Max Velocity of blood cell inside the vessel	m/s
$W(\tau)$	Defined as: $k(\tau) = jW$	$1/m$

Bibliography

[Abramowitz et al., 1988] Abramowitz, M., Stegun, I. A., and Romer, R. H. (1988). Handbook of mathematical functions with formulas, graphs, and mathematical tables.

[Akkermans and Montambaux, 2007] Akkermans, E. and Montambaux, G. (2007). *Mesoscopic physics of electrons and photons*. Cambridge university press.

[Belau et al., 2017] Belau, M., Scheffer, W., and Maret, G. (2017). Pulse wave analysis with diffusing-wave spectroscopy. *Biomedical optics express*, 8(7):3493–3500.

[Berne and Pecora, 2000] Berne, B. J. and Pecora, R. (2000). *Dynamic light scattering: with applications to chemistry, biology, and physics*. Courier Corporation.

[Biasetti et al., 2014] Biasetti, J., Spazzini, P. G., Hedin, U., and Gasser, T. C. (2014). Synergy between shear-induced migration and secondary flows on red blood cells transport in arteries: considerations on oxygen transport. *Journal of the Royal Society Interface*, 11(97):20140403.

[Blumgart and Yens, 1927] Blumgart, H. L. and Yens, O. C. (1927). Studies on the velocity of blood flow: I. the method utilized. *The Journal of clinical investigation*, 4(1):1–13.

[Boas et al., 1994] Boas, D., O'leary, M., Chance, B., and Yodh, A. (1994). Scattering of diffuse photon density waves by spherical inhomogeneities within turbid media: analytic solution and applications. *Proceedings of the National Academy of Sciences*, 91(11):4887–4891.

[Boas et al., 2016] Boas, D. A., Sakadžić, S., Selb, J. J., Farzam, P., Franceschini, M. A., and Carp, S. A. (2016). Establishing the diffuse correlation spectroscopy signal relationship with blood flow. *Neurophotonics*, 3(3):031412.

[Boas and Yodh, 1997] Boas, D. A. and Yodh, A. G. (1997). Spatially varying dynamical properties of turbid media probed with diffusing temporal light correlation. *JOSA A*, 14(1):192–215.

[Bourlier et al., 2013] Bourlier, C., Pinel, N., and Kubické, G. (2013). *Method of moments for 2D scattering problems: basic concepts and applications*. John Wiley & Sons.

[Colton and Kress, 2019] Colton, D. and Kress, R. (2019). *Inverse acoustic and electromagnetic scattering theory*, volume 93. Springer Nature.

[Cummins and Swinney, 1970] Cummins, H. Z. and Swinney, H. L. (1970). Iii light beating spectroscopy. In *Progress in optics*, volume 8, pages 133–200. Elsevier.

[Ding et al., 2005] Ding, H., Lu, J. Q., Jacobs, K. M., and Hu, X.-H. (2005). Determination of refractive indices of porcine skin tissues and intralipid at eight wavelengths between 325 and 1557 nm. *JOSA A*, 22(6):1151–1157.

[Durduran et al., 2010] Durduran, T., Choe, R., Baker, W. B., and Yodh, A. G. (2010). Diffuse optics for tissue monitoring and tomography. *Reports on Progress in Physics*, 73(7):076701.

[Durduran and Yodh, 2014] Durduran, T. and Yodh, A. G. (2014). Diffuse correlation spectroscopy for non-invasive, micro-vascular cerebral blood flow measurement. *Neuroimage*, 85:51–63.

[Flock et al., 1992] Flock, S. T., Jacques, S. L., Wilson, B. C., Star, W. M., and van Gemert, M. J. (1992). Optical properties of intralipid: a phantom medium for light propagation studies. *Lasers in surgery and medicine*, 12(5):510–519.

[Frenkel and Smit, 2001] Frenkel, D. and Smit, B. (2001). *Understanding molecular simulation: from algorithms to applications*, volume 1. Elsevier.

[Funck et al., 2018] Funck, C., Laun, F. B., and Wetscherek, A. (2018). Characterization of the diffusion coefficient of blood. *Magnetic resonance in medicine*, 79(5):2752–2758.

[Gabe et al., 1969] Gabe, I. T., GAULT, J. H., ROSS JR, J., MASON, D. T., MILLS, C. J., SCHILLINGFORD, J. P., and Braunwald, E. (1969). Measurement of instantaneous blood flow velocity and pressure in conscious man with a catheter-tip velocity probe. *Circulation*, 40(5):603–614.

[Goldsmith and Marlow, 1979] Goldsmith, H. and Marlow, J. (1979). Flow behavior of erythrocytes. ii. particle motions in concentrated suspensions of ghost cells. *Journal of Colloid and Interface Science*, 71(2):383–407.

[Graaff and Ten Bosch, 2000] Graaff, R. and Ten Bosch, J. (2000). Diffusion coefficient in photon diffusion theory. *Optics letters*, 25(1):43–45.

[Haskell et al., 1994] Haskell, R. C., Svaasand, L. O., Tsay, T.-T., Feng, T.-C., McAdams, M. S., and Tromberg, B. J. (1994). Boundary conditions for the diffusion equation in radiative transfer. *JOSA A*, 11(10):2727–2741.

[Higgins et al., 2009] Higgins, J. M., Eddington, D. T., Bhatia, S. N., and Mahadevan, L. (2009). Statistical dynamics of flowing red blood cells by morphological image processing. *PLoS computational biology*, 5(2).

[Ishimaru, 1978] Ishimaru, A. (1978). *Wave propagation and scattering in random media*, volume 2. Academic press New York.

[Isserlis, 1916] Isserlis, L. (1916). On certain probable errors and correlation coefficients of multiple frequency distributions with skew regression. *Biometrika*, 11(3):185–190.

[Jayanthy et al., 2011] Jayanthy, A., Sujatha, N., and Reddy, M. R. (2011). Measuring blood flow: techniques and applications–a review. *Int. J. Res. Review Appl. Sci*, 6:203–216.

[Kashima et al., 1992] Kashima, S., Nishihara, M., Kondo, T., and Ohsawa, T. (1992). Model for measurement of tissue oxygenated blood volume by the dynamic light scattering method. *Japanese journal of applied physics*, 31(12R):4097.

[Kashima et al., 1993] Kashima, S., Sohda, A., Takeuchi, H., and Ohsawa, T. (1993). Study of measuring the velocity of erythrocytes in tissue by the dynamic light scattering method. *Japanese journal of applied physics*, 32(5R):2177.

[Lai et al., 2014] Lai, P., Xu, X., and Wang, L. V. (2014). Dependence of optical scattering from intralipid in gelatin-gel based tissue-mimicking phantoms on mixing temperature and time. *Journal of biomedical optics*, 19(3):035002.

[Lang, 2004] Lang, P. (2004). Scattering methods: Basic principles and application to polymer and colloidal solutions.

[Morse and Feshbach, 1954] Morse, P. M. and Feshbach, H. (1954). Methods of theoretical physics. *American Journal of Physics*, 22(6):410–413.

[Nanne et al., 2010] Nanne, E. E., Aucoin, C. P., and Leonard, E. F. (2010). Shear rate and hematocrit effects on the apparent diffusivity of urea in suspensions of bovine erythrocytes. *ASAIO journal (American Society for Artificial Internal Organs: 1992)*, 56(3):151.

[Owen and Roberts, 2007] Owen, C. A. and Roberts, M. (2007). Arterial vascular hemodynamics. *Journal of Diagnostic Medical Sonography*, 23(3):129–140.

[Pietrangelo et al., 2018] Pietrangelo, S. J., Lee, H.-S., and Sodini, C. G. (2018). A wearable transcranial doppler ultrasound phased array system. In *Intracranial Pressure & Neuromonitoring XVI*, pages 111–114. Springer.

[Poelma et al., 2012] Poelma, C., Kloosterman, A., Hierck, B. P., and Westerweel, J. (2012). Accurate blood flow measurements: are artificial tracers necessary? *PloS one*, 7(9).

[Pogue and Patterson, 2006] Pogue, B. W. and Patterson, M. S. (2006). Review of tissue simulating phantoms for optical spectroscopy, imaging and dosimetry. *Journal of biomedical optics*, 11(4):041102.

[Rajan et al., 2009] Rajan, V., Varghese, B., van Leeuwen, T. G., and Steenbergen, W. (2009). Review of methodological developments in laser doppler flowmetry. *Lasers in medical science*, 24(2):269–283.

[Rička, 1993] Rička, J. (1993). Dynamic light scattering with single-mode and multimode receivers. *Applied optics*, 32(15):2860–2875.

[Sakadžić et al., 2017] Sakadžić, S., Boas, D. A., and Carp, S. A. (2017). Theoretical model of blood flow measurement by diffuse correlation spectroscopy. *Journal of biomedical optics*, 22(2):027006.

[Sommerfeld, 1949] Sommerfeld, A. (1949). *Partial differential equations in physics*. Academic press.

[Stewart et al., 2019] Stewart, K., Dangelmaier, S., Pott, P., and Anders, J. (2019). Investigation of a non-invasive venous blood flow measurement device: Using thermal mass measurement principles. *Current Directions in Biomedical Engineering*, 5(1):179–182.

[Tang et al., 2018] Tang, J., Erdener, S. E., Li, B., Fu, B., Sakadzic, S., Carp, S. A., Lee, J., and Boas, D. A. (2018). Shear-induced diffusion of red blood cells measured with dynamic light scattering-optical coherence tomography. *Journal of biophotonics*, 11(2):e201700070.

[Torricelli et al., 2014] Torricelli, A., Contini, D., Dalla Mora, A., Pifferi, A., Re, R., Zucchelli, L., Caffini, M., Farina, A., and Spinelli, L. (2014). Neurophotonics: non-invasive optical techniques for monitoring brain functions. *Functional neurology*, 29(4):223.

[Vishwanath and Zanfardino, 2019] Vishwanath, K. and Zanfardino, S. (2019). Diffuse correlation spectroscopy at short source-detector separations: Simulations, experiments and theoretical modeling. *Applied Sciences*, 9(15):3047.

[Wang et al., 2018] Wang, C., Li, X., Hu, H., Zhang, L., Huang, Z., Lin, M., Zhang, Z., Yin, Z., Huang, B., Gong, H., et al. (2018). Monitoring of the central blood pressure waveform via a conformal ultrasonic device. *Nature biomedical engineering*, 2(9):687.

[Wang and Wu, 2012] Wang, L. V. and Wu, H.-i. (2012). *Biomedical optics: principles and imaging*. John Wiley & Sons.

[Wu et al., 1990] Wu, X., Pine, D., Chaikin, P., Huang, J., and Weitz, D. (1990). Diffusing-wave spectroscopy in a shear flow. *JOSA B*, 7(1):15–20.

[Zanfardino and Vishwanath, 2018] Zanfardino, S. and Vishwanath, K. (2018). Sensitivity of diffuse correlation spectroscopy to flow rates: a study with tissue simulating optical phantoms. In *Medical Imaging 2018: Physics of Medical Imaging*, volume 10573, page 105732K. International Society for Optics and Photonics.